NOVEL APPROACHES TO ENGINEER GLUCOSE BIOSENSORS

A DISSERTATION

FOR THE DEGREE OF DOCTOR OF PHILOSOPHY

SUBMITTED TO THE BRUNEL INSTITUTE FOR BIOENGINEERING

AND THE COMMITTEE ON GRADUATE STUDIES

OF BRUNEL UNIVERSITY

LONDON

by

Jakub Trzebinski

December 2011

To my friends & family

Acknowledgements

First and foremost I would like to thank Professor Tony Cass for the scientific and mental support throughout my Ph.D. His immense knowledge, patients for my (often ridiculous) questions and enthusiasm for research was contagious and motivational for me. If I ever achieve anything in science all the blame should rest on his shoulders.

The work presented here would not be completed without the support of Dr Anna Radomska - Botelho Moniz and Dr Sanjiv Sharma. They made working long hours fun, have been patient enough to listen to me whenever I was excited about a new idea and provided me with a tremendous amount of mental support. I also thank all my labmates. It was a pleasure to work with so many talented and dedicated people!

Thanks are also given to Professor Francis Moussy for giving me the opportunity to start my Ph.D. and for his support together with Dr Krishna Burugapalli, both serving their advice throughout the whole project. Also, not much would have been achieved without the cheerful word from Jenny Kume and Professor Derek Fisher who both helped me in dealing with my rather 'unusual' problems!

I would also like to express my deepest gratitude to my family for all their love and encouragement, especially my grandfather Stefan Kupczyk who was always there for me.

Last but not least, I would like to thank all my friends back home and in London (you know who you are!) who sweetened; to a tremendous extent, this time of my life.

List of publications

Most of the results presented in this thesis have been published in the following journal articles (attached in the appendix) and a book chapter:

Sanjiv Sharma, Anna Radomska-Botelho Moniz, Iasonas Triantis, Kostis Michelakis, **Jakub Trzebinski**, Alireza Azarbadegan, Benjamin Field, Chris Toumazou, Ian Eames and Anthony E. G. Cass, *An integrated silicon sensor with microfluidic chip for monitoring potassium and pH*, Microfluidics and Nanofluidics, 2011, Vol: 10, Pages: 1119-1125, DOI: 10.1007/s10404-010-0740-y

Jakub Trzebinski, Anna Radomska-Botelho Moniz, Sanjiv Sharma, Krishna Burugapalli, Francis Moussy, Anthony E. G. Cass, *Hydrogel Membrane Improves Batch-to-Batch Reproducibility of an Enzymatic Glucose Biosensors,* Electroanalysis, 2011, DOI: 10.1002/elan.201100286

Jakub Trzebinski, Sanjiv Sharma, Anna Radomska-Botelho Moniz, Kostis Michelakis, Yang Yang Zhang and Anthony E.G. Cass, *Microfluidic device to investigate factors affecting performance in biosensors designed for transdermal applications,* Lab on a Chip, 2011, DOI: 10.1039/C1LC20885C

Anna Radomska-Botelho Moniz, Yang Yang Zhang, Kostis Michelakis, **Jakub Trzebinski**, Sanjiv Sharma, Desmond G Johnston , Nick Oliver and Anthony E.G. Cass, *Continuous glucose monitoring using minimally invasive microprobes,* Journal of Diabetes Science and Technology, 2012, Vol:6, Pages:479-480

Iasonas F. Triantis, Anna Radomska-Botelho Moniz, Kostis Michelakis, Sanjiv Sharma, **Jakub Trzebinski**, Belinda Garner and Amir Eftekhar, *Ionic Neural Sensing*. Springer Handbook of Medical Technology, Springer Verlag, 2011, ISBN: 9783540746577

Abstract

Designing a biosensor capable of continuously monitoring blood glucose concentration in people with diabetes has been a major challenge for over three decades. In this work we attempt to develop a novel microspike based minimally invasive biosensor for this purpose. Also, as a part of an ongoing study, we attempt to improve the current design of coil-type implantable biosensors.

Microspikes, which are able to painlessly penetrate the skin layer, were fabricated using lithographic techniques and sputtered with gold to serve as an electrode. The biosensor design is based on thiomalic acid self-assembled monolayer (SAM) on which glucose oxidase was immobilised by a simple coupling technique together with a tetrathiafulvalene mediator entrapped in an epoxy-polyurethane permselective membrane. Functional testing revealed that such modified sensors are capable of detecting glucose concentration within the clinically relevant range. This was followed by studying the microspike based biosensors incorporated into the microfluidics platform mimicking the sensor behaviour in interstitial fluid. Data from these experiments revealed that the sensor response is mainly dependent on enzyme kinetics rather than membrane permeability to glucose.

In contrast, an attempt to address the reproducibility issues of coil-type biosensors is presented. The hypothesis for this study was that a crosslinked hydrogel would have a sufficiently uniform porosity and hydrophilicity to address the variability in sensor sensitivity. The hydrogel was prepared

by crosslinking di-hydroxyethyl methacrylate, hydroxyethyl methacrylate and N-vinyl pyrrolidone with 2.5 mol% ethylene glycol dimethacrylate using the water soluble initiators – ammonium persulphate and sodium metabisulfite under a nitrogen atmosphere. The hydrogel was applied to the sensor by dip coating during polymerisation. Electrochemical measurements revealed that the response characteristics of sensors coated with this membrane are highly consistent. Scanning Electrochemical Microscopy (SECM) was used to spatially resolve glucose diffusion through the membrane by measuring the consequent hydrogen peroxide release and compared with an epoxy-polyurethane membrane.

Contents

List of figures

List of tables

List of abbreviations

Å	Angstrom
AFM	Atomic Force Microscopy
C	Bulk concentration
CV	Cyclic Voltammetry
C_E	Concentration of an enzyme
C_S	Concentration of a substrate
CGMS	Continuous glucose monitoring system
CNT	Carbon nanotubes
D	Diffusion coefficient
E	Potential of the electrochemical cell
$E°$	Sum of the individual potentials of the electrodes measured in standard state
$E_{p,ox}$/ $E_{p,red}$	Oxidation and reduction potentials
e^-	Electron
F	Faraday constant
FAD	Flavin adenine dinucleotide
FTIR	Fourier Transform Infrared Spectrometry
GOx	Glucose oxidase
GDH	Glucose dehydrogenase
H&E	Hematoxylin and eosin
I_p	Peak current
$I_{p,ox}$/ $I_{p,red}$	Peak oxidation/reduction current
$i_{T\infty}$	Steady state current
ISE	Ion-selective electrode
ISF	Interstitial fluid
J	Flux
$\mathrm{K_m}$	Michaelis – Menten constant
k_1, k_{-1} and k_2	Reaction kinetic parameters
LBL	Layer by layer assembly
n	Number of electrons transferred in the reaction
O	Oxidised species
S	Sensitivity

SAM	Self assembly monolayer
SCE	Saturated calomel electrode
SECM	Scanning Electrochemical Microscopy
SEM	Scanning Electron Microscopy
SHE	Standard hydrogen electrode
STM	Scanning Tunnelling Microscopy
R	Reduced species
R/G	Ratio of ultramicroelectrode radius and surround glass radius
T	Absolute temperature
UME	Ultramicroelectrode
v	Scan rate
V_{max}	Maximum enzyme turnover rate
z	Ionic charge of the electroactive species

Chapter 1

Introduction

1.1 Aims and objectives

The aim of this chapter is to introduce the reader to electrochemistry as a science and show examples of currently used techniques. Furthermore, some recent developments in biosensor applications are presented along with a literature review of the work performed in this field.

1.2 Electrochemistry

Electrochemistry is a bridge between chemistry and electricity, wherein, electrical quantities at the interface between the electrode and the solution are correlated to chemical parameters [1]. The understanding of this science began in the 16th century when English physician and scientist William Gilbert published his book *'De Magnete'* ('The Magnet') where he briefly touched on electricity matters. However, it is only at the beginning of the 19th century when two chemists William

Nicholson and Johann Wilhelm Ritter separated water into oxygen and hydrogen using electrolysis that electrochemistry branched from chemistry to become an independent science. Today, it is a well developed discipline applied to a vast range of applications including renewable energy, metal purification and biomedical analysis [1].

Electrochemistry takes place at the junction between an electrolyte (a conductive substance containing free ions) and at least two electrodes (electrical conductors) which constitute the electrochemical cell. Such a device can be categorized either as a galvanic cell (where the electrical energy is derived from the chemical reactions) or as an electrolytic cell (where the electrical energy is used to decompose chemical compounds). In two electrode cell the electrical conductors are classified as either a cathode (a negatively charged electrode where the electroactive species undergo reduction) or an anode (a positively charged electrode where the electroactive species undergo reduction oxidation). Both, reduction and oxidation (redox) reactions of the analyte can be described by equation 1.1, where O and R are the oxidised and reduced forms of the redox couple, respectively, and n is the number of electrons transferred in the reaction:

$$O + ne^{-} \rightleftarrows R \tag{1.1}$$

This reaction occurs when a potential is applied between the electrodes, making the transfer of electrons thermodynamically favourable. For a given reaction, the potential of the electrochemical cell (E) where the reaction could thermodynamically take place can be calculated using Nernst equation:

$$E = E^{\circ} - \frac{RT}{zF} \ln Q \tag{1.2}$$

where $E°$ is the standard cell potential (sum of the individual potentials of the electrodes measured in standard state), R is the universal gas constant (8.314 J K^{-1} mol^{-1}), T is the absolute temperature, z is the number of moles of electrons transferred in the cell reaction, F is the Faraday constant (96485 C mol^{-1}) and Q is the reaction quotient (the concentration of electroactive species).

The voltammetric response is determined by reactions between the electroactive species and the electrode and is the sum of Faradaic currents (current generated by the redox reactions of a substrate) and a background current (current flowing through an electrode usually caused by processes at the electrode surface). For a simple reaction, such process involves the heterogeneous electron transfer in the solution to the electrode interface, and transport of the product back to the solution. Thus, the overall response is determined either by the mass transport of the electroactive species or by the rate at which the electrons are transferred.

Mass transport limited reactions

Mass transport processes are present in electrochemical reactions in three modes:

- Migration; movement of charged molecules driven by an electric field
- Diffusion; random motion of particles driven by a concentration gradient
- Convection; motion of particles caused by physical (solution) movement

A mass transport phenomenon is described by flux (J), which can be defined as the rate of molecules flowing across an area in a unit of time. When all three modes of mass transport occur in a given system, flux can be calculated using Nernst – Planck equation, which is an extended version

of Fick's Law by a component representing particles movement as a response to electrostatic force (second term in the equation 1.3). In one dimension this is:

$$J(x,t) = \underbrace{-\frac{D\partial C(x,t)}{\partial x}}_{\text{Diffusion}} \underbrace{-\frac{zFDC}{RT}\frac{\partial \phi(x,t)}{\partial x}}_{\text{Migration}} + \underbrace{C(x,t)V(x,t)}_{\text{Convection}} \quad (1.3)$$

where D is the diffusion coefficient [$m^2\ s^{-1}$], C is the bulk concentration [M], z is the ionic charge of the electroactive species, ϕ is the potential and V is the hydrodynamic velocity. Usually in electrochemical measurements the potential gradient is kept at minimum by providing an excess of the supporting electrolyte, thus the second term of the equation can be neglected. Moreover, the experiments are often carried without any convection (i.e. stirring or flow of the solution), which is represented as the last term in the above equation, in which case it can be also neglected [1]. In such simplified experimental conditions, the flux is dependent on the concentration gradient and can be calculated from equation 1.4:

$$J(x,t) = -D\frac{\partial C(x,t)}{\partial x} \quad (1.4)$$

Since the current (i) is directly proportional to the flux, as shown below:

$$i = -nFAJ \quad (1.5)$$

the current response of an electrochemical system can be calculated from the equation:

$$i = nFAD\frac{\partial C(x,t)}{\partial x} \quad (1.6)$$

Thus, the equation 1.6 indicates that current is directly proportional to concentration gradient of the electroactive species.

Such approximations make an electrochemical system relatively easy to model. Electrochemistry also provides a wide range of techniques to study more complex systems.

1.3 Electrochemical techniques

Several methods have been established to study electrochemical reactions, which are reviewed elsewhere [1]. Thus, only the techniques relevant to this work are described here, namely:

- Cyclic Voltammetry
- Amperometry
- Scanning Electrochemical Microscopy

Cyclic Voltammetry (CV)

CV is simple to perform and most widely used electrochemical procedure, which provides crucial information about the thermodynamics and kinetics of redox processes. It is a potentiodynamic technique wherein the potential is varied through linear ramping and the resulting current is measured [2]. A typical voltage sweep in CV is presented in Figure 1.

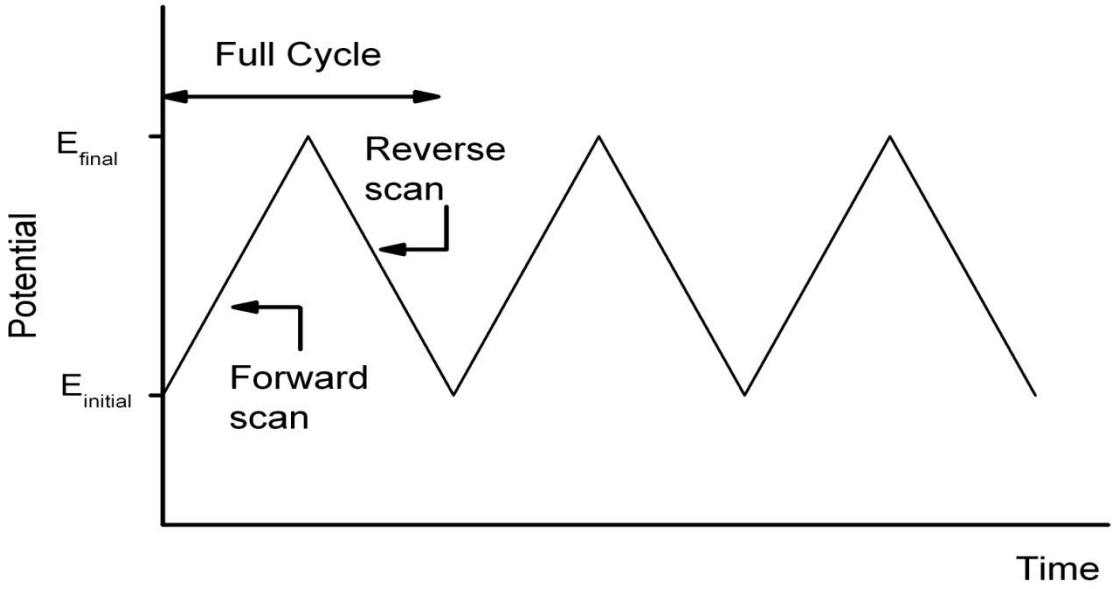

Figure 1: An example of potential vs. time plot for a typical cyclic voltammetry experiment.

A full cycle potential triangular waveform consists of a forward scan and a reverse scan. The slope of the potential ramp is called scan rate (v) and is expressed in V s^{-1}. The potential is applied between working and reference electrodes and the resulting current is measured between the working and counter electrodes (such combination is called three electrode setup). To neglect the mass transport of molecules caused by convection and migration (equation (1.3), CV is performed in unstirred solution with an excess of a supporting electrolyte. The results from a typical CV are presented as current versus potential plot and are called voltammograms (Figure 2).

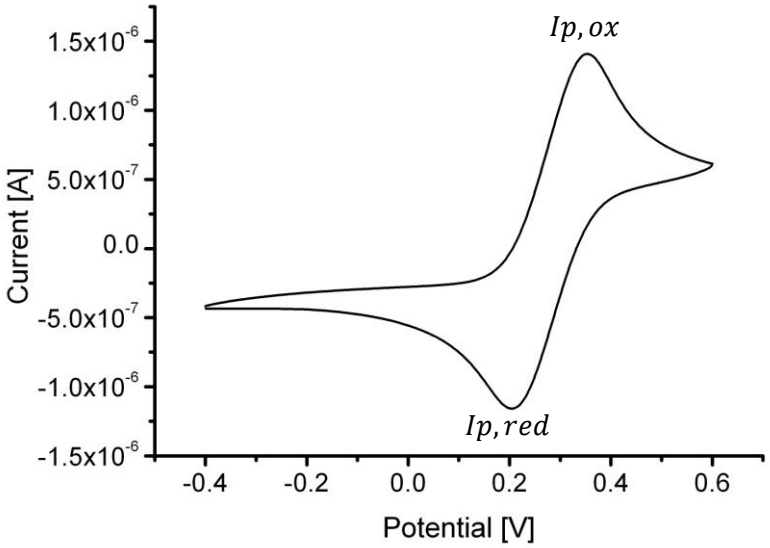

Figure 2: An example of a voltammogram for a gold disc electrode in 10mM $Fe(CN)_6^{3-}/Fe(CN)_6^{4-}$ at a scan rate of $100mVs^{-1}$

The initial potential is usually chosen where no redox reactions occur. When the potential is shifted forward past a threshold potential towards the oxidation potential the signal increases until the peak current I_p is reached. As the potential increases, the concentration of the reduced species on the surface of an electrode is depleted (redox process) which results in the change of concentration gradient and thus the increase of a cathodic current (equation (1.6). After the peak oxidation current $I_{p,ox}$ is reached the potential is shifted until the concentration of oxidised species is constant (i.e. constant current). At that point the current is mass transport limited and not potential limited. During the reverse scan, the accumulated oxidized species are reduced which results in decrease of anodic current $I_{p,red}$, after which the steady state current is reached.

Analysis of CV provides useful information about the electrodes – electrolyte system. CV is used to determine the kinetics of chemical reactions, especially whether the reaction is thermodynamically reversible. In particular, for a reversible couple (at 25°C) the peak current I_p is described by Randles – Sevcik equation:

$$i_p = (2.69 \cdot 10^5) n^{3/2} A C D^{1/2} v^{1/2} \quad (1.7)$$

where *n* is the number of electrons taking part in the reaction, *A* is the surface area of the electrode [cm^2], *C* is the concentration of the reverse couple [M cm^3], *D* is the diffusion coefficient [$cm^2\ s^{-1}$] and *v* is the scan rate [$V\ s^{-1}$]. Equation 1.7 can be used to determine the diffusion coefficient for an electroactive species as the current increases with the square root of the scan rate (for a Nernstian system, $E°$ is independent on the scan rate). Furthermore, varying the scan rate provides information useful to identify the type of the reaction (reversible, quasi – reversible or irreversible) [1]. For an ideal thermodynamically reversible (or electrochemically reversible) system the peak current ratio, $I_{p,ox}$ / $I_{p,red}$, is unity and the separation between the peak potentials is expressed as:

$$E_{p,ox} - E_{p,red} = \frac{59mV}{n} \quad (1.8)$$

where $E_{p,ox}$ and $E_{p,red}$ are the oxidation and reduction potentials, respectively, and n is the number of electrons transferred.

In reality, most electrochemical systems do not exhibit Nerstian behaviour. Such systems, referred to as quasi – reversible, process the electron transfer slower than the voltage scan rate as the barrier to electron transfer needs to be overcome by increased potential beyond E_{ox} In turn, this causes a separation of the oxidation and the reduction peaks observed on the voltammogram, which can be calculated from below equation (at 25 °C):

$$E_{p,ox} - E_{p,red} = \frac{48mV}{\alpha n_a} \tag{1.9}$$

where α is the transfer coefficient and n_a is the number of electrons exchanged during the charge - transfer step. Furthermore, CV of a system which is irreversible exhibits a shift of E_p with the scan rate, or absence of the reverse peak.

Amperometry

In amperometry a constant potential is applied to a working electrode and the resulting current is measured as a function of time. The applied potential is usually chosen (based on the CV experiments) such that the resulting current is mass transport limited thus, at steady state, it represents a concentration of the electroactive species, which are the analyte of interest or can be correlated to its concentration.

This technique is used to study the sensor response to a change of substrate concentration which is referred as titration. It involves the current measurements of a sensor under constant polarisation immersed in a buffer solution, while changing the analyte concentration (stepwise). The results are plotted on a current versus time curve. The time between the changes of analyte concentration is

determined by the properties of the sensor, namely by the time required for the current to reach equilibrium state.

Scanning Electrochemical Microscopy (SECM)

SECM is a type of Scanning Probe Microscopy (SPM), wherein measurements of surface properties are made using a customised tip [3]. In particular, SECM is used to measure the reactivity of the surface at a microscopic level. The basic principle involves positioning an ultramicroelectrode (UME), at close proximity to the sample surface and measuring the Faradaic currents while scanning the substrate immersed in an electrolyte solution. The measured current depends on the distance between the tip and the substrate, the characteristics of the UME, and the conductivity of the sample provides useful information about the electrochemical activity at nanometre to micrometer scale resolution.

The UME consists of a conductive material (usually Pt) insulated around the sides in a way that only the tip is exposed to the bulk solution (no lateral diffusion). The relation between the radius of the tip disc electrode R and the diameter of the insulator G, R/G, dictates the properties of the tip. Bigger R/G ratio results in larger collection area and smaller special resolution. Taking the above geometry into account, the steady state current, $i_{T\infty}$, when the UME is far from the surface, can be calculated from the fallowing equation:

$$i_{T\infty} = 4nFCDR \tag{1.10}$$

where *C* is the local concentration of a redox couple and R is the radius of the electrode.

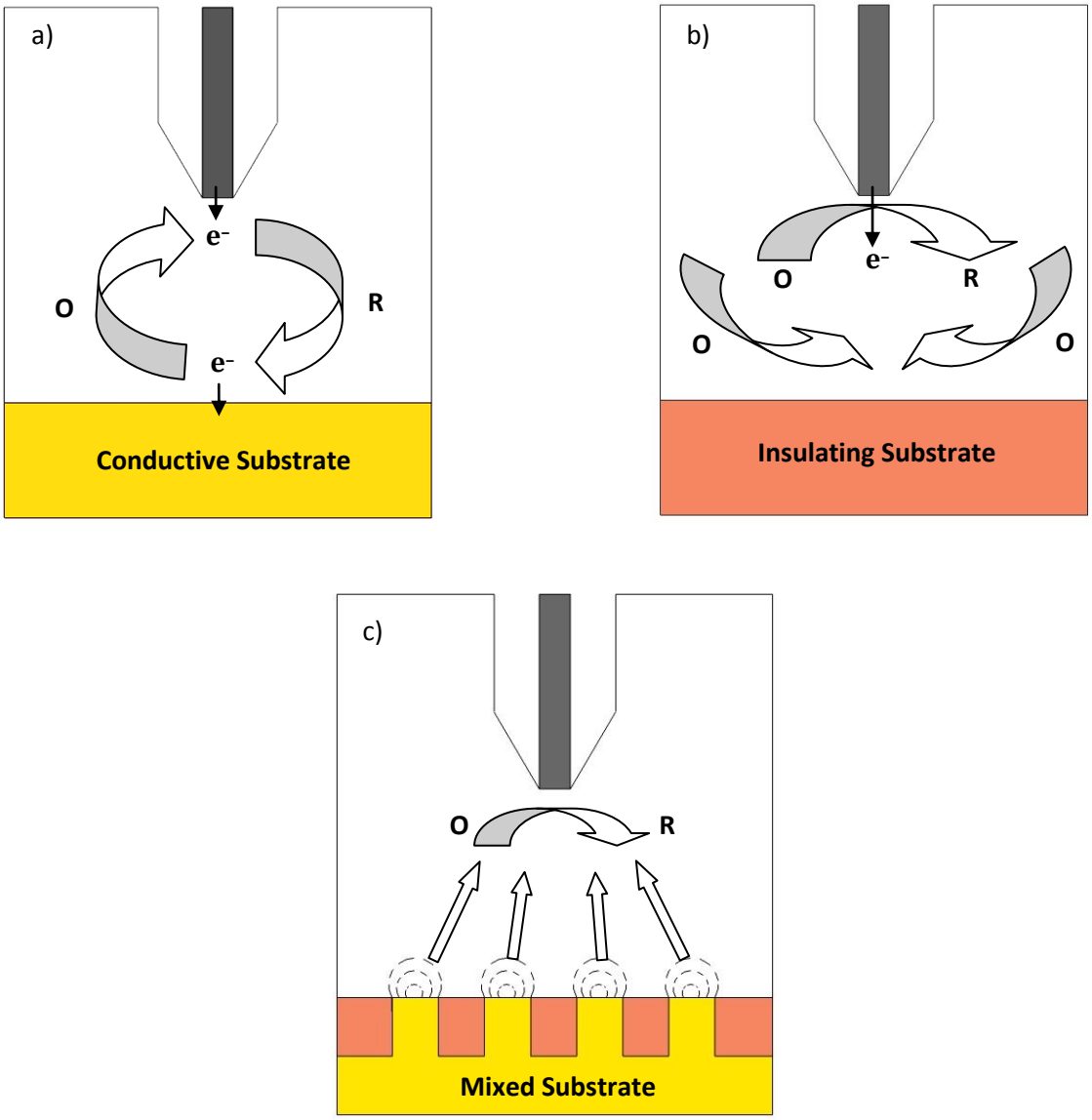

Figure 3: Schematic representations of the SECM methods of operation. a) positive feedback mode where the UME tip is in close proximity to a conductive substrate and the regeneration of electroactive species is present, b) negative feedback mode where the tip is positioned near the insulating substrate (the diffusion of oxidised species O is hindered) and c) generation – collection mode where the electroactive species are generated at the conducive interface.

When the UME is brought to a close proximity to the conductive sample (few tip diameters) the resulting current will be larger than a steady state current, i.e. $i_T > i_{T\infty}$, as the redox mediator is regenerated, increasing the flux of the reduced species to the UME tip. Such operation mode, called 'positive feedback' [4], is presented in Figure 3 (a). In contrast, when the UME is brought to a close proximity to the insulating surface (i.e. glass), the species oxidised at the tip of an electrode cannot be regenerated and its diffusion to the UME is hindered, as shown in Figure 3 (b). Such mode of operation is called 'negative feedback' and results in the decrease of measured current in comparison to a steady state current, $i_T < i_{T\infty}$.

A different approach is used in a SECM generation – collection mode, which is a method where the electroactive species are generated in a reaction involving the substrate and are collected by the UME tip. The tip is held at constant distance from the sample and a constant potential is applied to the UME as presented in Figure 3 (c). The measured current represents a concentration of redox species reacting with the tip. Thus, this mode allows mapping e.g. activity of an enzyme.

1.4 Enzymes

Many types of biosensors are described in the literature (reviewed in the next section). However in this work, enzyme based biosensors are of particular interest, as they exhibit exceptional specificity to a given substrate which is a highly desirable feature. In this section, a general description of enzymes is included and narrowed down to glucose oxidase which was used in this study.

Enzymes are globular proteins with amino acid residues ranging from few dozens to few thousands which, by lowering the activation energy, catalyze a chemical reaction. An enzyme comprises of an

active site (where the substrate is attached and the reaction takes place) and a shell surrounding it [5]. Enzymes are highly selective in binding to the substrate and the mechanism by which the catalysis is initiated involves specific non – covalent binding interactions. Specifically, there are four main routes by which the substrate can interact with the enzyme:

- Electrostatic interactions; charged substrate binds to the oppositely charged amino acid side chain
- Hydrogen bonding; hydrogen bond donor binds to a hydrogen bond acceptor containing acidic group of an enzyme. Both substrate and enzyme can be donors or acceptors
- Van der Waals interactions; when substrate and enzymes' active side are highly complementary with each other the binding can occur due to non – polar interactions
- Hydrophobic interactions; occurs when a hydrophobic group of a substrate binds to a hydrophobic group of an enzyme active site [5]

Enzymes, either alone or with a cofactor(s) improving the activity, can catalyze over a million reactions per second. They do not alter the position of chemical equilibrium but only 'speed up' the reaction rate aiming to reduce the concentration gradient between the substrate and the product. The rate at which the enzyme reacts with the substrate also depends on the temperature and the pH of the solution as both have an influence on the enzyme efficacy [5].

Enzyme kinetics

Enzyme kinetics is a study of the reaction rate, the speed at which a substrate is converted to a product (turnover rate) by an enzyme [5]. These studies help understanding the effect of various reaction conditions on enzyme performance.

The rate at which the enzyme catalyzes a reaction is dependent on its concentration, C_E, as well as the concentration of its substrate, C_S. For a given C_E and for a relatively low C_S the reaction rate increases linearly, which indicates that there is enough enzyme molecules to catalyse the reaction of a substrate. However, as the C_S increases, the reaction reaches a plateau, as it becomes limited by the enzyme turnover rate and finally arrives to a point where the maximum, V_{max} is reached [5]. An example of a saturation curve illustrating the dependence between the concentration of a substrate and the reaction rate is presented in Figure 4.

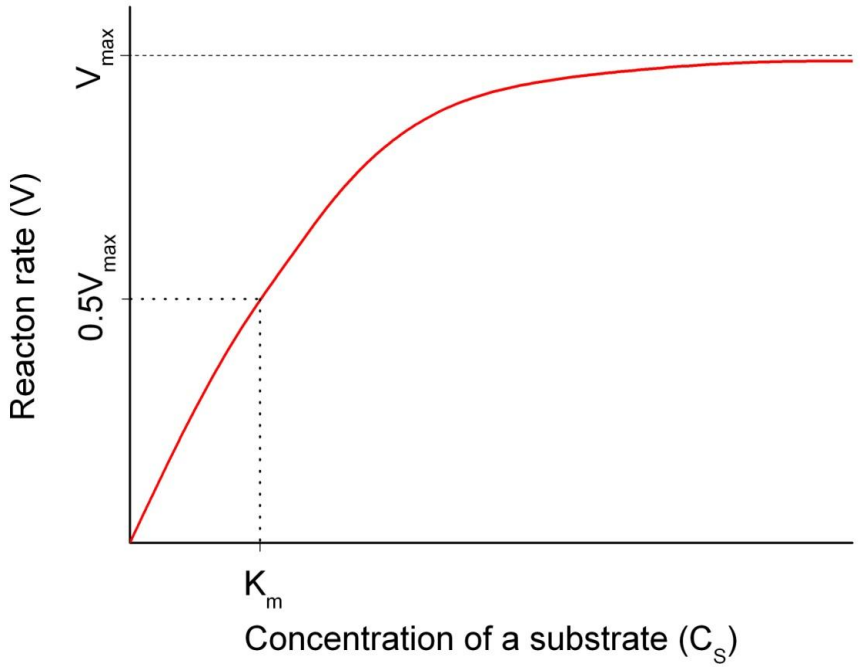

Figure 4: Typical enzyme saturation curve presenting the dependence of the reaction velocity versus the substrate concentration.

The mathematical description of enzyme kinetics was first presented by Michaelis and Menten in 1909 and is still widely used today. Their model is based on the assumption that that enzymatic reaction takes place in two stages. First, the enzyme E binds reversibly to a substrate S forming an ES complex. In the second stage, ES complex is catalysed by the enzyme and the product P is formed. This can be represented in a mathematical form as shown below:

$$E + S \underset{k_{-1}}{\overset{k_1}{\rightleftharpoons}} ES \overset{k_2}{\rightarrow} E + P \tag{1.11}$$

where k_1, k_{-1} and k_2 are the kinetic parameters [s^{-1}]. Such representation is called Michaelis – Menten kinetics model and is based on several assumptions:

- Enzyme binds to a single substrate
- The formation of a product is irreversible and the product does not bind to an enzyme
- The enzyme concentration does not change over time, which implies that the total enzyme concentration is the sum of the enzyme E and the enzyme – substrate complex ES
- The concentration of a ES complex changes much slower than the P and S concentration (the quasi – steady state assumption)
- There are no inhibitors involved in the reaction

The mathematical expression correlating the reaction rate to the substrate concentration derived from the Michaelis – Menten model can be formulated as:

$$\upsilon_0 = \frac{\upsilon_{max}\,[S]}{K_m + [S]} \tag{1.12}$$

where υ_0 is the initial rate of the enzymatic reaction, υ_{max} is the maximum rate, S is the substrate concentration and K_m (called a Michaelis – Menten constant) is equal to $\frac{k_{-1}+k_2}{k_1}$ and is defined as a substrate concentration at which the reaction rate is half of υ_{max} (as illustrated in Figure 4). This constant is inversely proportional to an approximate affinity of an enzyme (bigger K_m represents smaller enzyme affinity), and is often used to evaluate enzyme performance [5].

Most practical way for determining K_m is from a graphical representation of enzyme kinetics data, e.g. Lineweaver – Burk plot or Eadie – Hofstee diagram, which are used to present the Michaelis – Menten equation in a linear form. The description of all methods for the determination of K_m is beyond the scope of this work; however, an explanation of technique used is presented in the next chapter.

Glucose oxidase enzyme

The two most commonly used enzymes for the oxidation of glucose are flavoproteins glucose oxidase (GOx) sourced from *Aspergillus niger* (E.C.1.1.3.4) and quinoprotein glucose dehydrogenase (GDH) sourced from *Acinetobacter calcoaceticus* (E.C.1.1.1.47) [6]. In this work, GOx was used as the functional part of the biosensors, thus a brief description of its structure and properties is presented.

Glucose oxidase belongs to a group of flavoproteins, containing flavin adenine dinucleotide (FAD) cofactor. FAD is not covalently bound to the enzyme and is essential for the oxidation of glucose [7]. GOx is an oxido-reductase that catalyzes the transfer of electrons from the electron donor, glucose, to the electron acceptor, FAD cofactor. This reaction is presented in the figure below:

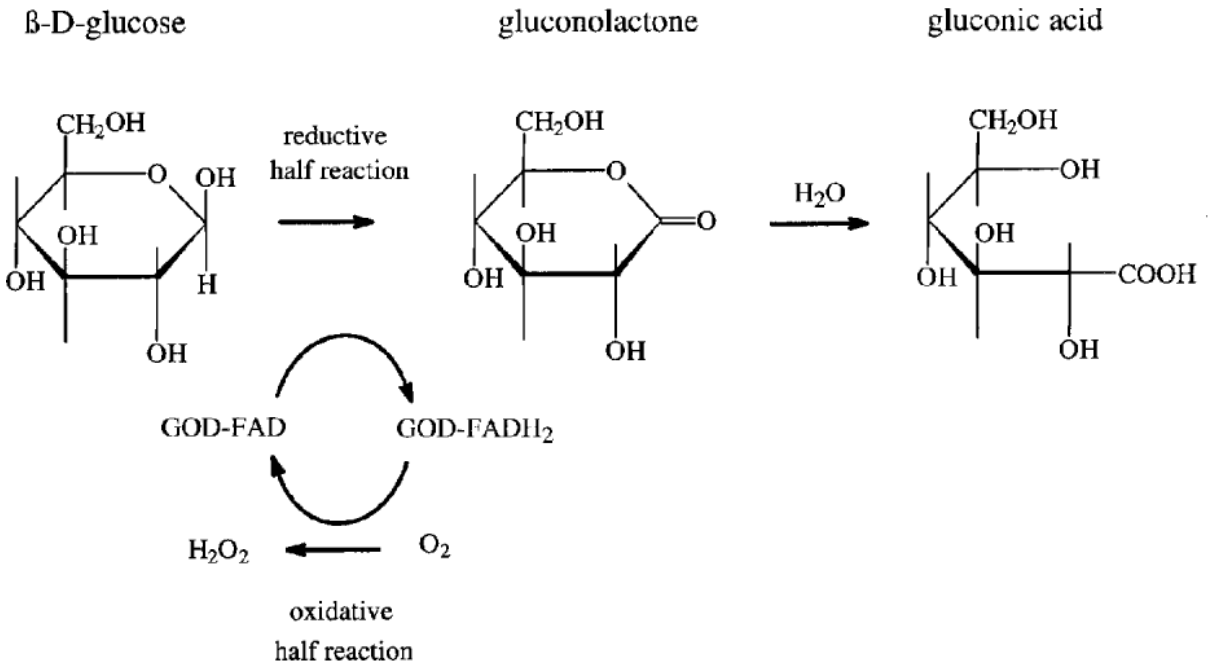

Figure 5: Schematic representation of GOx reaction with β-D-glucose. The image was adopted from [8].

As seen in Figure 5, in the first half-reaction β-D-glucose is oxidised by the enzyme to D-glucono-1,5-lactone (gluconolactone) which further hydrolyses spontaneously to gluconic acid. In the second half-reaction FAD cofactor acts as an electron acceptor and is reduced to $FADH_2$ which is than oxidised by molecular oxygen because it has higher reduction potential. Oxygen is than reduced to hydrogen peroxide which is the electroactive end product of the reaction [8].

GOx is highly specific and can only catalyse the reaction with β-D-glucose, which is one cyclic form, and not the other anomeric α-D-glucose form. However, since in humans both α- and β- D-glucose are in equilibrium, it is widely accepted to assume that the concentration of one is proportional to an overall glucose concentration [5, 7, 8].

1.5 Biosensor

A biosensor is a device containing a biological component capable of detecting an analyte. It comprises a sensing element having high affinity to an analyte of interest, a detector that transforms the signal from interactions between the sensing element and the analyte, and an instrument that amplifies, translates and presents the signal in a user friendly manner [1].

The choice of sensing element is dependent on the analyte of interest. Various biological materials have been used for this purpose, including enzymes, nucleic acids, antibodies and other components [9]. The main function of the sensing element is to interact with the analyte in a way which can be detected and processed. Ideally, the reaction should be quick, reversible and highly specific to a single analyte.

The main function of a detector (transducer) is to transform the signal generated by the interaction between the sensing element and the analyte of interest. The choice of the detector is dictated by the type of the physicochemical interaction between the sensing element and the analyte or by the biosensor application. Many types of transducers had been reported in the literature, including mechanical, thermal, electrical, optical or acoustic transducers [9].

In this work we have concentrated on electrochemical biosensors which take the advantage of biological elements capable of reacting with the analyte of interest, and producing a chemical signal, which can be measured using electrochemical methods.

1.5.1 Electrochemical biosensor

Electrochemical biosensors have been widely researched over the last three decades. They serve the advantage of detecting an analyte in an accurate and inexpensive fashion. The detection mechanism depends on the biorecognition processes and is based on the following electrochemical methods:

- Amperometric; constant potential is applied between electrodes to oxidise or reduce an electroactive species, a product of the biorecognition reaction, resulting in the generation of a measurable current signal
- Potentiometric; the signal (potential) is associated with the concentration of an analyte by the use of ion-selective electrode (ISE) and is measured between the working electrode and reference electrode (providing a reference potential) [1]

- Impedance; the signal (impedance – an extended form of resistance in AC current) is correlated to the selective binding of the analyte of interest immobilised on electrode surface [10]

Electrochemical biosensors based on enzymes have many applications in healthcare, environmental monitoring, and food industries, due to their accuracy and reliability in complex biological environments. Here, we attempt to improve current methods for the amperometric detection of glucose, thus a description of such sensors is presented below.

Enzyme based electrochemical biosensors

The basic working principle of enzyme based amperometric biosensors is presented in the figure below.

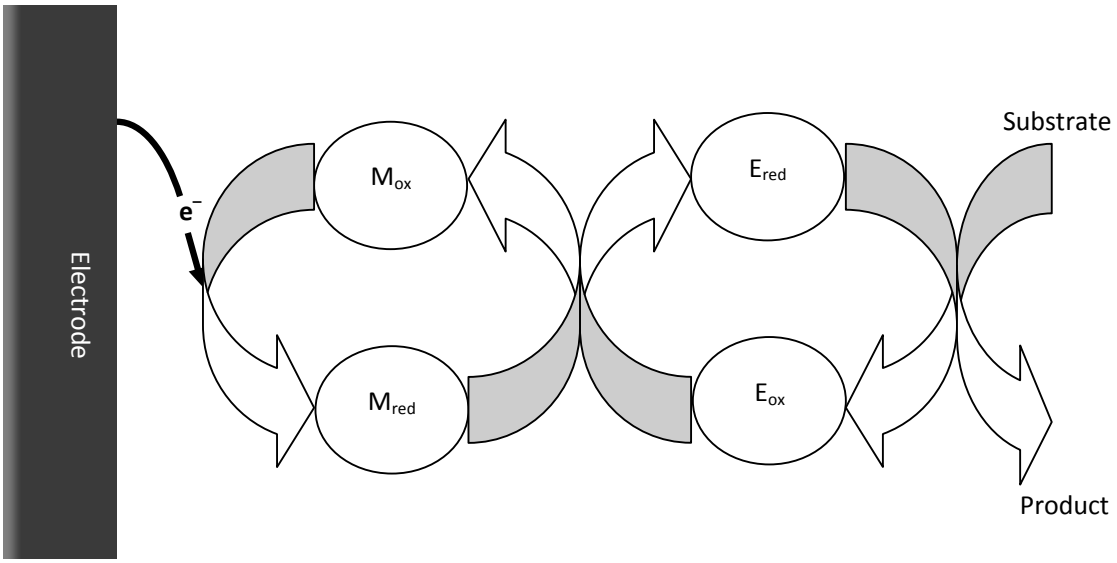

Figure 6: A schematic representation of a second generation biosensor (where a mediator is used to transfer the electrons between *E* and the electrode) working principle. *M* represents a mediator and *E* an enzyme.

The analyte of interest is catalysed by the enzyme layer in the same manner as described in section 1.4. When one of the products from such reaction is electroactive, a specific potential applied between working and counter electrode oxidises or reduces this species. The redox reaction involves electron e^- transfer from or to the electrode, which is proportional to the concentration of the reactant.

In case of glucose biosensors, where GOx is used as a biorecognition element to catalyse the reaction with the substrate, a potential of about 700mV is applied to oxidise hydrogen peroxide (which is an end product in the reaction) as shown below on the simplified version of the catalytic process:

$$\beta - D - glucose + GOx \cdot FAD \rightarrow D - glucono - 1{,}5 - lactone + GOx \cdot FADH_2 \qquad (1.13)$$

$$GOx \cdot FADH_2 + O_2 \rightarrow GOx \cdot FAD + H_2O_2$$

$$H_2O_2 \xrightarrow{700mV} 2H^+ + O_2 + 2e^-$$

It is important to note that in the oxygen mediated GOx catalysis process the measured current (transfer of e^-) is directly proportional to the concentration of hydrogen peroxide and not necessarily to the concentration of glucose. In the second step of the reaction presented above, the oxidation of $GOx \cdot FADH_2$ can be hindered by the availability of oxygen (e.g. when the sensors are implanted *in vivo*, sometimes they are exposed to oxygen depleted environment).

A solution to this problem was proposed by Cass *et al.* who used a ferrocene derivative (ferrocene monocarboxylic acid, $Fecp_2R$) to mediate the transfer of electrons between the GOx and the electrode [11] which made the reaction oxygen independent (see Figure 6), as presented in the stoichiometric equations below:

$$\beta - D - glucose + GOx \cdot FAD \rightarrow D - glucono - 1{,}5 - lactone + GOx \cdot FADH_2 \qquad (1.14)$$

$$GOx \cdot FADH_2 + 2Fecp_2R^+ \rightarrow GOx \cdot FAD + 2Fecp_2R + 2H^+$$

$$2Fecp_2R \xrightarrow{150mV} 2Fecp_2R^+ + 2e^-$$

Such an approach serves several advantages. First, the oxidation of the enzyme cofactor is independent from the molecular oxygen and any fluctuations of oxygen concentration in the solution containing the analyte will not have an effect on the reaction performance. Moreover, the regeneration of the mediator is usually done at much lower potential (approximately 150mV for ferrocene with comparison to 700mV for hydrogen peroxide) which decreases the risk of oxidising any unwanted molecules affecting the sensor response. However, a drawback from using mediators in implantable biosensors is that any leakage of these substances from the sensor can be potentially harmful to the host tissue.

1.6 Literature review

In this section, a literature review of the relevant subjects is presented, including a brief description of the need and techniques used to monitor the blood glucose level, and an in-depth review of minimally invasive and subcutaneously implantable glucose biosensors, which are the subject of this work.

1.6.1 Diabetes

Diabetes is a chronic disease which leads to an increase of blood glucose concentration (hyperglycaemia) either because the pancreas does not produce enough insulin (a hormone controlling the metabolism of glucose) or when the tissues in the organism do not respond to the insulin. The classification of this disease is as follows [12]:

- Type 1 diabetes (also called insulin dependent); is caused by the insufficient production of insulin by the pancreas
- Type 2 diabetes (also called non-insulin dependent); is characterised by the inability of the cells to use the insulin
- Gestational diabetes; involves high glucose levels secondary to pregnancy in woman (usually reversible)

If not managed properly, diabetes is a life threatening condition and can, through a series of complications (i.e. stroke, blindness or kidney failure), lead to death. According to the World Health Organisation (WHO), 220 million people worldwide have diabetes and in the year 2010 alone over 3.5 million people died as a consequence of this disease [12]. The cost for treating diabetics is approximately 10% of the total healthcare expenses in developed or developing countries [13].

There is no cure for this disease, and the cause of diabetes is usually obesity, unhealthy life style, genetic predisposition or viral infections. The treatment of diabetes involves controlling the glucose level close to normal by managing the diet, exercise and medications (mainly insulin in type 1 but also in combination with some oral medications in type 2 diabetes) which minimises the risk of complications [12].

For proper management of blood sugar levels and balancing it with insulin, a continuous (or at least often) monitoring of glucose is required. Many approaches to this problem have been researched in the last three decades, some of which are described below.

1.6.2 Glucose biosensors

The first attempt to improve the monitoring of the blood glucose level was made in mid 1960s resulting in the release of the Ames Reflectance Meter (ARM), which initially was for the doctor's office use only. The device was based on a cellulose strip, containing glucose oxidise, peroxidise and a chromogen (dye), which changed colour when a drop of blood was deposited onto it. The strip had to be compared with the colour chart which gave an rough estimation of blood glucose level [14]. The first clinical trial studies for home use ARM based devices were published 1978 by Peterson *et al.* where a group of patients was able to test their blood glucose levels at home [15]. Since then the general public noticed the importance of glucose monitoring in diabetic patients, which was underpinned in a joint statement issued in 1986 by the American Diabetes Association, Food and Drugs Administration and the National Institutes of Health recommending such practice for diabetic patients [16].

The ideal glucose sensor should provide continuous, real time, accurate readings for rapid change in blood glucose concentration. It should be non-invasive, long lasting and not require calibration from the user. Today, most popular technologies available on the market fulfil only some of the above criteria as they are based on off-line sampling either blood (glucometers which require finger pricking) or urine (urine dipstick) [16]. Such sensors typically comprise of a screen printed electrode (with PVC or ceramic as a substrate and carbon as a conductive ink; often mixed with a mediator) on which enzyme (glucose oxidase or glucose dehydrogenase) is deposited and protect with an outer layer (e.g. Nafion which also prevents from interferences) [17]. The biggest disadvantage of these sensors is that they do not provide continuous monitoring, which can lead to errors in adjusting the

glucose level with insulin. However, they are still the most popular in diabetic patients' community as there is no feasible alternative for these sensors. Other technologies (majority under constant development) which aim to address this issue are presented in the figure below.

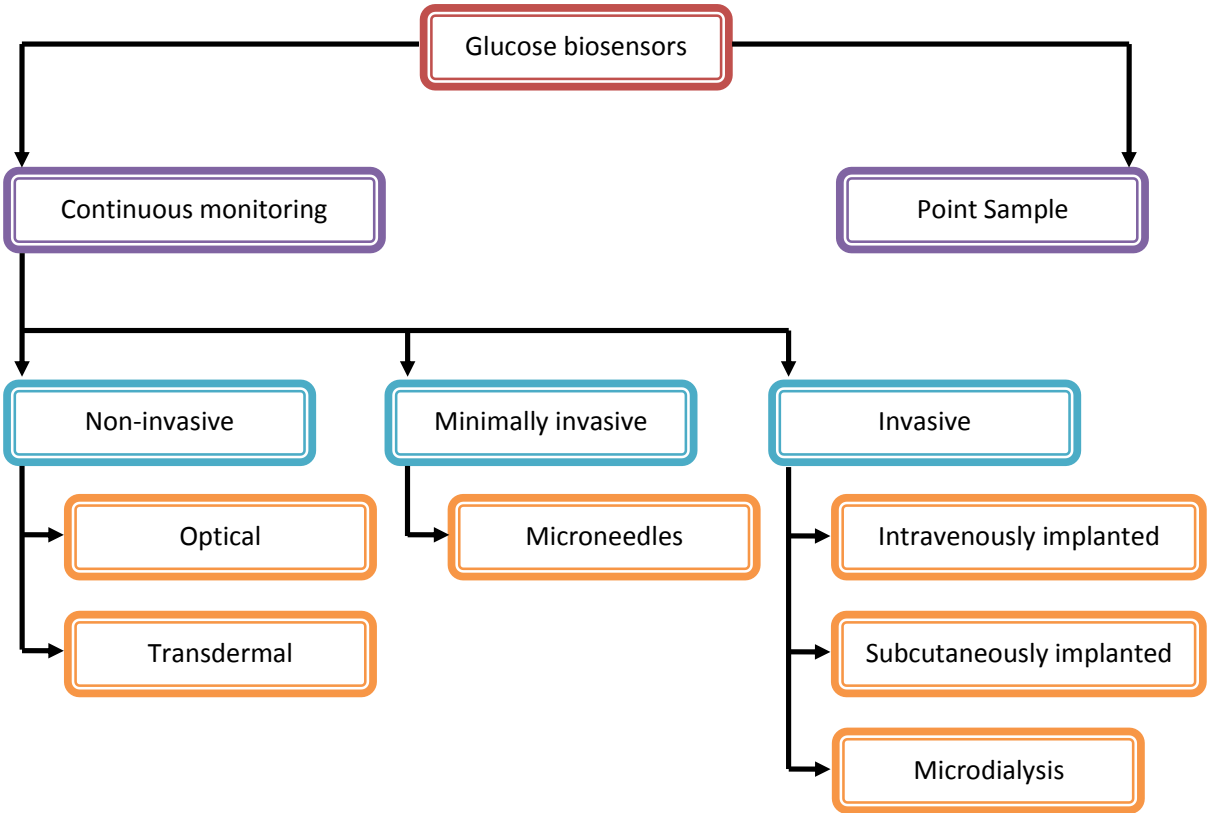

Figure 7: Schematic representation of the glucose sensor technologies [16].

The continuous glucose monitoring system (CGMS) is highly desirable as it allows correlation of the blood glucose level with factors which have an influence on it, like exercise, food or the insulin level. Traditional meters based on a point-sampling provide only a measurement at a given moment, based on which it is impossible for the patient to predict whether the glucose level increases or decrease and thus accordingly adjust it with insulin. CGMS would allow the user to obtain the reading without his/her involvement, which leaves no room for error, and applying an appropriate

dosage of insulin [18]. This would allow to remotely controlling the blood glucose level in a close loop insulin delivery system.

Glucose biosensor technology is still a rapidly growing field, with over 600 publications just in 2010. Many technologies (Figure 7) have been used to develop CGMS however, as for today; none was approved to fully replace the traditional meters. The review presented below gives a flavour of the work published on glucose biosensors and indicates the direction of possible future research.

Non – invasive optical glucose biosensors

Non – invasive biosensors are designed to measure the glucose concentration without accessing the blood or breaching the skin layer. To achieve this, optical techniques have been used in the recent past and some devices are already in clinical trial phase (e.g. Grove Instruments [19]). The main reasoning behind using optical techniques is that the beam of light can, to some extent, penetrate the tissue layer and interact with the molecules inside it.

Infrared (IR) spectroscopy technique takes advantage of the fact that molecules adsorb specific frequencies which than can be correlated to their structure. IR has been used for measuring the blood glucose concentration [20]. Both, near – infrared (NIR; wavelength 0.7 – 1.4 μm) and mid – infrared (MIR; wavelength 2.5 – 50 μm) spectroscopes have been used with some success for this purpose allowing the detection of glucose spectra window where absorption band intensities for interferences like melanin, hemoglobin, and water are low [21]. It has been shown that these techniques allow the beam of light passing through the skin layer to a subcutaneous region where various molecules can be detected [22]. Furthermore, Burmeister *et al.* used NIR to measure the

blood glucose level across the human tongue [23] which is very promising as the oral mucosa is highly vascularised. The drawback however, is that such measurements are performed in the presence of saliva containing traces of glucose, which can compromise the accuracy of the results [16].

A more general problem related to the use of IR spectroscopy for blood glucose measurements is that the skin through which the light is passing can vary between the individuals (e.g. by the amount of fat deposited or its hydration) or change its properties (e.g. temperature) over a short time; hence the sensors often require calibration [16]. These parameters also have an influence on the scattering of the light beam which results in the increase of signal to noise ratio.

Scattering of light can be exploited, and also used as a method for glucose detection. As the light passes through the tissue the amount of scatter depends on the relative refractive index of any obstacles (e.g. blood, cell membrane or fat). Therefore, as the concentration of glucose changes, the amount of scattered light will vary which was demonstrated by Heinemann *et al*. [24]. However, this technique is also susceptible to the change of skin characteristics mentioned above.

Similar problems occur when using MIR for measuring the thermal emission from cutaneous microcirculation of the blood vessel which depends on the blood glucose concentration [25]. This issue can be overcome by using Surface – Enhanced Raman spectroscopy, which studies a form of light scattering (named Raman scattering) enhanced by metal particles [26]. However, this technique requires an implantation of these particles to improve the signal, as without them the Raman Effect is too weak to distinguish glucose from similar particles [16] or the time required to acquire a full

spectrum is long which can be harmful to the tissues [27]. Furthermore, sources of error affecting the Raman scattering include the skin thickness or the concentration of erythrocytes [26].

Another attempt to measure the glucose concentration, without breaching the tissue layer, was done using polarimetry. This technique relays on measuring optically active molecules (such as glucose), exhibiting double refraction of the polarised light. The limitation of polarimetry is that it is impossible to detect the blood glucose concentration through the skin as the polarization needs to be measured in the tissue less than 4mm thick [16]. However, it is feasible to implement this technique in the anterior chamber of an eye [28, 29] and correlate the measurements with blood glucose concentration [30]. The biggest challenge for the scientists working on using polarimetry for glucose measurements is optimising a feedback mode to eliminate the eye motion artefacts and on modifying the current system for the *in vitro* measurements [28].

Optical coherence tomography (OCT) is based on the principle that backscattered radiation can be recorded from the skin irradiated with coherent light. Using this technique the change of glucose concentration in interstitial fluid can be measured, as it affects the scattering coefficient of tissue [31]. The disadvantage of OCT is that the changes of skin temperature or motion affect the measured signal [32]. Nevertheless, tests of products based on this technology (e.g. Sentris-100™, GlucoLight, Bethlehem, PA) suggest good performance *in vivo* [33].

Photoacoustic spectroscopy is another technique used for glucose detection. When a optical beam is illuminated onto a tissue the absorbed energy is transformed into a kinetic energy which results in heat generation [34]. Based on the physical and optical characteristics of the tissue, the blood glucose concentration can be determined noninvasively [34]. *In vivo* studies show 20% correlation

between the Aprise photoacoustic sensor (Glucon Inc., Boulder, CO) and oral glucose tolerance test [35]. This method also suffers from similar problems as the above described optical sensors [16].

Affinity based fluorescent techniques seem to be very promising candidates for biosensors as they exhibit fast, accurate and reversible response to a change of glucose concentration [36]. The main working principle involves competitive binding of glucose and fluorescently labelled binding agent to a receptor, which results in concentration dependent change in fluorescence emission. This technique can be used to analyse the glucose concentration in interstitial fluid (e.g. 'smart tattoos' [37]) or, when incorporated into contact lenses, in tears [38]. Several companies are looking into commercialisation of this technology and some are already on clinical trials stage (e.g. The Charles Stark Draper Laboratory Inc., Cambridge, MA).

Non – invasive transdermal glucose biosensors

It has been shown that transdermal glucose measurements in interstitial fluid (ISF) can be directly correlated to venous glucose concentration (with the first one lagging behind the other for 12.4 ± 4.9 min [39] also however, depending of the method of evaluation [40]). Among sensors taking advantage of this phenomena are the transdermal sensors which exploit the skin properties to noninvasively access the ISF.

The most mature method in transdermal glucose sensing is based on reverse iontophoresis. This technique involves applying current (usually DC) to an electrodes attached to the skin [41]. The flowing current induces migration of molecules either through electromigration (of e.g. negatively charged lactate) or electroosmosis (of e.g. uncharged glucose) [41]. The concentration of glucose

collected using reverse iontophoresis is much lower than in ISF; however it is still possible to measure it using enzymatic biosensors and correlate to the blood concentration [42]. This technology was incorporated into first transdermal glucose sensor called GlucoWatch (Cygnus Inc., Redwood City, CA) in 1999 [43]. However, the device was causing unpleasant skin rashes and was unreliable during perspiration, which resulted in its withdrawal from the market in 2008 [44].

Similar effects on the skin can be induced with another technique called sonophoresis. It relays on applying an ultrasound wave to the skin which increases its transdermal permeation and makes it easier to extract the ISF for glucose measurements (usually done using enzymatic biosensors) [45]. The advantage of sonophoresis is that, by making the skin more permeable, it allows removing ISF and injecting insulin with the same piece of equipment [46]. A prototype of such device was introduced in 2000 [46], however, there is still no product based on this technique available on the market.

Impedance spectroscopy is a method for noninvasively determining the glucose concentration. It is an indirect measurement technique, where an AC current is applied to the skin and the impedance is measured as a function of frequency [16]. The results (often referred as bioimpedance) can be correlated to the blood glucose concentration as it affects the impedance of the tissue – blood system [47]. However, the impedance measurements can also be affected by the change of skin temperature or sweating [47, 48].

Minimally invasive glucose biosensors

Minimally invasive sensors consist of a platform comprising of a needle-like microprobes and a sensing element (either combined with the platform or as a separate unit). Such structures are able to painlessly [49] penetrate the skin barrier (stratum corneum) and access the ISF or blood [50]. Such structures were firstly introduced in the 1970s, however not until 1990s, when microfabrication become more common, microprobes become extensively studied [51, 52]. Such platforms can be broadly classified in two categories, namely hollow microneedles and microspikes. Both types can be fabricated from various materials, including silicon, metals, biodegradable polymers or glass [53, 54]. The fabrication of hollow microneedles usually involves etching the silicon substrate using lithographically patterned silicon wafer, which leads to the development of microspikes. To fabricate microneedles with a channel trough the centre, an additional round of etching needs to be performed [53]. Such structures can serve as a mask for fabricating a micromould which can be used to manufacture these devices with variety of materials [53].

For sensing applications, microneedles are used for extraction of either blood (when 2mm in length [50]) or ISF (700-1500µm long [55]) from underneath the skin (either through capillary forces or vacuum), where the medium is examined by an external sensor. Earlier studies suggest that it is feasible to use microdialysis to sample the ISF for glucose measurements [56]. The biggest challenges for this technique are fouling of the catheter with large molecules which than can interfere with the sensor function, relatively long sampling lag (with combination to a interstitial fluid glucose concentration being approximately 60% of that in blood and its change being in the compartment lag 6-7 minutes behind changes in blood [40]) and local trauma at the site of the catheter insertion [57]. Hollow microneedles serve the advantage over the above as they are small

enough to minimise the local tissue irritations when inserted into the skin [49], can be modified to act as size – exclusion membrane and prevent unwanted molecules to pass through [58], and, with the help of a vacuum pump, dramatically increase the sampling time [56]. However, clogging of microneedles by large proteins is still an issue which, to our knowledge, has not been solved.

Microspikes have been extensively developed for painless drug delivery as they allow puncturing the skin structure creating small cavities hence making it permeable for large drug molecules to diffuse through [52, 59, 60]. Similar devices serving the same function were also fabricated from biodegradable materials (e.g. PLA or PLGA), mixed [51] or coated [61] with a model drug which was released after inserting through the skin.

Invasive glucose biosensors

Invasive glucose biosensors are designed to access either the ISF or the capillary blood and take measurements directly or in offline analysis. This is the most developed group of biosensors for continuous glucose monitoring and most commercially available products are based on this technology [16].

Microdialysis is one of such technologies and involves implanting a fibre into the adipose tissue, where the ISF perfuse out under pressure and is pumped to an external electrochemical glucose sensor [62]. Such fibre usually consists of a membrane for initial filtration of cells and large molecules, allowing the clean matrix to perfuse [62]. The fluid which is used for measurements is mixed with Ringer's solution containing GOx enzyme and passed to the electrolytic cell which minimises the need for calibration (usually done once a day) [63]. Adding enzyme to the solution

also reduces the risk of enzyme degradation and, since the measurements are done *ex vivo*, the risk of inflammation or biofouling [64]. However, the bacterial contamination of the catheter and the lag time for the analyte to be pumped from the adipose tissue to a biosensor still reminds an issue [64]. An example of such device available on the market is GlucoDay S system (Menarini Diagnostics, Firenze, Italy) [65].

Among invasive sensors, subcutaneously implanted needle – type amperometric glucose biosensors are the most commonly used for CGMS [64]. Such a sensor implanted into the subcutaneous space comprises of a working electrode (on which the enzyme is immobilised) and a reference/counter electrode. The working principle involves measuring the current resulting from enzyme catalysed electrooxidation of glucose mediated either by oxygen or a redox active couple (see section 1.5.1 for details). As the GOx enzyme becomes saturated at high glucose concentrations which results in inaccurate readings, such sensors are coated with a membrane which serves several functions. It limits the flux of glucose (which increases the limit of detection making sensors feasible to work at physiological glucose concentration range) and acts as a protective coating providing the bioactive interface between the electrodes and the body tissues [66]. These sensors are shown to function *in vitro* for ≥ 3 months under constant polarisation [67] and some reports suggest that they are capable to work *in vivo* for over a year [68]. However, as soon as such sensors are implanted in the body, they start losing their sensitivity due to biofouling and immune responses triggered by implantation injury, and these ultimately lead to the sensors failure [66]. Several attempts were made to minimise these effects [69-72], however most such approaches increase the *in vivo* sensing life of the sensors, but often, only one of many ostensibly identical sensors functions longer than a few weeks [73].

Several sensors based on this technology are available on the market, some of which are presented in Figure 8.

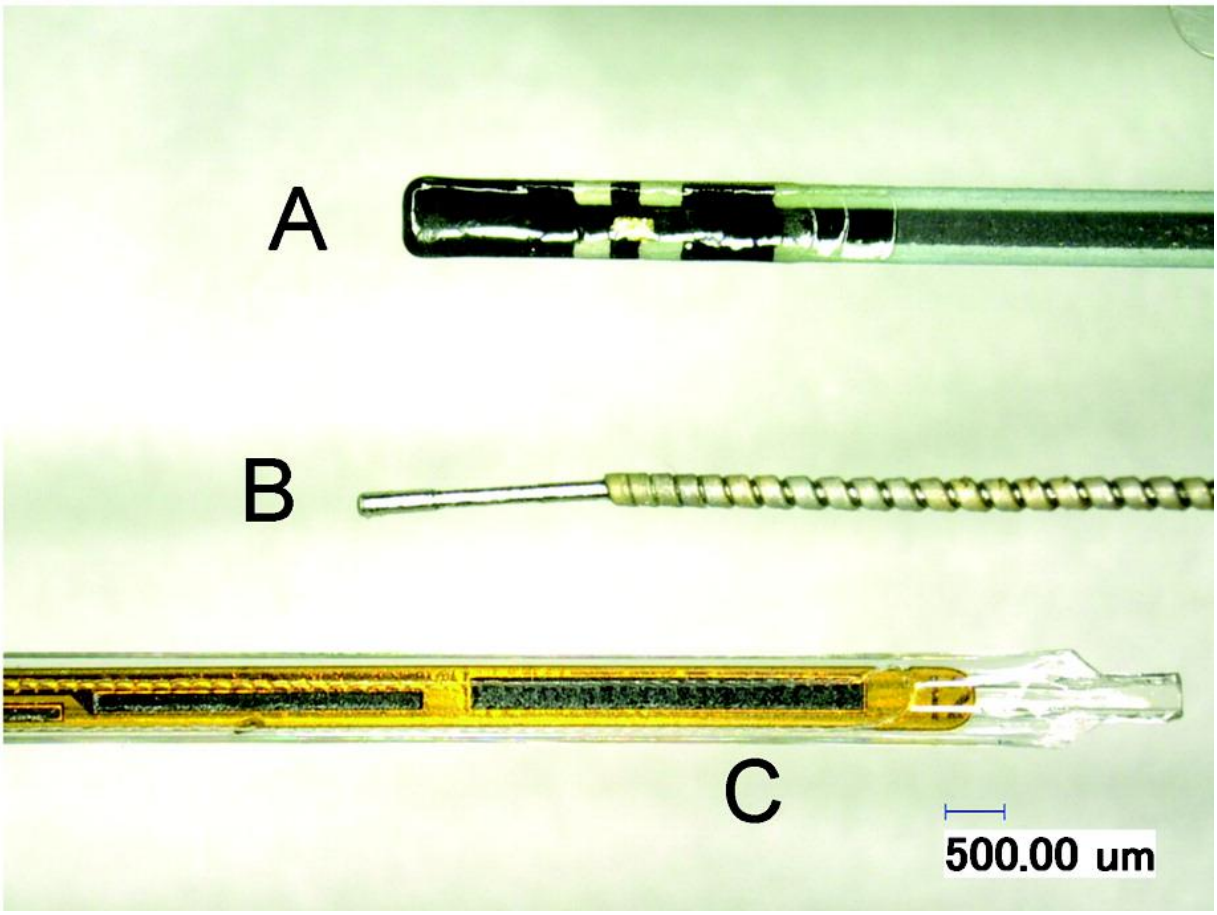

Figure 8: Examples of commercially available needle – type amperometric glucose biosensors. A) FreeStyle Navigator (Abbott Diabetes Care, Alameda, CA); B) Dexcom STS (DexCom, Inc, San Diego, CA) and C) Guardian RT (Medtronic Diabetes, Northridge, CA). The image was adapted from [64]

The sensors presented in the above figure are subcutaneously implanted for between 3 – 7 days and, after 1 – 10h equilibration period *in vivo*, require daily calibration typically done using finger prick method. Such sensors are not individually tested *in vitro* since it could influence their

performance. The need for calibration is mainly because the variability of subcutaneous environment, sensor drift, sensor to sensor variation due to manufacturing processes (FDA agrees on 10 % variation for implantable, and 3–5% for the test strip biosensors used for calibration [64]) and the immune response from the host caused by the sensor implantation [74] . The attempt to address the reproducibility of enzymatic glucose sensors is presented in this work, thus a review of such devices, including theoretical consideration of the operation modes is presented below.

1.6.3 Enzymatic biosensors

Leland C. Clark, who is widely considered as a father of electrochemical biosensors, designed first sensor capable of measuring the concentration of oxygen dissolved in a solution, which is now known as 'Clark type' electrode. Such sensor comprises of a platinum cathode immersed in potassium chloride solution separated from the bulk with a Teflon permselective membrane and silver chloride anode. When a constant voltage of -600mV is applied between the electrodes, the change of current is proportional to the partial pressure of oxygen as the following reaction occurs:

$$O_2 + 4H^+ + 4e^- \rightarrow 2H_2O \qquad (1.15)$$

$$4Ag + 4Cl^- \rightarrow 4AgCl + 4e^-$$

Clark further exploited this technology and designed a sensor comprised of glucose oxidase enzyme sandwiched between the electrode and Teflon permselective membrane. The catalytic reaction of glucose, consuming oxygen as a substrate, causes the oxygen depletion in proximity to the electrode making it possible to indirectly measure the concentration of glucose. However, a drawback from

such determination of glucose *in vivo* is that the local fluctuations of oxygen concentration significantly influence the measurements. The solution for this problem was proposed in 1967 by Updike and Hicks, who designed a sensor with two working electrodes, one used to indirectly measure glucose concentration and the other to detect dissolved oxygen in solution [75]. This allowed subtracting the background current caused by the local oxygen variations from the indirect measurements of glucose concentration.

The first sensor which was capable of detecting glucose by measuring the hydrogen peroxide produced in the catalytic reaction involving GOx presented in equation (1.13), was described in 1972 by Guilbault and Lubrano [76]. Since then the development of glucose biosensors has progressed through three generations, as shown below:

- First generation biosensors; makes use of the oxygen co-substrate depletion or the hydrogen peroxide production during the catalytic reaction of glucose
- Second generation biosensors; synthetic electron acceptors (mediators) are used instead of oxygen in the catalytic reaction of glucose making the electron transfer more efficient. Such approach allows the sensor to work independently from oxygen and at much lower potentials
- Third generation biosensors; the goal for this type of sensors is to allow the direct electron transfer between the enzyme active sites and the electrode, which abandons the need for using a mediator. It can be achieved either by positioning of the GOx redox centre (FAD) at a close proximity (less than about 3 – 5 Å) to the electrode, or by developing an electrode which allows such electron transfer (e.g. tetrathiafulvalene – tetracyanoquinodimethane electrodes) [77].

As described earlier in this report, enzymatic biosensors comprise of three components: sensing element, detector and a signal processing component. The design of a biosensor depends on the technique used for immobilising the enzyme on a detector (electrode), choice of the redox couple, and selection of a permselective membrane. These components are described below.

Enzyme immobilisation

For glucose biosensors there are several strategies for the enzyme immobilisation on the electrode surface. GOx can be physically entrapped between the electrode surface and the permselective polymeric film such as Teflon or Nafion [77]. Although such approach allows not only to entrap the enzyme but also to extend its linear working range by reducing the local glucose concentration, it is not efficient especially considering long term sensor performance [1]. More elegant way is to covalently couple the enzyme within a polymer/protein film and casting it on top of the electrode. The advantage of this method is that it allows entrapping large quantities of GOx which results in larger hydrogen peroxide production (higher current density) and can enhance the enzyme activity [78]. The most commonly used protein for this purpose is bovine serum albumin which can be crosslinked using glutaraldehyde [69, 78].

Electropolymerisation is another technique which allows controlled immobilisation of enzyme on the surface of an electrode. GOx can be entrapped in the metal oxide (e.g. TiO_2 or CeO_2 [79, 80]) or polymeric (e.g. poly(pyrrole) or poly(1,2-diaminobenzene) [81, 82]) film produced by applying a potential on the electrode surface. If done using chronoamperometry, this technique allows controlling the thickness of the deposited film which accounts for sensor reproducibility.

More sophisticated method is the deposition of an enzyme using self assembly monolayer (SAM) technique. Gold electrode can be functionalised with e.g. thiomalic acid providing carboxylic groups with which GOx forms an amide bond and attaches covalently to the surface [83, 84]. This strategy allows the 2D enzyme deposition in a controlled fashion, which is beneficial especially when one wants to uniformly coat a 3D electrode surfaces [85]. Despite this, the long term stability of enzyme assembled using SAMs is poor unless such complex is further crosslinked [86].

Improved electron transfer can be achieved by 'wiring' the GOx redox centre with an electrode, which shortens the distance for the electrons to travel. This can be accomplished by, for example, wiring the enzyme with a polymer containing covalently attached electron acceptors (e.g. polyvinyl pyrrolidone with densely packed osmium complexes) [87], conductive nanoparticles (e.g. Ag) [88] or carbon nanotubes (CNT) [89].

Mediators

Mediators are a key feature in the second generation glucose biosensors. The main working principle involves the reaction of mediator with the reduced form of an enzyme and then diffusion to the electrode surface where it undergoes electron transfer. Their advantage of using the mediators in amperometric glucose sensors is that the artificial electron acceptors allow functioning independently from the dissolved oxygen concentration (which is a crucial substrate in the catalytic reaction of GOx) and requires much lower oxidation potentials in comparison to hydrogen peroxide (see section 1.5.1).

An ideal mediator should require low oxidation potential, close to that of an enzymes redox centre, to avoid oxidation of unwanted species (e.g. ascorbic acid or uric acid which are oxidised at the same potential as hydrogen peroxide). Further, mediators should function independent of changes in pH or temperature, have stable oxidised and reduced forms and not react with dissolved oxygen or participate in other side reactions which otherwise lead to inaccurate readings. They should also have low toxicity, especially when used for invasive or minimally invasive sensors [90].

Over the years many types of mediators have been developed to achieve these goals. They can be categorised into three groups, namely organic, inorganic and metal – organic mediators. Examples of such electron transferring agents are presented in the table below:

Organic	Quinoid dyes Quinines Oxidized viologens Quinone and its derivatives Heterocyclic dihydropolyazines Tetrathiafulvalene Tetracyanoquinodimethane Conducting salts
Inorganic	Oxygen Hydrogen peroxide Hexacyano-complexes of iron, cobalt and ruthenium
Metal – organic	Ferrocene derivatives Osmium complexes Chromium derivatives Ruthenium complexes

Table 1: Examples of artificial mediator – redox couples based on [64, 90].

Among the organic mediators, all presented above have been reported to mediate the signal in GOx catalysed enzymatic reaction [64]. However, some quinones and its derivatives have been shown to

also react with other proteins [91]. In addition, the performance of most organic dyes (e.g. prussian blue or methylene blue) vary with changes in pH, and often their stability is questionable [90].

In the group of organic mediators, tetrathiafulvalene (TTF) and its derivatives have been widely used as electron transfer agents especially for flavo enzymes [92-94]. The oxidation potential for these compounds is within 0.1 – 0.3 V (versus SCE) range which is low enough to prevent the interference from unwanted species [90]. Moreover the single and repeated application of saturated solutions of these mediators does not cause any local skin irritation [95], which suggest relatively low toxicity.

Oxygen and hydrogen peroxide are also considered as naturally occurring mediators for GOx, however, as discussed above, they require high oxidation potential (0.7 V versus SCE) for peroxide (which is similar to that of some interferences) and are affected by low oxygen solubility in physiological solutions [64].

Hexacyano-complexes (e.g. $Fe(CN)_6^{3-/4-}$, $Co(CN)_6^{3-/4-}$, $Ru(CN)_6^{3-/4-}$[96]) are widely used for the electron transfer enhancement in enzymatic biosensors [97, 98]. Their relatively low molecular weight (small size) allows them to reach the enzyme redox centre. Good performance when they were incorporated on screen printed carbon electrodes lead to the development of strip-based glucose meters [64].

Metal – organic mediators have been successfully used for fabrication of glucose biosensors, especially ferrocene and osmium complexes, which are known for their good stability and fast electron transfer rate between the enzyme and the electrode [11, 64]. Strip-based glucose meters comprised of these mediators (e.g. first electrochemical glucose meter for home use - ExacTech from Medisense [99]) were also developed.

Recent research also shows that it is possible to mediate the electron transfer from the enzyme flavin redox centre to the electrode using carbon nanotubes (CNT) [100, 101], which significantly enhance the electron transfer. The nano-size, cylindrical structure with high aspect ratio and end to end ballistic transport of electrons along CNTs was suggested to cause such rapid electron exchange [100]. Effectively, they are said to wire the redox centre of GOx to the electrode. However, a report suggests that the spontaneous interaction of CNTs with enzyme causes conformational changes (partial protein unfolding) exposing the active sites of GOx for faster electron transfer [102].

Another recent development is to use metal particles for the electron transfer enhancement. Gold [103], Platinum [104], Silver [105], Silicone particles [106] and Laponite (polycrystalline silicon) crystals [107] with sub-nanometre diameters have been reported to increase the electron transfer rate between the enzyme and the electrode [108]. Although these particles are reported to dramatically increase the enzyme performance (e.g. 5000 s^{-1} turnover rate for Ag nanoparticles/GOx complex [109] versus 600-700 s^{-1} for GOx [110]) very little is known about their interaction with the enzyme or the long term stability [109].

Permselective membrane

The permselective membranes (also referred as mass transport limiting or flux limiting membranes) are widely used for controlling the diffusion of substrate (e.g. glucose) to the sensing element. Although the purpose of such membrane remains the same in most types of sensors, the properties and coating technique varies depending on the application. The primary function of the membranes is to allow sensors to operate in physiological glucose concentration range by controlling solute transport, such that glucose concentration reaching the sensing element is rate limiting for the

sensing reaction. This allows measurements on un-diluted biological fluids, making implantable CGM a possibility [111, 112]. Secondly, the membranes also slow down or prevent the interferences from reaching the electrode. In the case of metal electrodes, especially platinum, they also prevent electrode poisoning by electrolytes in body fluids including chloride ions. A third function for the membranes is to protect underlying mediators, enzyme SAM, or electrodeposited films from degradation and leaching.

Polymers and co-polymers such as Nafion, cellulose acetate, polycarbonate, polyurethane, polyvinyl chloride, polyvinyl alcohol, tetrafluoroethylene, polyethylene, polypropylene, polyacrylamide, polymethylmethacrylate, collagen, perflurocarbon, and polyallylamine-polyaziridine, have been tested as mass transport limiting membranes [111, 113-121]. They are primarily deposited on sensors through solvent casting. Often additives such as epoxy resins are used to reinforce the polymers for improving mechanical integrity and long term durability [122]. The polymer membranes prepared by solvent casting/phase separation typically have tortuous pores of size >100nm, medium distribution and high density [123].

Most polymers tested are porous. However, Updike's group reported the use of monolithic membranes based on polyurethane on glucose sensors. The monolithic membrane is non-porous, yet it acts as barrier due to its preferential dissolution and diffusion of solutes [111]. The polyurethanes were based on block co-polymers having hydrophobic and hydrophilic domains (containing carboxylate groups and polyether segments) that limit solute transport. Another membrane that has hydrophobic and hydrophilic components is Nafion (a perfluorosulfonic acid polymer), whose sulfonic acid residues also repel anionic interferants [124, 125]. Moussy's group extensively tested both polyurethane and Nafion membranes as mass transport limiting membranes

[67, 78, 126-131]. In their studies, Moussy *et al.* reinforced polyurethane with epoxy resin for better mechanical and long term durability. These membranes also have good mechanical properties, provide sufficient glucose limiting barrier and limit the amount of interferants passing through. Unfortunately, the properties of PU (and Nafion) based membranes are highly depended on the polymerisation conditions (e.g. temperature and humidity) [74, 132] which cause high within the production batch variability in sensor performance.

Well organised, uniform and thin membrane made with high precision LBL assembly is another choice for mass transport limiting. Galeska *et al.* and more recently, Tipnis *et al.* used this technique to construct layers with humic acids/ferric cations (HAs/Fe^{3+}), humic acids/poly diallyldimethylammonium chloride (HAs/PDDA), and poly styrene sulfonate / poly diallyldimethylammonium chloride (PSS/PDDA) and optimised the diffusion of glucose and hydrogen peroxide through the membranes [133, 134]. Stein *et al.* assembled nanometre size (12nm) layers of poly allylamine hydrochloride (PAH) and poly sodium 4-styrenesulfonate (PSS) on glucose sensitive microspheres and by varying the assembly conditions and the number of layers adjusted the sensitivity to cover the hypo -, normo- and hyperglycemic levels [135, 136]. However, the physical or ionic affinity binding in LBL assemblies can be susceptible to local variations in pH and ionic strength, often compromising the long term stability of the membranes, especially when implanted.

Composites have also been used to obtain better controlled porosities, than solvent cast polymers [123]. Uehara *et al.* proposed the use of nanofiltration composite membranes (with well controlled pore size in a range between 5 and 30nm) made of polystyrene (PS) from PS-block-poly(methyl methacrylate) (PMMA) with homo-polymer PMMA to optimise the glucose diffusion and, at the same time, prevent large molecules (e.g. bovine serum albumin) to pass through [137]. To allow

flexibility and, at the same time, limit the diffusion of glucose and hydrogen peroxide Chu *et al* used porous polytetrafluoroethylene (PTFE) membrane with phospholipid polymer (2-methacryloyloxyethyl phosphorylcholine (MPC) copolymerized with 2-ethylhexylmethacrylate (EHMA) called PMEH which has a similar molecular configuration as a cell membrane [138]. Further, a novel, multifunctional membrane composed of MPC and n-butylmethacrylate (BMA) was proposed to sustain sensor performance [132].

Modern fabrication methods such as lithography and ion-track etching for polymers; micromachining, anodization, powder sintering and sol-gel approaches for ceramics and semiconductor materials have been utilized to generate membranes with well controlled pore sizes ranging between 1 and 50 nm [123]. Such membranes, due to their molecular sieving abilities, function as excellent mass-transport limiting. But, in practice, they are primarily used as enzyme or affinity molecule entrapping membranes than as mass-transport limiting membranes for glucose sensing [139-150].

Another important function for permselective membranes is to exclude interferants based on their size, charge or polarity. Size exclusion is primarily dependent on the pore size and distribution within the membrane. Uniform pore size is commonly achieved through electropolymerization using materials such as poly(phenylenediamine), polyphenol, poly(aminophenol) and poly(1,2-diaminobenzene) [145, 151-157]. The advantage of the electro-polymerization method is that miniature sensors can be coated with uniform, thin and compact films [158]. Furthermore, plasma polymerization method is also used to deposit size exclusion membranes based on cellulose acetate and mercaptosilane on sensors [159-161]. Electrostatic repulsion using membranes containing charged functional groups, especially a negatively charged perfluorinated ionomer Nafion, is also

widely studied for elimination of interferants [127]. In addition, hydrophobic membranes made of alkanethiol or lipid layers are used to exclude hydrophilic interferants [162]. Often, different membranes are used in combinations to eliminate multiple interferants in complex biological fluids. For instance, Moussy *et al.* sandwiched GOx immobilization layer between an electro-deposited poly(phenylenediamine) inner layer and a Nafion outer layer [127]. Combinations of Nafion and cellulose acetate have been used to eliminate the interference of the neutral acetaminophen and negatively charged ascorbic and uric acids, respectively [163, 164]. Rodriguez *et al.* prepared a LBL assembly of polyethylenimine, Nafion, polyetylenimine, and DNA followed by alternate deposition of polyethylenimine and GOx, on thiolated gold surface, considerably improving the selectivity and sensitivity of the glucose biosensor [165].

1.7 Research motivation

A continuous glucose monitoring platform together with closed loop insulin delivery could significantly reduce the risk of complications in diabetes, as it would reduce the need for patient compliance. In this work we attempt to develop and improve a platform which could be used for this purpose. In particular, we have concentrated on two types of sensors for glucose monitoring: microspike based (minimally invasive) and subcutaneously implantable (invasive) enzyme based biosensors, both having some advantages and disadvantages over the other.

Minimally invasive glucose biosensors have a great potential to be combined with CGMS and improve the treatment for diabetes [16]. Currently, many scientists have concentrated on the development of hollow, micron size structures, which are referred to as microneedles [166, 167].

The use of such structures for delivery of drug molecules and vaccines [168] has become popular among scientific community over the last decade because it is minimally invasive and painless [169-176]. Polymer and silicon based microneedles have been used for transdermal drug delivery of small biomolecules such as insulin [177]. The approaches of using these structures as biosensors are based on sampling the ISF followed by offline analysis. However, in this specific application it was more beneficial to use microspikes ('blind' microneedles) as they exhibit extensive robustness and eliminate the problem of clogging associated with hollow microneedles. Moreover, compared to other planar electrochemical sensors, the 3D structure of the microspikes provides larger surface area (greater compactness of an enzyme) which results in an increased current, hence greater signal to noise ratio. It also allows higher enzyme loading which in turn leads to longer term performance. To our knowledge, no one reported a successful fabrication of such structures for sensing applications. Taking the above into account, the aim of this work was to develop a method of fabricating and functionalising such structures to act as glucose biosensors and characterise their performance.

In contrast, we also have concentrated on improving the current development of coil – type implanted glucose biosensors. The advantage of such sensors is that they can provide reliable glucose measurements for a relatively long period of time *in vitro* [78] and *in vivo* [68]. The main trends in developing these type of sensor are concentrated in improving the sensor biocompatibility using various techniques (e.g. hydrogel [69], collagen [71] or PLA [73] as a protective coating, the suppression of immune responses using corticosteroids [70] or the promotion of neovascularisation using growth factors [72]). However studying the biocompatibility of these sensors still remains challenging due to the lack of sensor reproducibility. This was often correlated with the fact that

coil – type sensors are partially handmade, which leaves a lot of room for variation [131]. It was also reported that the performance of the sensors (e.g. sensitivity or time response) is mainly dictated by the permselective membrane coated on the sensor surface [131]. Both conclusions were based on the current response of sensors coated with Nafion or Polyurethane (PU) based membranes [78, 128]. These polymers seems to be good materials for permselective membranes as they block interfering agents from reacting with the enzyme and significantly reduce glucose diffusion rates thus extending the sensors' linear range. A major disadvantage with permselective membranes for biosensors based on Nafion and PU is that small variations in curing time, humidity, or temperature during their polymerisation can cause significant variation in porosity, leading to high variability in sensor performance [178].

The advantage of being able to fabricate reproducible sensors is that the host influence on implantable biosensors can be assessed when studying their *in vivo* response compared with that *in vitro*. Also, because the poor reproducibility of such sensors there is a need for frequent recalibration before and while implanted in the host tissue [179]. As previous reports suggest [180] this could be overcome by implanting two sensors fabricated the same way, one with and one without the enzyme. As both sensors will experience very similar environmental effects after implantation the response for the sensor without the enzyme can be correlated to background current and extracted from glucose measurements. Such set up allows measuring current caused by known (e.g. l-ascorbic acid, acetaminophen or uric acid) [131] as well as any unknown interfering agents.

In this work, we have concentrated on developing a novel hydrogel coating for such amperometric glucose sensors which acts as a permselective membrane making the sensors more reproducible.

Hydrogels used in our study were developed for contact lenses and are widely acknowledged as a biocompatible [69]. In this case, however, the hydrogel is used as a permselective membrane. The advantage of hydrogel over Nafion or PU based membranes is that its properties are much less dependent on environmental changes (e.g. temperature, humidity or curing time) during the polymerisation, meaning that the final alignment and compactness of the polymer chains (which in turn dictates the material properties) are mainly determined by the chemical composition and not by conditions at which the polymerisation has occurred. Thus, the aim was to develop hydrogels having a high degree of crosslinking and uniform porosity, which can function as permselective membranes for biosensors, improving their performance and reproducibility.

Chapter 2

Materials and Methods

2.1 Introduction

The aim of this chapter is to describe various techniques used to fabricate and characterise the sensors.

2.2 Chemicals

Thiomalic acid (TMA), ethyl-dimethyl-aminopropylcarbodiimide (EDC), N-hydroxy-succinimide (NHS), poly-l-lysine, Nafion 117, tetrathiafulvalene (TTF), bovine serum albumin (BSA), glutaraldehyde (GA), glucose oxidase (GOx, from *Aspergillus niger*, lyophilized, powder, ~200 units/mg), ATACS5104 epoxy adhesive, polyurethane (PU), polyethylene glycol dodecyl ether (Brij 30), tetrahydrofuran (THF), ammonium peroxodisulfate (APS), sodium metabisulfite (SMS), 2-hydroxyethyl methacrylate (HEMA), 1-vinyl-2-pyrrolidone (NVP), ethylene glycol dimethacrylate (EGDMA), Benacure 1173,

polyethylenimine (M_w 25,000) branched (PEI), phosphate buffer saline (PBS) tablets and eosin were obtained from Sigma-Aldrich, UK.

HEMA, NVP and EGDMA were purified by vacuum distillation before use.

Polydimethylsiloxane (Sylguard 184 monomer, PDMS) was obtained from VWR Internatinal Limited, and the SU-8 photoresist from Chestech Ltd, UK.

Image reverse photoresist (AZ5214E) was purchased from Clariant, GmbH, Germany.

2 mm thick polyvinyl acetate (PVA) sheets were purchased from Ceiba Technologies (Chandler, AZ, USA).

Full bright cyanide free gold plating solution (Gold ECF 60) was purchased from Metalor Technologies (Birmingham, UK)

2,3-dihydroxypropyl methacrylate (DHPMA) was purchased from Polysciences Inc. (Warrington, PA, USA).

Teflon coated Platinum–Iridium (Pt-Ir, 9:1 weight ratio, Ø0.125mm) and Silver (Ag, Ø0.125mm) wires were obtained from Medwire (Mt. Vermon, NY, USA).

Deionised (DI) water purified with a Millipore system was used throughout these experiments.

2.3 Fabrication of microprobe arrays

The fabrication of microspikes was done in collaboration with Dr Kostis Michelakis and Dr Sanjiv Sharma.

The microspikes were fabricated using method reported by Kim et al. [181]. Negative photoresist polymer (SU-8) was used for the microfabrication. Microprobe arrays were fabricated to have over 1000 needles varying from 56µm to 700µm in length and from 15 to 30µm diameter at the tip. An SU-8 mesa was formed on a Pyrex glass substrate and a second SU-8 layer was then deposited on to the first SU-8. When exposed to UV, SU-8's long molecular chains cross-link, causing the solidification of the material. An array of SU-8 tapered pillar structures, with angles in the range of 3.1˚–5˚, was formed on top of the SU-8 mesa structure. This was followed by a conformal electrodeposition step involving sputtering of gold. In order to lower the resistance of obtained material, an additional, uniform layer of gold was deposited electrochemically on the microprobe array.

2.4 Electroplating gold on microspikes

The electroplating was done on two different microspike based platforms. First was used to test the microspikes performance as glucose biosensors and the other on microspikes incorporated in the microfluidics platform. In both cases, electroplating was performed using CHI 1000A Multi Potentiostat (CH Instruments, Llanelli, UK).

2.4.1 Microspikes

Prior to the electroplating, a single microspike array was gently separated from the glass substrate. Acetone, which dissolves the positive photoresist, was used to expose gold coated surface (see Figure 9) to which a metal wire was attached using a silver epoxy resin. After 1h drying time the connection between microspikes' exposed gold surface and the wire was insulated using 2 part epoxy resin.

The microspikes were immersed in 0.5M H_2SO_4 and electrochemically cleaned by shifting the potential from -0.4 to 1.6V (2 cycyles) vs. Ag/AgCl acting as reference and counter electrode (scan rate 0.05V s^{-1}, E step 10mV). Electrochemical deposition of gold was performed using a conventional three-electrode configuration, namely Au microspikes as working electrode, platinum gauze counter electrode and an Ag/AgCl reference electrode. For electroplating commercial full bright cyanide free gold plating solution (Gold ECF 60) containing 10 g/L gold (pH= 9) was used. The Au layer was deposited under potentiostatic conditions. Electrodeposition was carried out using 8 cycles of a three potential sequence consisting of first 300mV for 20s, second -600mV for 0.1s, then -500mV for 800s.

To determine whether the electrodeposition procedure was successful, thereby ensuring good electrical contact between the golden deposit and the underlying golden microspikes the films were tested using a potassium ferricyanide redox couple.

2.4.2 Microspikes for microfluidics platform

Prior to the electroplating, a single microspike array was glued onto a glass slide with silver electrodes. A fraction of the front side (see Figure 9) was gently cleaned with acetone, to dissolve the photoresist covering the bulk of the chip excluding the microspike tips, and connected to the silver electrode contact pads using silver epoxy resin. A separate silver pattern was modified with 0.1M $FeCl_3$ as described in [182] and served as both reference and counter electrode. When tested in bulk solution an external Ag/AgCl reference electrode was used.

The microspikes were cleaned with 0.5M H_2SO_4 by shifting the potential from -0.4 to 1.6V vs. external Ag/AgCl reference and counter electrode. The electrochemical deposition of gold was done using full bright cyanide free gold plating solution (Gold ECF 60, 10g/l of Au, pH=9) in order to lower the resistance of the electrode. A standard three electrode cell comprising of working, reference and counter electrodes consisting of microspikes, Ag/AgCl and platinum gauze, respectively was used. Only the gold coated part of the microspikes (i.e. without the silver patterns) was exposed to the electroplating solution. Gold metallization was conducted using eight cycles of three potential sequences (300mV for 20s, -600mV for 0.1s and -500mV for 800s). Such prepared samples were tested using cyclic voltammetry (0-400mV at 50mV/s scan rate) in 0.1M PBS solution containing 1mM potassium ferricyanide to confirm the proper gold attachment to the underlying microspikes.

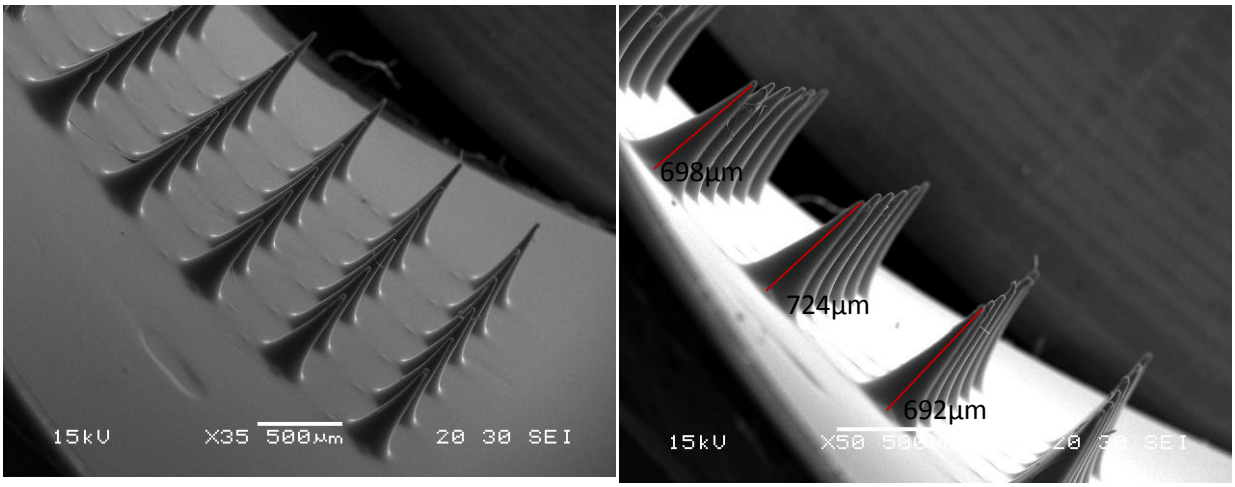

Figure 9: Scanning Electron Microscope images of microspikes array before functionalising it to act as biosensor and the estimates of microspikes heights.

2.4.3 Thickness calculations

We have used the following formula to calculate the thickness T[cm] of deposited gold

$$T = \frac{Mw}{nFAD} \int I\, dt \tag{2.1}$$

where Mw is the molecular weight of the deposited metal [g mol^{-1}] , n is the number of electrons taking part in the reaction, F is the Faraday constant [s A mol^{-1}], A is the surface area of microspikes [cm^2] and D is the density of gold [g cm^3]. $\int I\, dt$ was calculated from the i-t curves. The surface area was calculated based on the SEM measurements.

2.5 Microspikes functionalization

After an additional cleaning with 0.5M H_2SO_4 microspikes were functionalised with 0.4M thiomalic acid (TMA) for 1h at room temperature. Subsequently, to activate TMA's carboxyl groups, the microspikes were incubating at room temperature for 2h in 2mM ethyl-dimethyl-aminopropylcarbodiimide (EDC) and 5mM and N-hydroxy-succinimide (NHS). The microspikes were than immersed in 0.1M PBS, 0.001% poly-l-lysine and 10mg/l of glucose oxide enzyme overnight at 4˚C. This was followed by coating the microspikes with either Nafion or epoxy – PU permselective membrane. The schematic representation of a final sensor design is presented in Figure 10.

Coating with epoxy - polyurethane (PU) based membrane

An epoxy-PU membrane was prepared by dissolving 0.5 M TTF, 17.8 mg each of Part A and Part B of ATACS5104 epoxy adhesive and 26.7 mg of PU in 4 ml of THF and 1 ml of Brij 30. 1µl of such membrane was deposited onto the microspikes and left for drying in room temperature for 20min.

Coating with Nafion based membrane

The dried microspikes surface was coated with a 1µl aliquot solution composed of 0.5M TTF in 1% Nafion 117 perfluorinated ion-exchange membrane. Prior to use, the microspikes were left for 1h to dry.

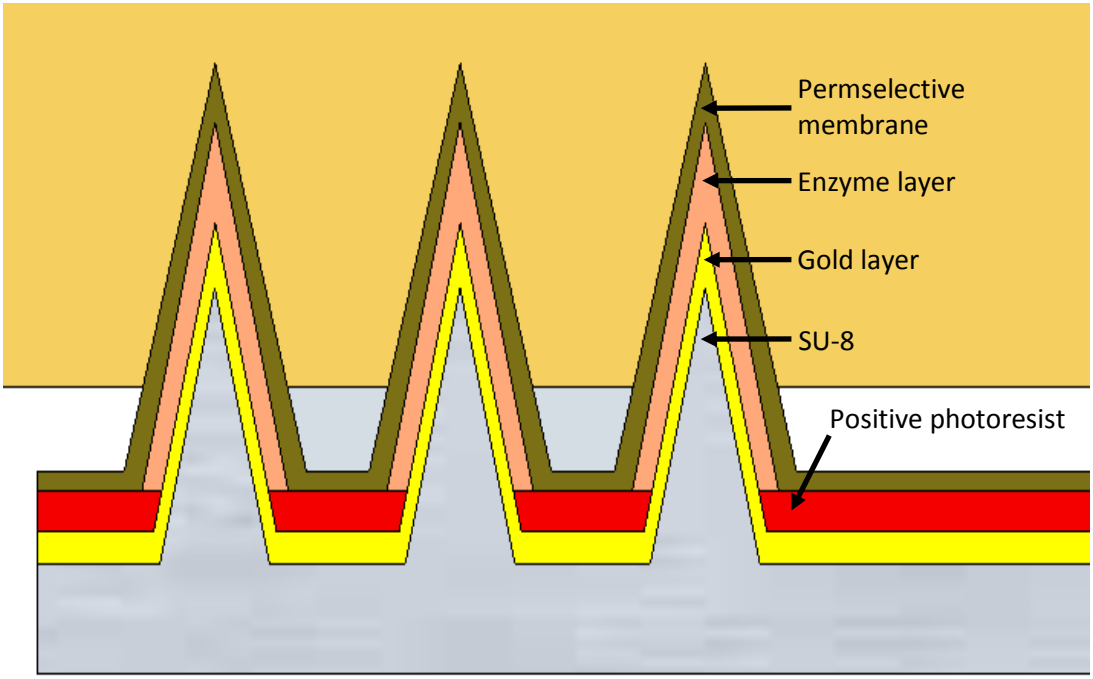

Figure 10: Schematic representation of microspikes based glucose biosensor.

2.6 Incorporation of microspikes into a microfluidics platform

As shown in Figure 11, the microfluidic platform comprises of a Polydimethylsiloxane (PDMS) microfluidic chip, and a microspike array layer. Sylguard 184 monomer and the curing agent (ratio 10:1) were poured into a pre-fabricated SU-8 mould and left to cure overnight. The PDMS was cut and peeled off the mould. This chip design had 2 inlets with meanders leading to hexagonal chamber which finally terminates into a single outlet. The microchannels were 1.0 mm wide and 1.0 mm deep. The microfluidic chip was bonded with a glass slide consisting of the microspike array by exposing it to Oxygen Plasma (Diener Technologies, Warrington, UK) for 120s at 60 % flow rate.

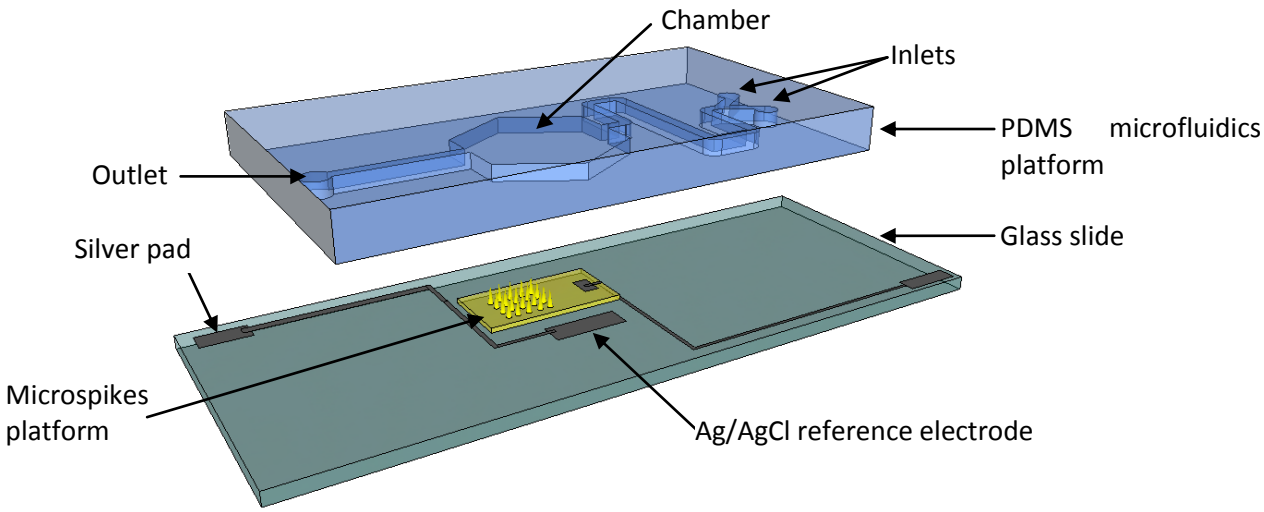

Figure 11: A schematic representation of microfluidics based system to study mass transport phenomena in microspike based biosensors.

2.7 Electrochemical measurements of microspikes

The electrochemical response of microspikes was characterised using various techniques described below on either of the two instruments:

- Single channel Ivium CompactStat (Ivium Technologies, Eindhoven, The Netherlands)
- Eight channel CHI 1000A Multi Potentiostat (CH Instruments, Llanelli, UK)

All measurements were done in a custom made Faraday cage to reduce the interferences from the surrounding electromagnetic fields.

2.7.1 Titration

Cyclic voltammetry revealed that the optimal potential for TTF mediator oxidation is 150mV and this was used throughout this study. Microspikes were used as a working electrode and an Ag/AgCl as a reference and counter electrode. The sensors were calibrated in 0.1M PBS under constant stirring by stepwise glucose concentration increase from 0 – 25mM.

2.7.2 Calculations of apparent Michaelis – Menten constant

The response of amperometric biosensor can be limited by either enzyme kinetics or mass transport effects [183]. Although these phenomena have been investigated for simple planar sensor designs [184] there is not enough evidence for more complex electrode geometries such as out-of-plane three dimensional electrodes. Thus, to characterise enzyme kinetics of biosensors, Michaelis – Menten constant $\mathrm{K_M}$, which correlates the affinity of the enzyme and the substrate, was determined. In case of microspike based glucose sensor containing a permselective membrane, the reaction is mass transport controlled and the calculated constant has no longer the true significance with respect to Michaelis – Menten kinetics. However, it is still valid for comparison of similar sensors [184]. Thus, the apparent Michaelis – Menten constant ($\mathrm{K_M^{app}}$) was calculated using Lineweaver – Burk type approximation [184]:

$$\frac{1}{i} = \left(\frac{\mathrm{K_M^{app}}}{i_{max}}\right)\left(\frac{1}{C}\right) + \frac{1}{i_{max}} \tag{2.2}$$

where C is a substrate concentration, i is steady state current, i_{max} is maximum steady state current, and $\mathrm{K_M^{app}}$ is an apparent Michaelis – Menten constant [185]. In order to calculate the $\mathrm{K_M^{app}}$, a plot of 1/i vs 1/c was constructed and apparent Michaelis – Menten constant was calculated from the slop of the linear fit. Such plot is presented in section 3.1.4.

2.7.3 Electrochemical response of microspikes incorporated into a microfluidics platform

The sensors were tested using Ivium CompactStat potentiostat with microspikes as working electrode and modified Ag/AgCl pattern as reference and counter electrode. The current was measured after applying 150mV which proved to be sufficient for TTF oxidation.

The injection of solutions was done using two syringe pumps connected to the two inlets of microfluidics platform. To determine the response to the change of glucose concentration, the sensor was first stabilised with PBS flowing at a constant rate until a stable current was observed. The PBS flow was stopped and a 5mM glucose solution was introduced through the second inlet keeping the same flow rate. The experiment was continued until the steady state current was reached. To evaluate the sensor performance 50, 100 and 200µl/min flow rates were used. The background current was subtracted from all measurements. The device lifetime was determined by repeating experiments with the same sensor over seven days.

2.8 Hydrogel preparation

To develop a membrane for coil-type amperometric biosensors hydrogels were prepared by mixing predefined amounts of NVP, HEMA, DHPMA and EGDMA monomers in a glass vial and diluted 1:1 with DI water. Free radical addition polymerisation of the monomer mixtures was carried out using chemical- or photo- initiation.

Free radical polymerization using chemical initiators

This method involved adding 1.5 mol% (of the total monomer content) of APS and SMS initiators, which decompose at room temperature in aqueous solutions producing free radicals necessary to catalyse the polymerisation reaction [186]. Prior to that, the monomer mixture was purged with nitrogen for 5min to remove the dissolved oxygen and ensure that the reaction takes place in oxygen-free atmosphere. Polymerization was stopped usually after 10-15min by immersing the hydrogels in DI water. The samples were than washed 5 times with DI water to remove any unreacted monomers. When not in use, the hydrogels were stored in DI water or PBS at 4^{o}C.

Photopolymerization

For the photopolymerization, 1.5 mole % (of the total monomer content) of Benacure 1173 photoinitiator was added to the monomer mixtures and purged with nitrogen gas for about 5 minutes to remove dissolved oxygen in the monomer solution. The reaction mixture was poured into petri dishes and exposed to 245nm UV radiation for the photo-polymerisation. The petri dishes were placed at about 1 to 2 cm distance from the 245 nm UV light bulb (30W, 254nm & 365nm UV lamps,

ALLEN 425, LCF-750-Q, P. W. Allen & Co., London) in a closed chamber. The chamber was purged continuously with nitrogen gas during the reaction to provide inert atmosphere. The reaction time was constant for all hydrogels and was 100 min after which the UV light was turned off. The reaction was stopped by adding DI water to the petri dishes with the hydrogels. The gels were stored at 4^{o}C overnight. The hydrogel films were then carefully dislodged from the petri dishes and washed 5 times in DI water to remove any unreacted monomers in the hydrogels. Thereafter the hydrogels were stored in DI water at 4^{o}C until future use.

2.9 Hydrogel characterisation

Hydrogels were characterised in terms of their micro-structure and chemical composition using the techniques described below.

2.9.1 Fourier Transform Infrared Spectrometry (FTIR)

The chemical composition of hydrogels was characterised using FTIR.

Prior to characterisation the samples were freeze dried (Heto Power-Dry, LL3000 freeze dryer, Thermo Electron Corporation, equipped with Edwards RV12 Vacuum pump) overnight at -76^{o}C (collector temperature). The freeze dried samples were stored in vacuum desiccator. IR spectra were recorded at room temperature in the mid-infrared range (4000–650 cm^{-1}) using Attenuated Total Reflectance Fourier Transform Infrared (ATR-FTIR) spectrometer (FTIR-8300, Shimadzu Europe Ltd.,

Duisburg, Germany). Typically, 10 scans were signal-averaged for a single spectrum at a resolution of ±8 cm^{-1} using a ZnSe crystal at an incident angle of 45°.

2.9.2 Temperature measurements

The temperature measurements were conducted using Apollo 4000 Amperometric Analyzer (World Precision Instruments Inc., Sarasota FL) equipped with high quality miniature platinum RTD (Resistance Temperature Detector) electrode (2.0mm tip diameter). Continuous temperature monitoring was used to determine the gel temperatures for the free radical polymerization using water soluble initiators APS and SMS.

2.9.3 Scanning Electron Microscopy (SEM)

Depending on whether dry or hydrated, the morphology, especially porosity of hydrogels differs significantly. In dry state the hydrogels usually appear non-porous. In order to see the porosity, the hydrogels were first hydrated in PBS and then freeze dried (Heto Power-Dry, LL3000 freeze dryer, Thermo Electron Corporation, equipped with Edwards RV12 Vacuum pump) overnight. The freeze dried samples were then coated with a 20-30 nm conductive layer of gold using the gold sputter (Quorum Emitech K850 Critical Point Drier and a Polaron SC7620 Mini Gold Sputter) under vacuum by applying 25mA current for 2min. The gold coated samples were examined in SEM (Variable Pressure SEM JEOL JSM 5610 LV) under high vacuum mode and an accelerating voltage of 15kV.

2.10 Needle type enzyme based amperometric biosensor fabrication

The sensors were prepared similar to that previously described [69, 131]. The sensor is a two electrode system containing a coil-type Pt-Ir anode as the working electrode and silver/silver chloride (Ag/AgCl) cathode as the reference/counter electrode.

2.10.1 Working electrode

1 cm of Teflon coating was stripped from each end of 7cm long Teflon coated Pt–Ir wire. One end was carefully cleaned with absolute ethanol and sonicated for 5 min in DI water to remove any impurities and plastic residues. The same end was wound around a 30 gauge ½ inch hypodermic needle to obtain a coil end (8 windings) of the sensor. The coil chamber was reinforced with sterile cotton to ensure stability of immobilised enzyme gel and prevention of air bubble formation. The cotton reinforced Pt-Ir coils were then sonicated in DI water for 30min followed by 20 min wash in absolute ethanol to remove any impurities and dried at 60^{o}C for 20 min.

2.10.2 Enzyme loading

About 2.5 µl of enzyme loading solution (12 mg of BSA, 2.5 mg GOx and 5 µl of GA dissolved in 300 µl of DI water) was applied on the cotton reinforced Pt-Ir coil and air dried at room temperature for

about 1 h. This procedure was repeated three times and the resulting enzyme gels on sensor coils were allowed to crosslink overnight at room temperature.

2.10.3 Reference electrode

1 cm of Teflon coating was stripped from each end of a 6 cm long Teflon coated silver wire. One end was carefully wound around a 30 gauge ½ inch hypodermic needle to obtain a coil end (8 windings) of the sensor. The Ag-coil was treated with ammonia solution for 30 sec, rinsed in DI water for 30 sec followed by 6M nitric acid treatment for 10 sec. The coil was then washed in DI water and electroplated in 0.01M HCl at a constant current of 0.1mA using a galvanostat (263A, Princeton Applied Research, TN, US) overnight. The resulting Ag/AgCl reference electrode coils were rinsed with DI water. The sensors were assembled by passing the free-end of the Pt-Ir working electrode wire through the Ag/AgCl reference electrode coil. The Teflon coated Ag and Pt-Ir wires were wound up such that the Ag/AgCl coil is separated from the enzyme loaded Pt-Ir coil by a distance of about 5 mm.

2.10.4 Permselective membrane coating

The Ag/AgCl reference and enzyme coated working electrodes of the sensors were coated with either epoxy-polyurethane (PU) or hydrogel permselective membrane. Epoxy-PU coated sensors were used as positive controls as they are well characterized in the literature [67, 131, 187].

Epoxy - polyurethane membrane coating

The epoxy-polyurethane loading solution was prepared by dissolving 26.7 mg of PU in 4 ml of THF and 1 mg Brij 30, 17.8 mg each of Part A and Part B of ATACS5104 epoxy adhesive. The sensors were coated by applying 1-1.5 µl of the loading solution and air dried at room temperature for 30min followed by 20min curing in an oven at 80 ˚C. The sensors were then cooled to room temperature, followed by storage immersed in PBS (pH 7.4) at 4^{o}C until further use.

Hydrogel membrane coating

In order to increase the affinity of the polymer chains of hydrogel for the enzyme surface, the sensor assembly including the enzyme coated Pt-Ir coil and Ag/AgCl reference coil were dipped in a 0.1M PEI (MW= 25kDa, branched polycation) solution under continuous stirring for 30 min followed by 30 min washing in DI water.

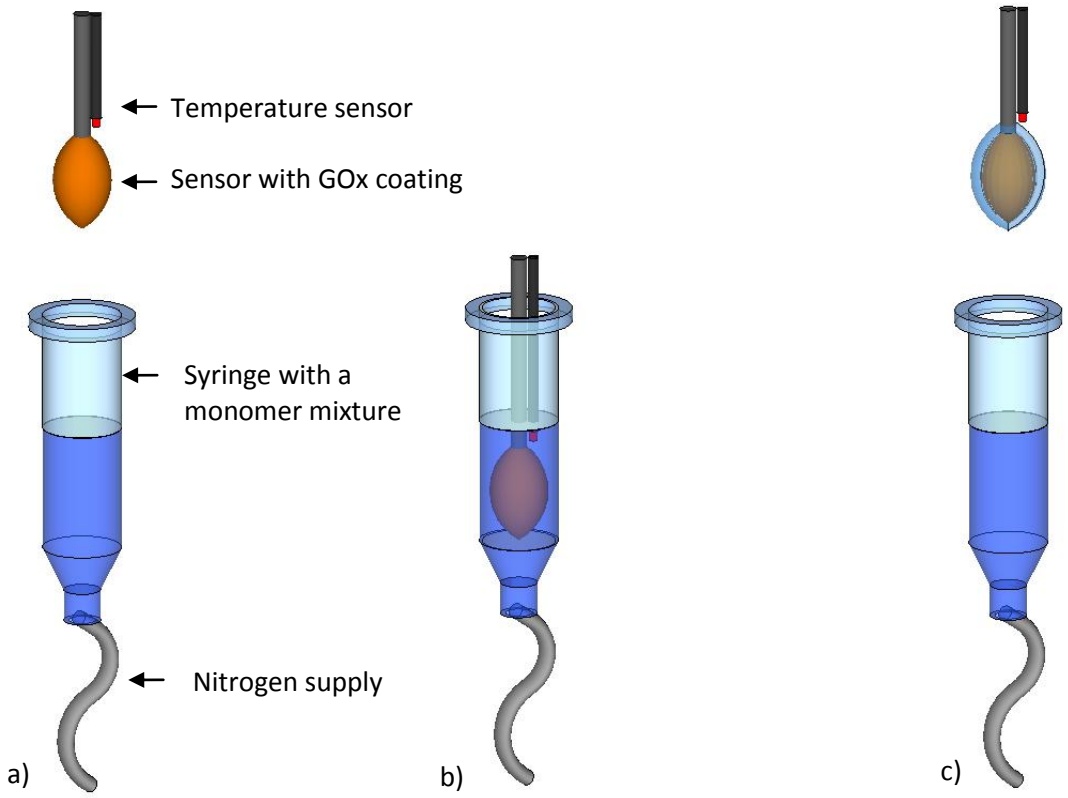

Figure 12: A schematic representation of sensor coating technique. The sensor was lowered perpendicularly into a syringe containing a monomer mixture to which a nitrogen supply was attached (a-b) and removed when the gel point was reached which was indicated by the increase of the temperature (c).

To coat the sensors with hydrogel, a vertically aligned 3ml disposable syringe with plunger removed and nitrogen supply attached to the needle end was used, as shown on the Figure 12. The monomer mixture was poured into the syringe, and held within the syringe by nitrogen gas flow. The solution was deoxygenated for at least 5 min with N_2 gas bubbling. For the free-radical polymerization, 1.5 mol % SMS was added to monomer mixture and allowed to mix uniformly (assisted by N_2 gas bubbling). After about 5 min 1.5 mol % APS was added drop-wise to initiate the polymerization as described in section 2.3 'Free radical polymerization'. The temperature of the reaction was constantly monitored using an Apollo 4000 temperature microsensor (World Precision Instruments,

Inc. Sarasota, FL). Three or four sensors were firstly immersed in the monomer solution and then raised above it before the reaction gel point was reached. A rapid increase in the temperature was used as the indication for removing the sensors from the reaction mixture. The sensors were left in the N_2 atmosphere within the syringe, but above the reaction mixture, for about 20min after the gel point was reached. Care was taken to prevent the sensors touching each other or the syringe walls. Thereafter, the sensors were suspended vertically in air at room temperature for an additional 2h, then transferred to PBS and stored at 4°C until further use. The schematic representation of the sensor final design and its working principle is shown in Figure 13.

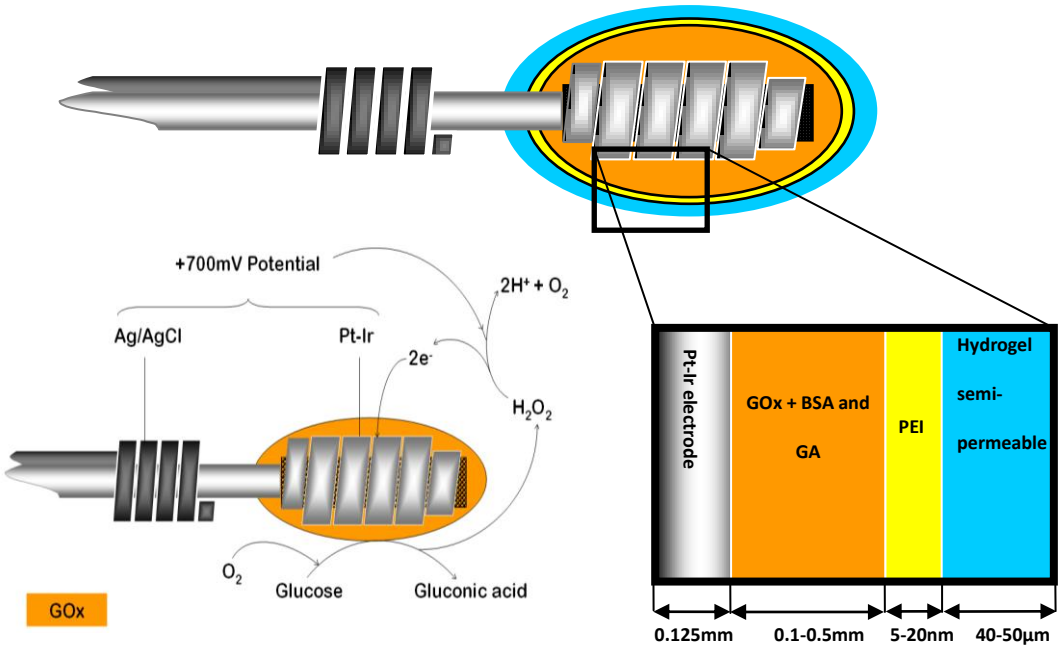

Figure 13: Schematic representation of hydrogel coated sensor with a description of each layer and a diagram presenting enzyme based amperometric sensor working principles.

2.10.5 Characterisation of hydrogel coating on sensors

The integrity and nature of the hydrogel coating on the sensor was tested using hematoxylin-eosin staining. The hydrogel coated sensors were stained in hematoxylin solution for 20 min, washed in running tap water for 10 min, stained in eosin for 20 min, washed in running tap water for 10 min and finally washed in DI water. The stained sensor was examined visually for staining under a Nikon Eclipse optical microscope. The cross-section of the sensor coatings was also observed using an optical microscope. The sensor was glued vertically on a glass slide and the coatings at the tip of the sensor were manually cut using a scalpel blade to expose coating cross-section for microscopic observation.

2.11 Electrochemical measurements

The electrochemical measurements were performed using Apollo 4000 Amperometric Analyzer (World Precision Instruments Inc., Sarasota FL). The sensors were tested in a beaker containing PBS (pH 7.4) solution with vigorous stirring. Before measurements the sensors were polarized at 0.7V vs. Ag/AgCl reference electrode until a stable current was observed. Calibration plots were obtained by measuring the current while increasing the glucose concentration from 0 – 30mM (stepwise). The response time was calculated as 90% of the maximum response time after increasing the glucose concentration from 5 to 15mM. The sensitivity S [A mM^{-1}] of each sensor was calculated from the following formula:

$$S = \frac{I_{15mM} - I_{5mM}}{10} \tag{2.3}$$

where I_{15mM} and I_{5mM} are the equilibrium current for 15 and 5 mM glucose concentration respectively. The background current was subtracted from the data at the end of the experiment.

2.12 Scanning Electrochemical Microscope (SECM) experiments

SECM is a commonly used technique to analyse and map the enzyme activity of surfaces [188-190]. In this study it was demonstrated that SECM is also a feasible method to characterise membrane functional performance and permeability to the substrate. The constant height, generation – collection imaging mode was used. The GOx enzyme catalyses the reaction of glucose resulting in production of a redox – active species (hydrogen peroxide), which than is used for mapping the permeability of the membranes.

2.12.1 Sample preparation

In order to analyze the membrane properties, epoxy – PU and hydrogel coated sensor surrogates were prepared. 1mm thick PVA film was glued to a glass microscope cover slip. Care was taken in order to ensure that the film is laid flat on the glass slide. Next, the samples were coated with glucose oxidase followed by either the epoxy – PU or hydrogel membrane deposition in the same manner as for the sensors (section 2.10.4). Subsequently the samples were scanned using an Optical

Profilometer (Xyris 4000 CL, TaiCaan Technologies, Southampton, UK) in order to assess their flatness. When not in use, the surrogate sensors were stored in PBS at +4 ˚C.

2.12.2 SECM measurements

The measurements were done using a 10µm diameter Ultra microelectrode (UME, Uniscan Instruments Ltd, Buxton, UK) with *R/G* ratio 10 (where *R* is the radius of the glass disk insulator and *G* the electrode radius) and an SECM M370 (Uniscan Instruments Ltd, Buxton, UK). Ag/AgCl and platinum plate were used as reference and counter electrodes respectively. Prior to each experiment the UME was electrochemically cleaned in H_2SO_4 by cycling the potential from +1.1V to -0.24V for 100 cycles at a 50mVs^{-1} scan rate. The samples were tested in 50mM glucose/PBS solution and in all experiments a potential of 0.7V was used as cyclic voltammetry confirmed this is suitable for hydrogen peroxide detection at the UME. The sample was positioned in the middle of the SECM three–electrode cell and an approach curve (also called tip-substrate distance curve) was measured in order to obtain exact information about the distance from the sample. Subsequently the UME was positioned 100µm above the sample surface and an area of 36cm^2 was scanned. The measurements were taken at 100µm intervals in both x and y direction with a 10µm s^{-1} scan velocity and a 1 s sample pre-delay. All results were converted from American to European sign convention.

Chapter 3

The development of microspikes for minimally invasive glucose sensing

3.1 Microspikes for continuous monitoring of glucose

Microspikes are a micro size structures which, unlike microneedles, are not hollow and are made of a smart material that acts as sensor surface. Such structures have the potential to penetrate the skin layer without causing pain and, with appropriate functionalization, measure the substrate concentration in ISF. The aim of this study was to develop a platform for continuous monitoring of glucose with microspikes acting as a sensing element. In this section, steps taken to functionalize the microspikes to act as glucose biosensors along with the techniques used for characterisation are described.

3.1.1 Introduction

In our research group, a novel platform technology - microspikes based electrode was developed. This section describes the application of the microspikes electrode for glucose biosensing. The microspikes electrodes were functionalised with enzyme and permselective membrane coatings to design the minimally invasive glucose biosensor. The efficacy of two different permselective membranes was tested.

3.1.2 Fabrication and characterisation

The microspikes were fabricated as described in section 2.3. Prior to electroplating, the microspikes surface was cleaned in 0.5M H_2SO_4 with cyclic voltammetry to remove debris and impurities such as organic, non-metallic (non conductive) film or oxide layers, which can lead to poor adhesion of gold, thus adversely affecting electrode performance. An example voltammogram acquired during this procedure is presented in Figure 14.

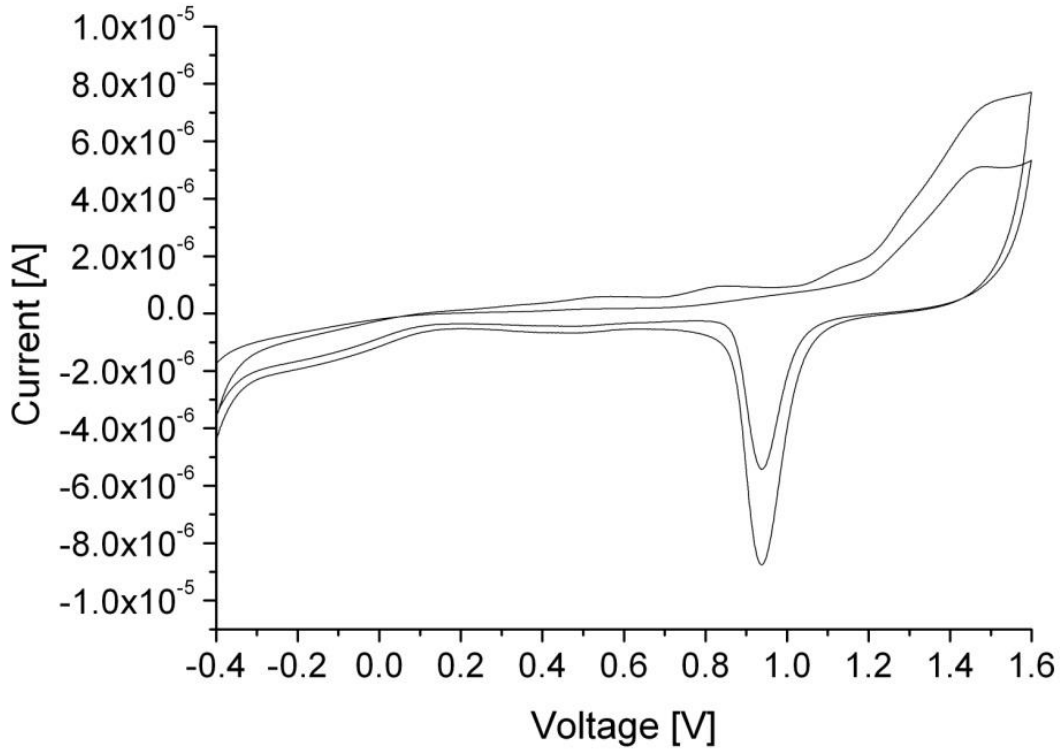

Figure 14: Example cyclic voltammogram for microspikes done prior to gold electroplating. The electrodes were cleaned in 0.5M H_2SO_4 by cycling the potential vs. Ag/AgCl reference electrode from -0.4 to 1.6V twice (scan rate 50m V s^{-1})

We have observed that each microspike array requires maximum two CV cycles for cleaning since overexposure to high currents leads to gold corrosion and removal of the conductive layer from the anode [191]. A reproducible reduction peak at approximately 0.9V indicated that the electrode surface is cleaned and can be used for further study.

To ensure uniform coating and to improve the resistance of sensors' conductive layer, an additional gold cover was electrochemically deposited on the microspikes (section 2.4.1). An example voltammogram from this experiment is presented in Figure 15.

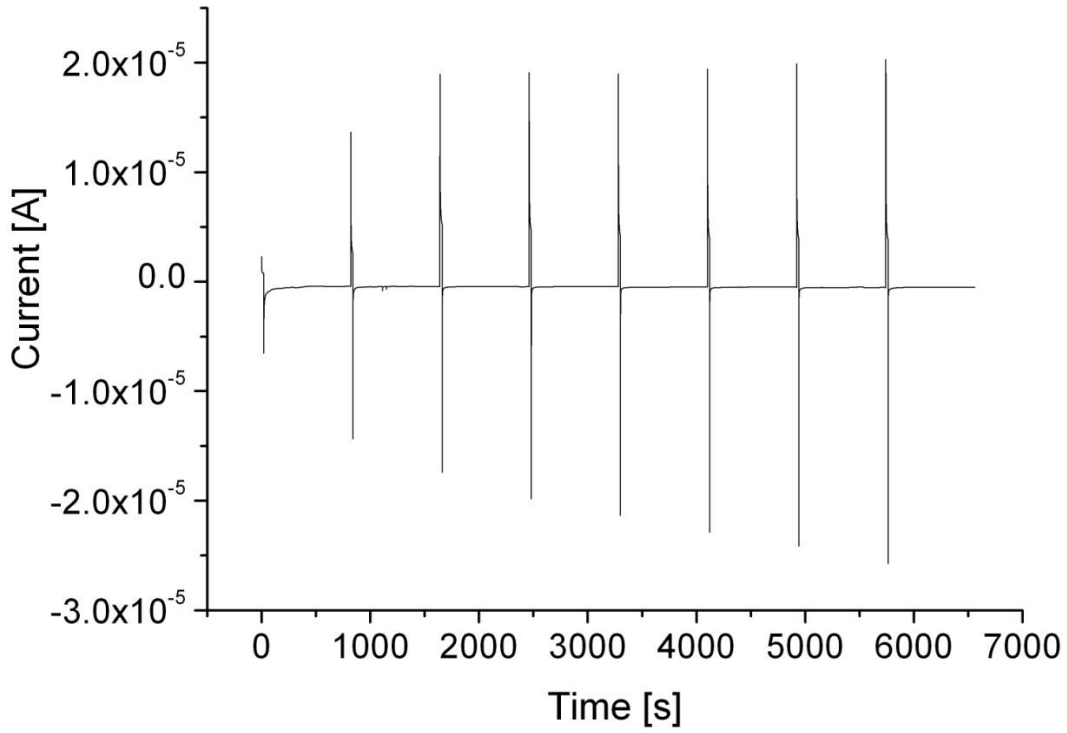

Figure 15: Electrochemical deposition of gold on microspikes. 8 cycles of a three potential sequence consisting of first 300mV for 20s, second -600mV for 0.1s, then -500mV for 800s were applied to microspikes acting as working electrode and Ag/AgCl as reference and counter electrode.

Figure 15 was used to estimate the thickness of gold layer electrodeposited on top of microspikes. The surface area of the microspikes electrode was estimated from SEM images of the same silicon wafer from which the microspikes were acquired, and was equal to $2.927 \cdot 10^{-2}$ cm^2. Gathering this information and substituting in equation 2.1 described in section 2.4.3, an estimated 43nm thick layer of gold was deposited on top of this microspike electrode.

To confirm the successful deposition of gold on the microspikes 'native' layer, the electrodes were tested with the potassium ferricyanide redox couple. A typical CV is presented in Figure 16.

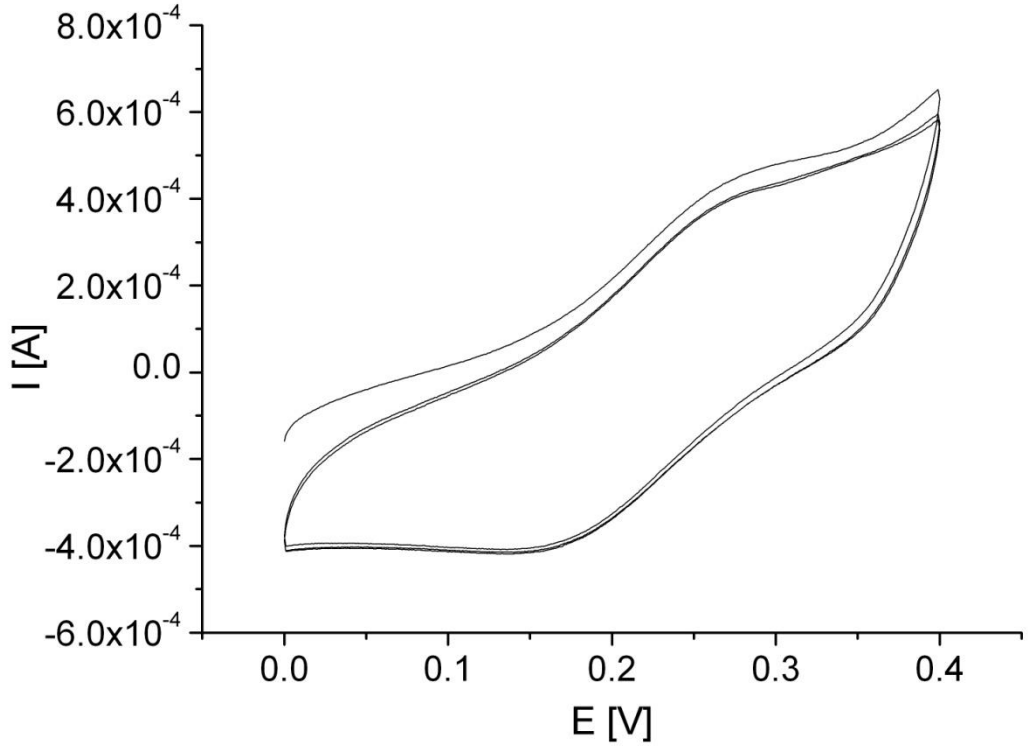

Figure 16: Cyclic voltammogram of microspikes in 1 mM $K_3[Fe(CN)_6]$ in 0.1M PBS solution conducted after gold electroplating. The potential was ramped from 0 to 400mV at a scan rate of 50mV s^{-1}.

After an additional washing in 0.5M H_2SO_4 the gold coated microspikes electrodes were functionalized with enzyme and permselective membranes to fabricate glucose biosensors as described in section 2.5.

3.1.3 Electrochemical sensor response

A second generation biosensor's working principle involves the reduction of a substrate by the enzyme, re-oxidation of the enzyme by the mediator and oxidation of the mediator by the electrode.

This allows the sensors to work at lower operating potentials and independent of the ambient oxygen concentration. In this study, the TTF mediator was incorporated in Nafion permselective membrane deposited on the microspikes electrode. To determine the operating potential for such prepared glucose sensor, cyclic voltammograms of the TTF-modified gold microelectrode were recorded in the range -300 and 500mV versus Ag/AgCl reference electrode. The procedure was carried out in 10mL of 0.1M PBS (pH 7.4). The oxidation peak was obtained at 150mV as shown in Figure 17 and this potential was chosen for further study. At potentials higher than 500mV a strong leakage of TTF from the electrode surface was observed and the sensor was destroyed. It is likely that this effect was induced after irreversible oxidation of TTF^{+} to TTF^{2+} which becomes soluble in aqueous solution and decomposes.

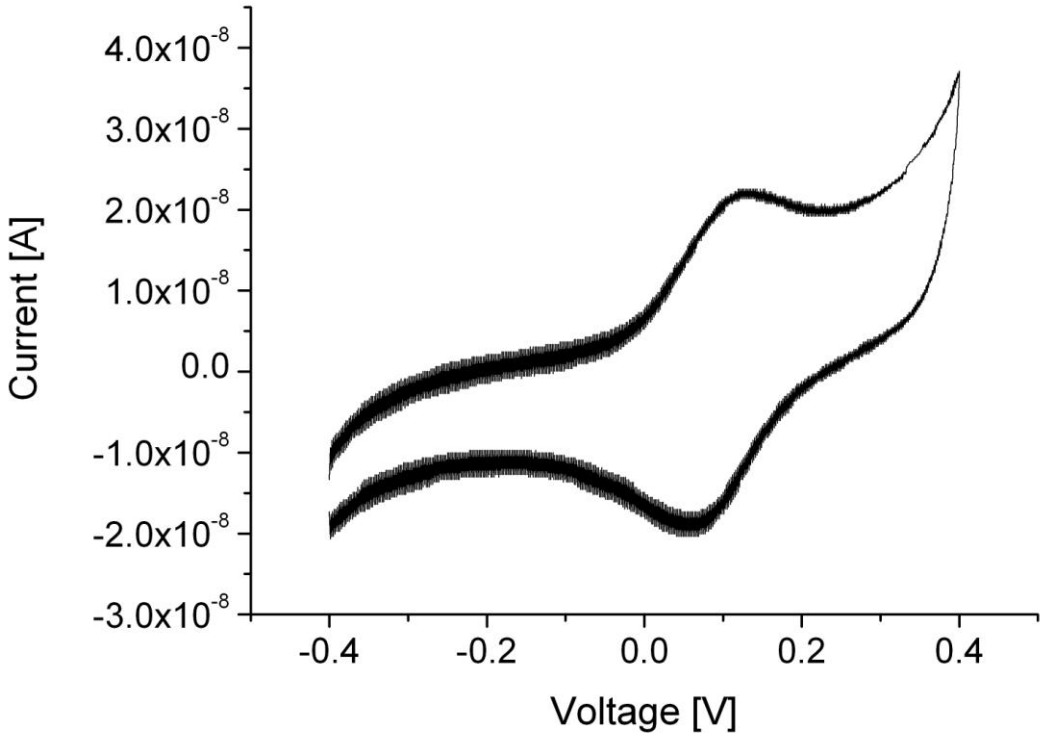

Figure 17 An example of cyclic voltammograms of the TTF-modified gold. The potential was ramped between -300 and 500mV versus Ag/AgCl reference electrode at a 50mV/s scan rate.

The TTF-Nafion coated microspikes sensors were calibrated by a stepwise glucose addition (section 2.7) at 150mV against Ag/AgCl reference and counter electrode (Figure 18).

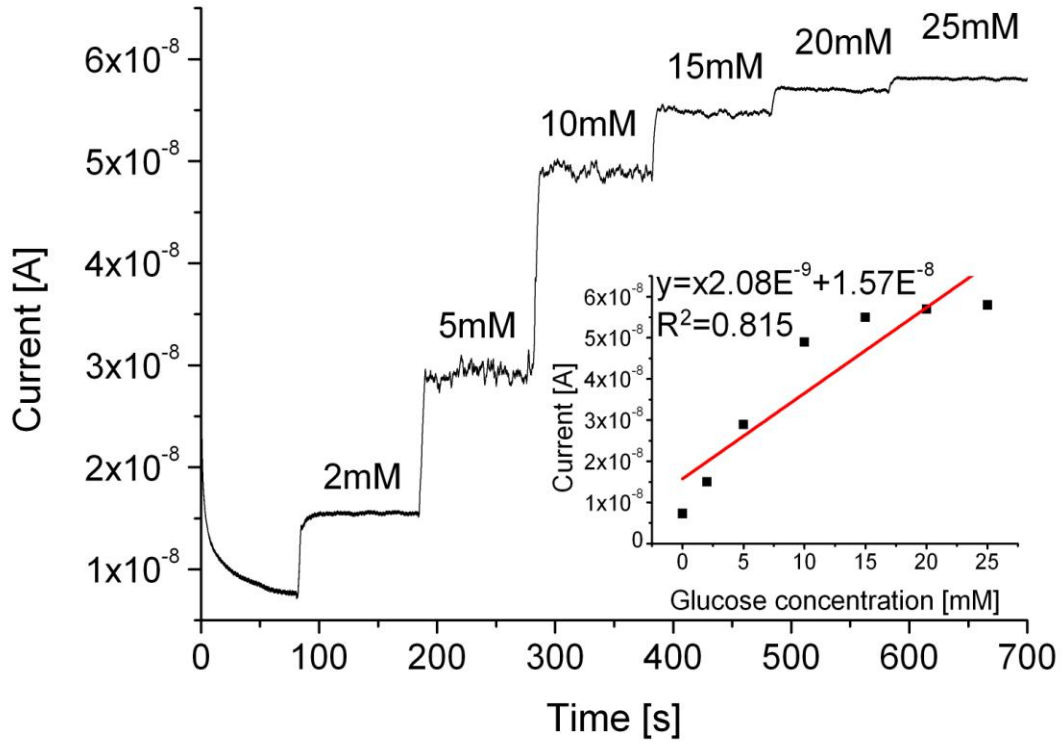

Figure 18: Current response to a stepwise glucose concentration increase for microspike sensors coated with Nafion permselective membrane and the calibration curve in insert. The operating potential was 150mV vs. SCE. More examples of such sensor responses are attached in the Appendix 1.

The TTF-Nafion based sensors showed linear response up to about 10mM glucose concentration after which the enzyme gets saturated and the signal flattens up. The range of 2 to 10mM glucose concentration is insufficient for monitoring the glucose level in ISF. Nevertheless, the time required for the sensor to reach maximum current for a particular glucose concentration is relatively fast (13±4 s), which is highly desirable for monitoring ISF glucose levels.

To improve the sensor functional performance and extend its liner working range, a different permselective membrane was selected. We have decided to apply an epoxy-polyurethane

membrane previously used for implantable glucose biosensors [67]. This membrane proved to be resistant to interfering agents such as dopamine, ascorbic acid, acetaminophen, or uric acid and functions reliably *in vivo* [67]. Thus, the enzyme functionalized microspikes were coated with epoxy-PU membrane (section 2.5). The resulting sensors were calibrated *in vitro* under constant potential of 150mV against Ag/AgCl reference and counter electrode. A typical sensor response curve and its corresponding linear regression curve are illustrated in Figure 19.

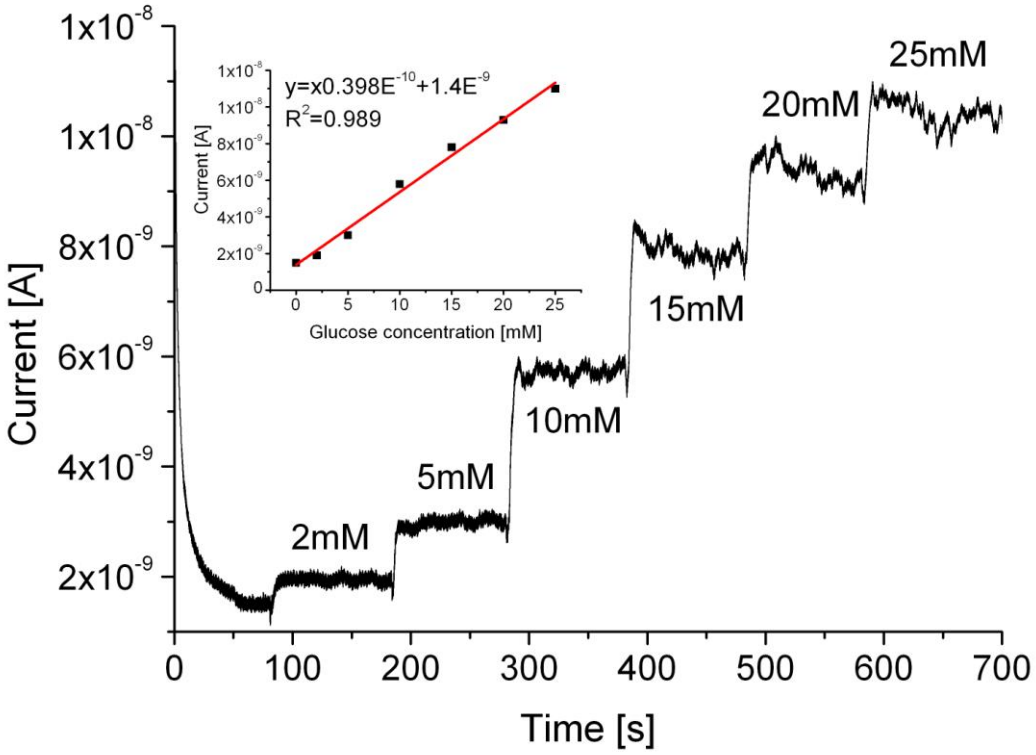

Figure 19: Current response to a stepwise glucose concentration increase for microspike sensors coated with epoxy-PU permselective membrane and the calibration curve in insert. The operating potential was 150mV vs. Ag/AgCl reference and counter electrode. More examples of such sensor responses are attached in the Appendix 1.

The linearity of the microspikes coated with epoxy-PU membrane (R^2=0.989) has been improved with comparison to Nafion coated sensors (R^2=0.972) within clinically relevant glucose concentration ranging of 0-25mM [16]. Moreover, the relatively fast response time for epoxy-PU sensors (15±9 s), which is comparable to Nafion (13±4 s), is favourable for sampling the ISF.

3.1.4 Determination of the apparent Michaelis – Menten constant

The electrochemical response of both types of sensors can be described by the apparent Michaelis-Menten constant, K_M^{app},which expresses a specific characteristic of the electrode – enzyme system. To determine K_M^{app} from the equation 2.2 described in section 2.7 a reciprocals of current vs. concentration were plotted (Figure 20) using Lineweaver–Burk approximation. The apparent Michaelis-Menten constant was calculated from the slope of the linear fit.

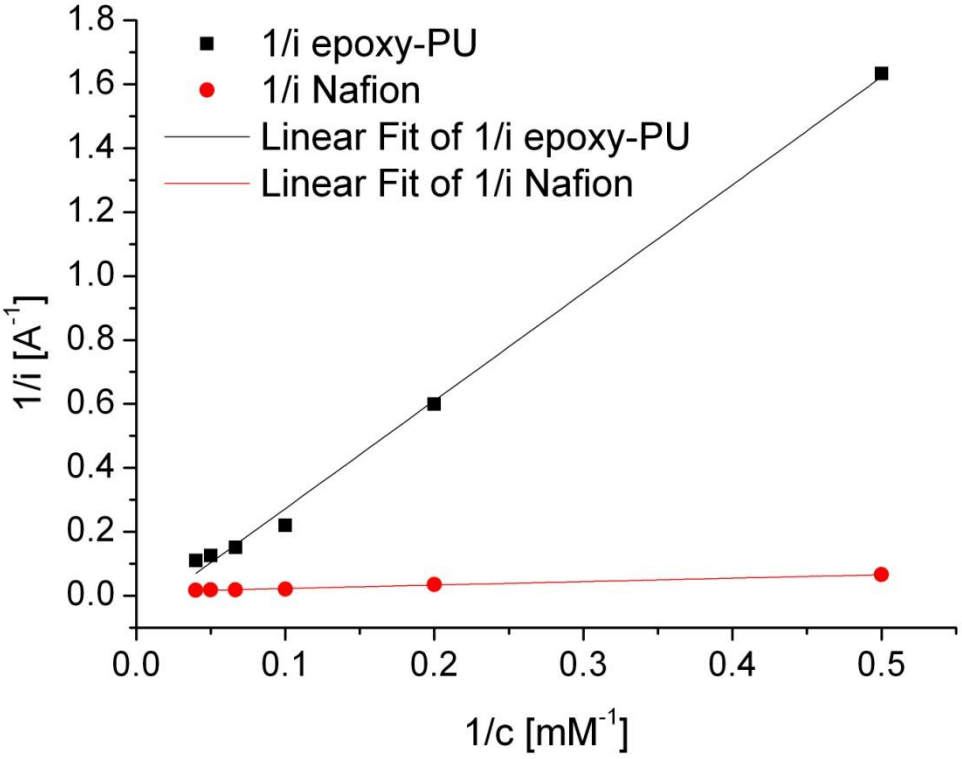

Figure 20: Lineweaver–Burk type plot for the determination of K_M^{app} . The current values for epoxy-PU and Nafion based membranes are taken from the titration curves presented above.

In case of sensors coated with epoxy-PU membrane, the apparent constant K_M^{app}=51.8mM is much higher than those coated with Nafion membrane (K_M^{app} =9.2mM). Since the sensors are composed of a membrane and a mediator (which affect the K_M^{app} values) the results cannot be compared to the literature values for saturated enzymes. However, the high K_M^{app} value for the epoxy-PU sensors confirms that the sensors can work in much higher substrate concentration range than the Nafion coated sensors. In contrast, these results indicate that the Nafion coated sensors are more sensitive at the lower substrate concentrations than the sensors coated with epoxy-PU membrane.

3.1.5 Conclusion

In this section, functionalization of microspikes with glucose oxidase and permselective membrane was described. The microspikes were fabricated as described in [181] and characterised by electrochemical techniques. The functionalization was done using EDC/NHS coupling technique to immobilise the glucose oxidase enzyme on the electrode. Furthermore, two permselective membranes were tested to improve the sensitivity and increase the linear working range of the sensors.

It was concluded that epoxy-PU membrane improves the sensor performance in glucose concentration range varying from 0-25mM when compared to Nafion membranes (0 – 10mM). The linearity and time response were sufficient for monitoring the blood glucose concentration in ISF [192]. The relatively low currents observed in sensors coated with epoxy-PU membrane are also beneficial for minimally invasive monitoring since high current values can lead to adverse tissue reactions. The low currents can be explained by the fact that, due to a three dimensional structure of the microspikes based electrodes, sensors surface area is relatively large in comparison to the plainer electrodes, which improves the mass transport efficacy. This also leads to a better signal: noise ratio and thus improves the accuracy and reproducibility of the sensors.

The drawback from conducting the experiments under constant stirring is that the electromagnetic field generated to rotate the stir bar has a high influence on the measured currents noises which can be easily observed when analysing i.e. Figure 19. On the other hand, stirring was necessary to allow quick mixing after the addition of glucose solution and minimise the risk of measuring the glucose

concentration at the electrode interface. Thus, to better characterise the sensor performance and minimise the influence of these effects, microspikes were incorporated into a microfluidics platform.

3.2 Microfluidic device to investigate factors affecting performance in biosensors designed for transdermal applications

3.2.1 Introduction

As discussed in section 1.5.1 biosensor performance is controlled either by enzyme kinetics or mass transport. Microfluidics platform was used to control convection and to more deeply understand biosensor behaviour. Microfluidics systems have been extended to various fields such as point of care diagnostic devices [193], microreactor systems [194], cell culture assays [195] and combinatorial chemistry & drug discovery systems[196]. Microfluidic based *in vivo* - surrogate assay platform for cell - based studies [197] and microscale cell culture analogue system [198] have been also described before. In this study we attempt using a simple microfluidic system incorporated with a functionalised set of microspike electrodes to mimic the behaviour of sensors monitoring the transdermal substrate concentration. These studies are useful in optimizing the physical and chemical aspects of the biosensor to ensure high performance before *in vivo* studies. A functional performance of microspikes incorporated in microfluidics platform is presented. The hypothesis for this study was that such device will allow controlling the environment at the interface between the sensor membrane and the solution, which can be used for studying the mass transport effect in microspike based biosensors.

3.2.2 Electrochemical response of microspikes incorporated into a microfluidics platform

The microspikes were fabricated as described in section 2.3 and 2.4.2. In order to study the mass transport effect, the microspikes were bound to a glass substrate and wired with the silver patterns. Based on the experiments presented above, it was determined that most suitable membrane for such glucose sensors is epoxy – PU thus, it was chosen for this study (detailed procedure described in section 2.5). Functionalized microspikes attached to a glass slide were incorporated into a microfluidics platform using oxygen plasma bounding, as described in section 2.6 (final design is presented in Figure 11 in the previous chapter).

As shown in Figure 21, in the initial stage the sensor response is dependent on the flow rate. As discussed below this is a consequence of the design of the flow chamber resulting in a period during which the concentration reaches a constant value. Once this chamber concentration has stabilised the plateau current is independent of flow rate. This implies that once the steady state is reached the current is limited either by the enzyme kinetics or membrane diffusion and not by external mass transport. In other words, the unstirred layer at the membrane surface is sufficiently thin at all flow rates studied for diffusion across this layer not to be rate limiting.

The sensor response is much longer when incorporated into a microfluidic platform than in bulk measurements (see Figure 19). The main reason for that is the relatively slow mixing in the microfluidic chamber which has been described earlier [199]. It has been reported that in a hexagonal chamber reaching concentration equilibrium takes several minutes [199]. The sensor

response for two different measurements at 100 µL /min flow rate indicates the reproducibility of the device.

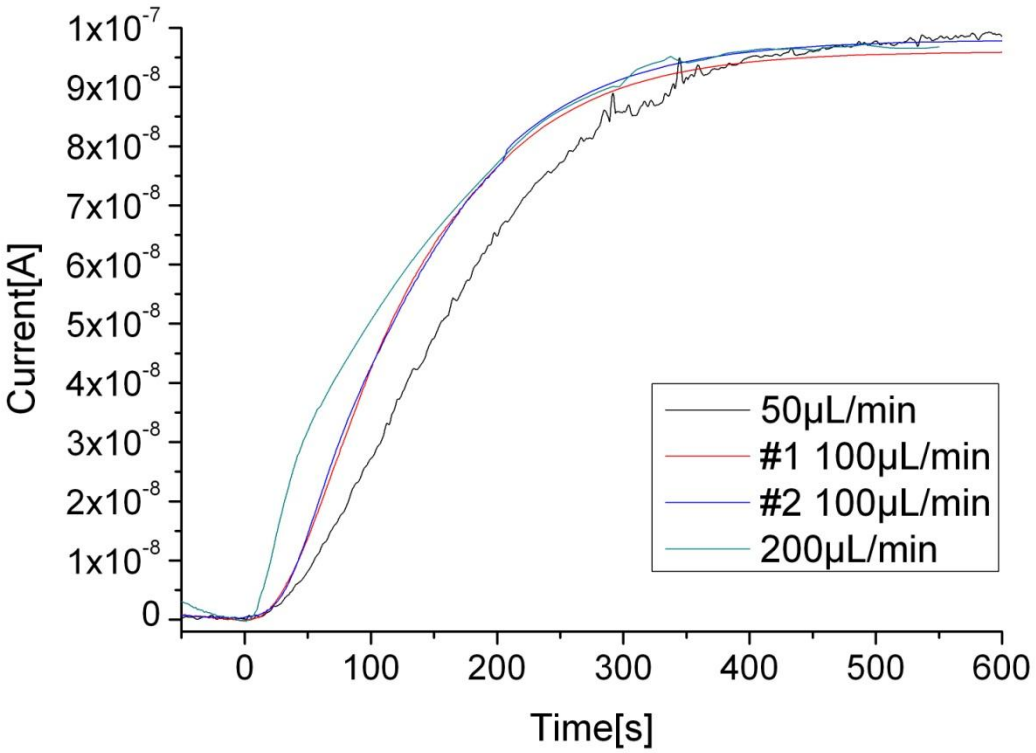

Figure 21: Electrochemical response of glucose sensing microspikes incorporated into a microfluidics platform. The increase of glucose concentration from 0 to 5mM is presented (background current was subtracted from the measurements). Two sensor responses at a flow rate of 100µL/min are shown to present the stability and reproducibility of the method

In the second generation biosensors, it is important to determine whether there are any membrane defects as they could allow the leakage of a mediator, which would affect the sensor performance and lead to loss of functionality. Incorporating microspikes into a microfluidics platform proved to be a very useful technique to study this phenomenon, as it allows the amplification of the mediator loss with comparison to the stationary measurements, and provides us with a very stable, well controlled

system where any such loss can be reliably measured. Thus, during the experiments described above the flow-through solution was collected and analyzed for TTF by applying 150mV to homemade gold (working) electrode vs. Ag/AgCl reference and counter electrode. Based on these results it was concluded that the epoxy – PU membrane was not damaged or cracked and there was no detectable leakage of TTF as the current was stable and remind at background level throughout the experiment.

3.2.3 Conclusions

We have demonstrated that microfluidics system is a useful technique for characterising microspikes based sensor behaviour. Microfluidics experiments involving out-of-plane microspikes revealed that the sensor response is flow rate dependent in the initial stage and independent of flow rate thereafter. The glucose sensors with epoxy – PU membrane show a long response time in the microfluidic platform. This can be attributed to the slow mixing of the solutions in the hexagonal chamber. The parabolic flow profile due to the syringe pumps coupled with laminar flow and backpressure [199] in the hexagonal chamber explain the high response time. This is further compounded by the use of two syringe pumps in sequence which further leads to backpressure near the inlets. The microfluidic platform described here provides valuable information on the kinetic processes which affect the sensor performance.

3.3 Summary

The non-flow cell set-up allowed determining the working range and the time response of glucose sensors. It was concluded that sensors with epoxy – PU membrane can operate in clinically relevant range with quick response time (less than 20s). Sensors coated with epoxy – PU membrane exhibit much higher working range than Nafion coated sensors, which was confirmed by the calculated apparent Michaelis - Menten constant.

Microspikes functionalized with epoxy – PU membrane are suitable candidates for minimally invasive glucose sensors. Functionalized set of microspikes was incorporated into a microfluidics platform. Such approach allowed controlling the environment at the interface between the sensor and the surrounding fluid by varying the flow rate. The results indicate that the functionalized microspikes coated with epoxy – PU membrane are sensitive to the changes in flow rate only at the initial stage of sensor response. However, the maximum current observed remained independent of the flow rate.

Transdermal biosensors can potentially be used as disposable devices for measuring glucose concentration in interstitial fluid. Our results suggest that microspike based glucose sensors functionalized with the enzyme using EDC/NHS chemistry, followed by casting of epoxy-PU membrane, meet the criteria for minimally invasive biosensors. The microfluidics device design presented here can be further customized. Modifications such as having two different subsets of functionalised microspikes incorporated into the microfluidic platform will enable simultaneous measurements of glucose and lactate concentrations.

Chapter 4

Improving batch to batch reproducibility of an enzymatic glucose biosensor

4.1 Development of hydrogel based permselective membrane

Hydrogels are hydrophilic materials commonly used as biomaterials to minimise adverse tissue reaction [200]. The hypothesis for this study was that hydrogels with higher molar concentration of the crosslinker would act as a permselective membrane while still keeping its superior *in vivo* performance. In this section the steps taken to evaluate the chemical composition of hydrogel which can be used as permselective membrane are described.

4.1.1 Introduction

The selection of monomers was based on previous reports by [69] where authors used hydrogels as bioactive coating for glucose biosensors and observed a significant improvement in performance *in vivo,* with comparison to PU coated sensors. Moreover, hydrogels with similar chemical composition are widely used as materials for contact lenses [201] and have been known for their biocompatibility properties [202]. In this section a series of studies is presented, which lead to the development of novel permselective membrane.

4.1.2 Hydrogel fabrication for FTIR experiments

To determine the incorporation of all monomers and select most appropriate chemical composition for further study, two series of hydrogels were prepared as described in section 2.3. In the series 1, four different hydrogels were prepared by varying the NVP concentration. The molar ratios used as against the rest of the monomers were 0, 15, 30 and 45 mol%. Of the rest, the molar ratio between HEMA and DHPMA monomers for all four hydrogels was kept constant at 1:8. EGDMA concentration for all hydrogels of this series was kept at 1 mol%. In the series 2 the molar ratios of NVP was 30 mol% and the molar ratio between HEMA and DHPMA for all four hydrogels was 1:8 of the total monomer concentration. The summary for both series is presented in Table 2 and Table 3.

Series 1	Molar Ratios			
	NVP	HEMA	DHPMA	EGDMA
VP0	0	11.0	88.0	1
VP15	15	9.3	74.7	1
VP30	30	7.7	61.3	1
VP45	45	6.0	48.0	1

Table 2: Molar ratios of monomers for synthesis of hydrogels of series 1

Series 2	Molar Ratios			
	NVP	HEMA	DHPMA	EGDMA
EGDMA0.5	30	7.7	61.6	0.5
EGDMA1	30	7.7	61.3	1
EGDMA3	30	7.5	60.1	3
EGDMA5	30	7.4	58.9	5

Table 3: Molar ratios of monomers for synthesis of hydrogels of series 2

4.1.3 Chemical characterisation of hydrogels using FTIR

The FTIR spectra of the monomers used for the hydrogel preparation are presented in Figure 22. The chemical composition of HEMA and DHPMA are similar, thus the similarity of the FTIR spectra. The stronger appearance of the absorption peak for DHPMA at approximately 3390 cm^{-1} indicates higher concentration of hydroxyl groups with comparison to EGDMA. Characteristic absorption peaks for NVP and EGDMA were also observed at 1450 cm^{-1} and 1650 cm^{-1}, respectively.

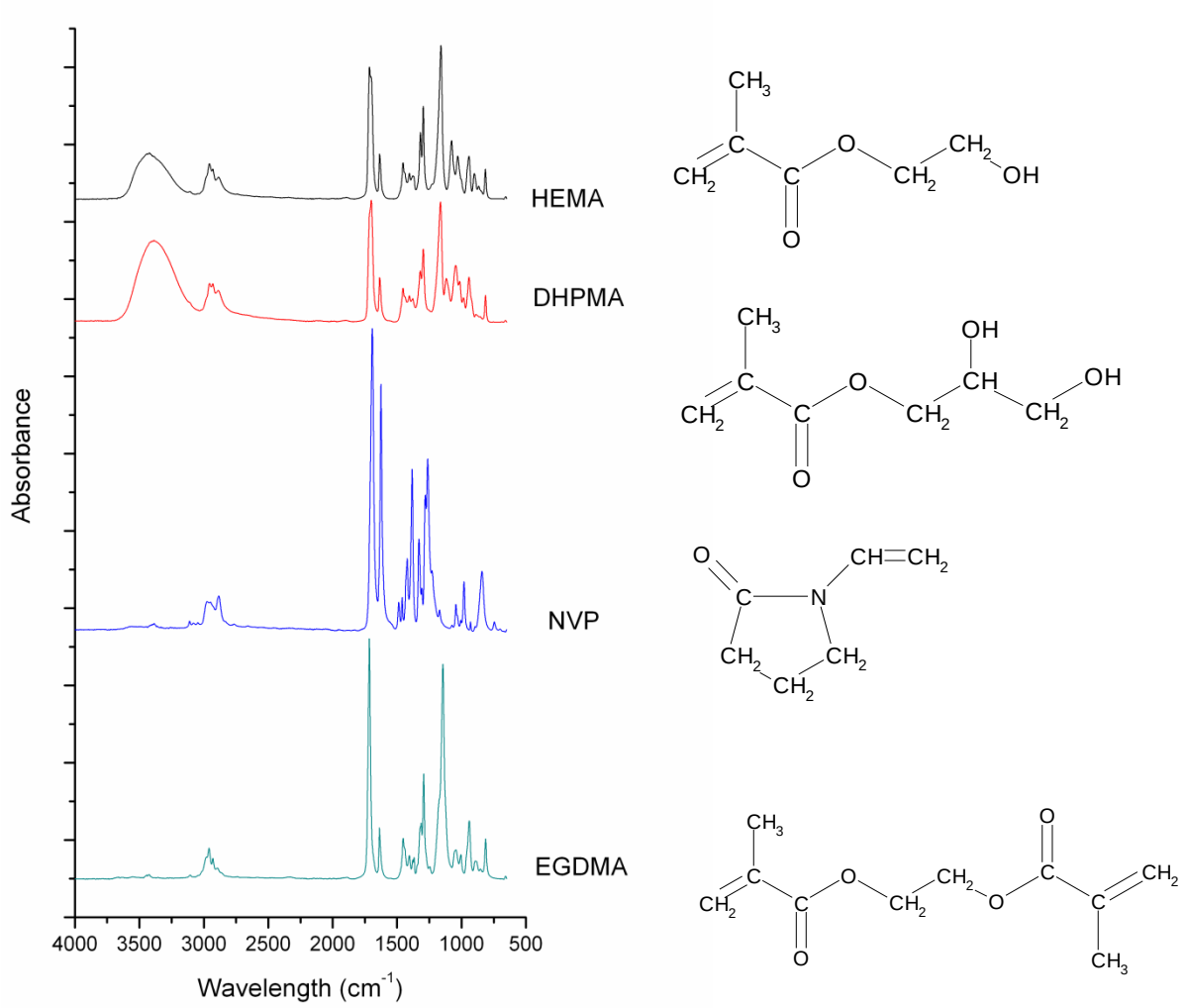

Figure 22: FTIR spectra (left) and structure (right) of monomers and crosslinker used in hydrogel preparation

Since NVP is a cyclic monomer and its concentration is correlated with hydrogel pore size and distribution [203], it was important to determine whether it is well incorporated into the copolymer structure. As seen on Figure 23 the absorption peak for NVP at approximately 1450 cm^{-1} increases with increased concentration of NVP. These results suggest that the NVP is well integrated into the hydrogel structure even at high concentration.

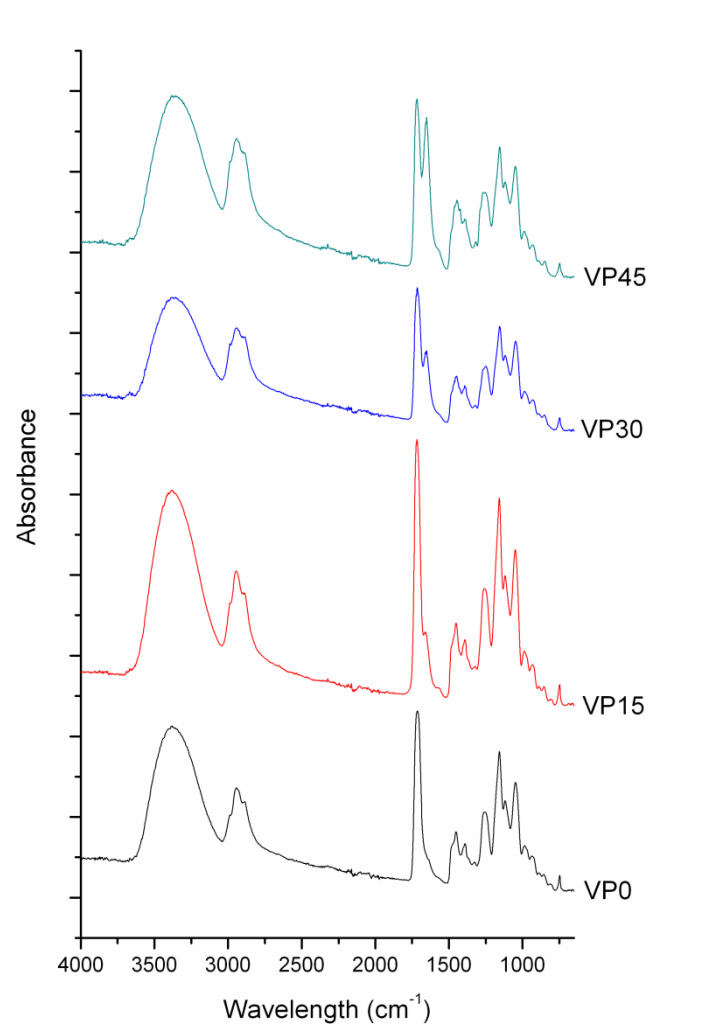

Figure 23: FTIR Spectra of DHPMA-HEMA-NVP hydrogels crosslinked with EGDMA, as function of NVP concentration

High crosslinker concentration was required to provide 'tight' structure of hydrogel which allows it to act as a permselective membrane. As seen on Figure 24, the absorbance pick at 1650 cm^{-1}, which is characteristic for EGDAM, increase with increased concentration of the crosslinker. However, during the experiments it was observed that hydrogels with high crosslinker concentration (EGDMA5 and EGDMA3) were too brittle and could easily be damaged when coated on a sensor.

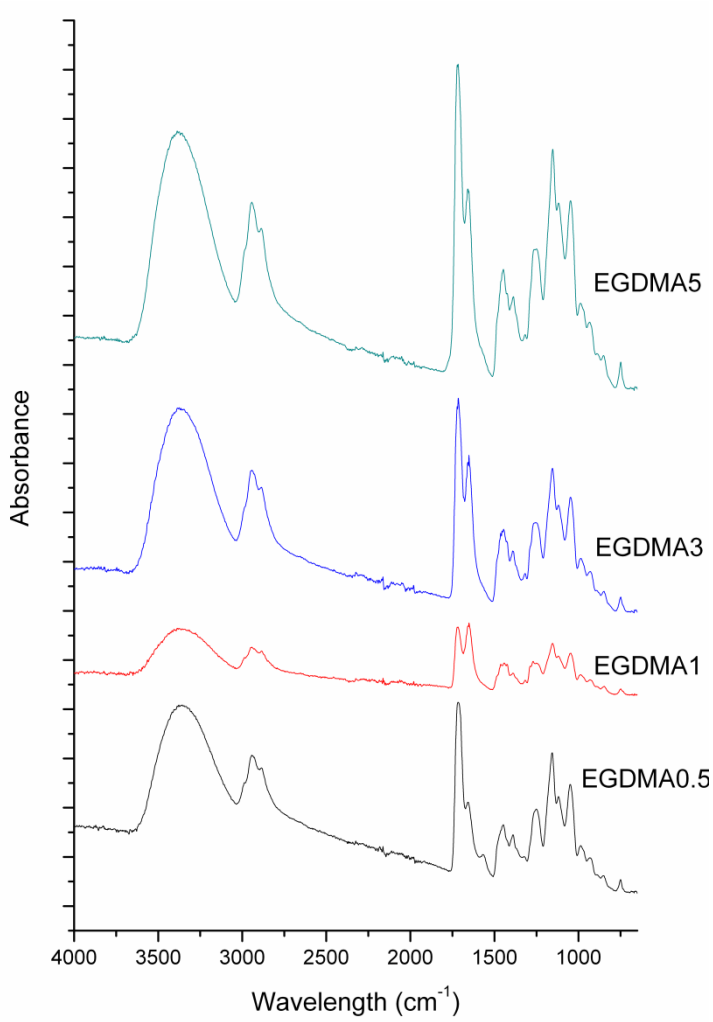

Figure 24: FTIR spectra of DHPMA-HEMA-NVP hydrogels as a function of crosslinking concentration of EDGMA

4.1.4 Conclusion

The chemical composition of hydrogels could be adjusted to suit the application by changing the NVP concentration from 0-45 mol%. The highest possible concentration of the crosslinker was 2-3 mol% since, although it incorporates well into the hydrogel structure, higher concentration affects

the mechanical properties of the hydrogel. The next step involved investigating the performance of hydrogel membrane, which was assessed through the functional studies of the sensors.

4.2 Preparation of glucose biosensor coated with hydrogel membrane

In this section a combination of epoxy-PU and hydrogel coated sensors characteristics are discussed. The device performance and the structure/morphology of the hydrogel permselective membrane are also described. Furthermore, a novel method based on Scanning Electrochemical Microscopy was developed to examine the performance of these membranes.

4.2.1 Introduction

As previously reported [131] the response of coil type amperometric glucose sensors is mainly determined by the permselective membrane properties (morphology and pore structure) and their distribution across the sensor surface. Although not widely acknowledged in the scientific literature, the reproducibility of such sensors is often poor. In this work we attempted to address this issue by using hydrophilic material with high crosslinker concentration. For comparison PU coated sensors, which were commonly used in previous work done in our group, are also presented.

4.2.2 Response characteristics sensors coated with epoxy – PU membrane

Sensors coated with epoxy – PU membrane were fabricated according to section 2.10 and electrochemical measurements were performed according to section 2.11. A typical response to change in glucose concentration for such sensors is presented below.

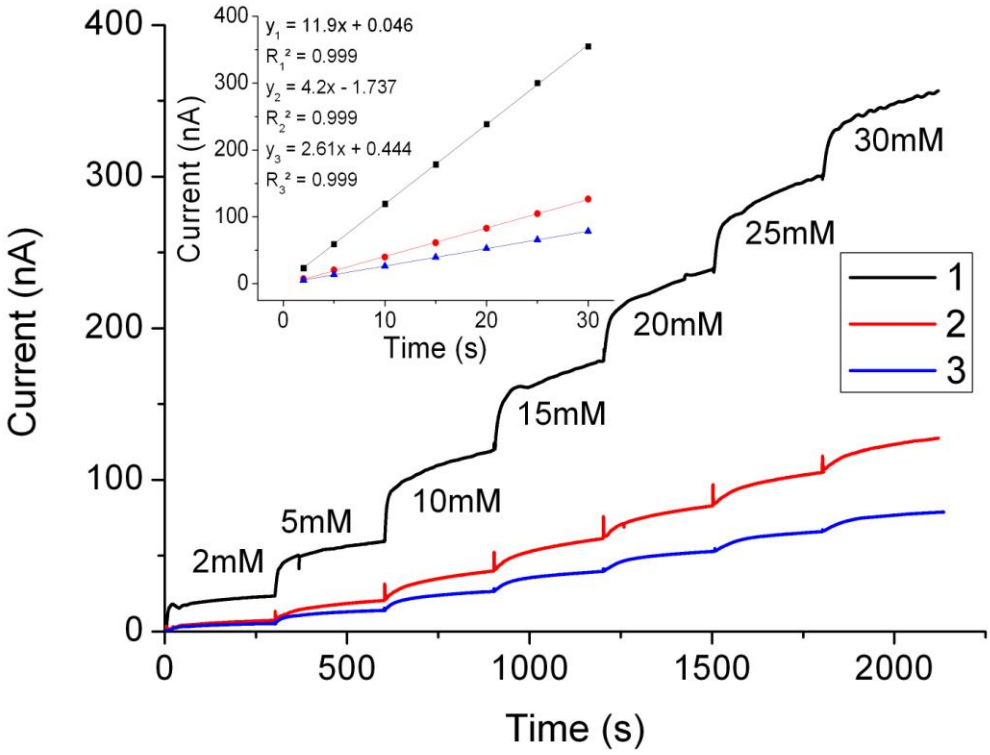

Figure 25: Typical current response to a stepwise glucose concentration increase (0-30 mM) for three sensors coated with epoxy – PU permselective membrane and the calibration curve in insert.

The sensors presented above were prepared in the same batch and tested one day after fabrication. The within-batch and batch-to-batch variation in sensor response was typical (see Figure 25)

although a lot of care was taken to ensure identical fabrication conditions. It is worth nothing, however, that the linearity of such sensors is exceptional (in the above example R^2 for all three sensors was 0.999).

To address the reproducibility issues of coil-type amperometric sensors, hydrogel membrane was used. The coating technique and the characteristics of such sensors are presented below.

4.2.3 Temperature measurements

APS and SMS initiators were used to induce the polymerisation of hydrogels as specified in section 2.3. The time after which APS and SMS decomposition generate enough free radicals to initiate the polymerisation depends on many factors including the solution/room temperature or freshness of the initiator solutions [204]. For coating the sensors, it was crucial to determine the exact moment when the polymerization begins. If the sensors were left for too long after the initiators had been mixed with the monomer solution, the membrane formed was irregular and uneven. On the other hand, if the sensors were left for too short the polymerization wouldn't occur equally on the sensor surface. Thus, it was crucial to design a system which allows monitoring the progress of polymerization for controlling the coating process of the sensors.

Since free radical polymerization is an exothermic reaction where the release of energy is in form of heat, the temperature was chosen as an indicator for the progress of the reaction. Thus, monomer solution containing 5 mol% of NVP, 46.25 mol% HEMA, 46.25 mol% DHPMA and 2.5 mol% of EGDMA was prepared and polymerized as described in section 2.3 using 1.5mol% of APS and SMS. During the

process of polymerization the temperature was measured as described in section 2.9.2. An example of temperature- time curve for free radical polymerized hydrogels is presented below.

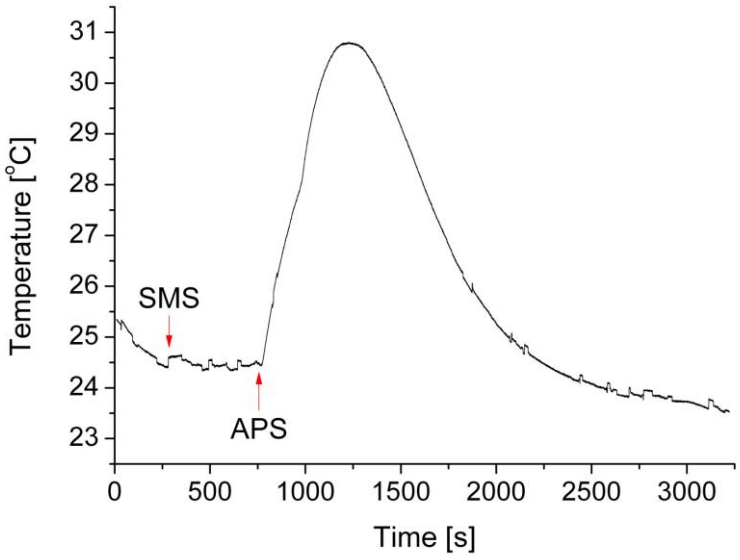

Figure 26: A typical temperature change when polymerising the hydrogels. The points at which the SMS and APS free radical initiators were added are marked

As seen on Figure 26 when both initiators were added to the solution the temperature increased exponentially, which indicates that the rate of heat transfer out from the sample was much lower than the heat created by the polymerization process [204]. In this phase the polymer chain growth is most rapid which results in rise of heat and increase of viscosity. Since the goal of this study was to form a uniform layer of a hydrogel membrane, the sensors were dipped into the monomer solution and, removed when the temperature started to increase rapidly. This allowed the polymers adsorbed on top of the sensors to polymerise and create a uniform thin coating. Based on these

results a detailed protocol for coating the sensors with hydrogel membrane was developed and is described in section 2.10.4.

4.2.4 Response characteristics of sensors coated with hydrogel membrane

Increased NVP concentration improves the porosity and water content of copolymers [69] thus, its concentration influences the structural properties of hydrogel. To determine the optimal concentration of NVP in hydrogel acting as a permselective membrane a series of functional performance studies was conducted.

Based on results from FTIR measurements (section 4.1) it was concluded that the maximum concentration of the EGDMA crosslinker, which can be used in hydrogels without compromising its mechanical stability, is between 2 - 3mol%. At such high crosslinking concentration, the hydrogels were expected to have very low porosity allowing it to function as a permselective membrane for the sensors. Moreover, since OH groups may favour the attachment and entrapment of cells[205], HEMA and DHPMA were kept at 1:1 ratio. To determine the functional performance of the sensors coated with hydrogel membrane, monomer mixture was prepared by mixing 2.5mol% of EGDMA, HEMA and DHPMA were kept at 1:1 ratio while that of NVP was 5, 10 and 15 mol % of total monomer content. Calibration curves for these sensors are presented in Figure 27.

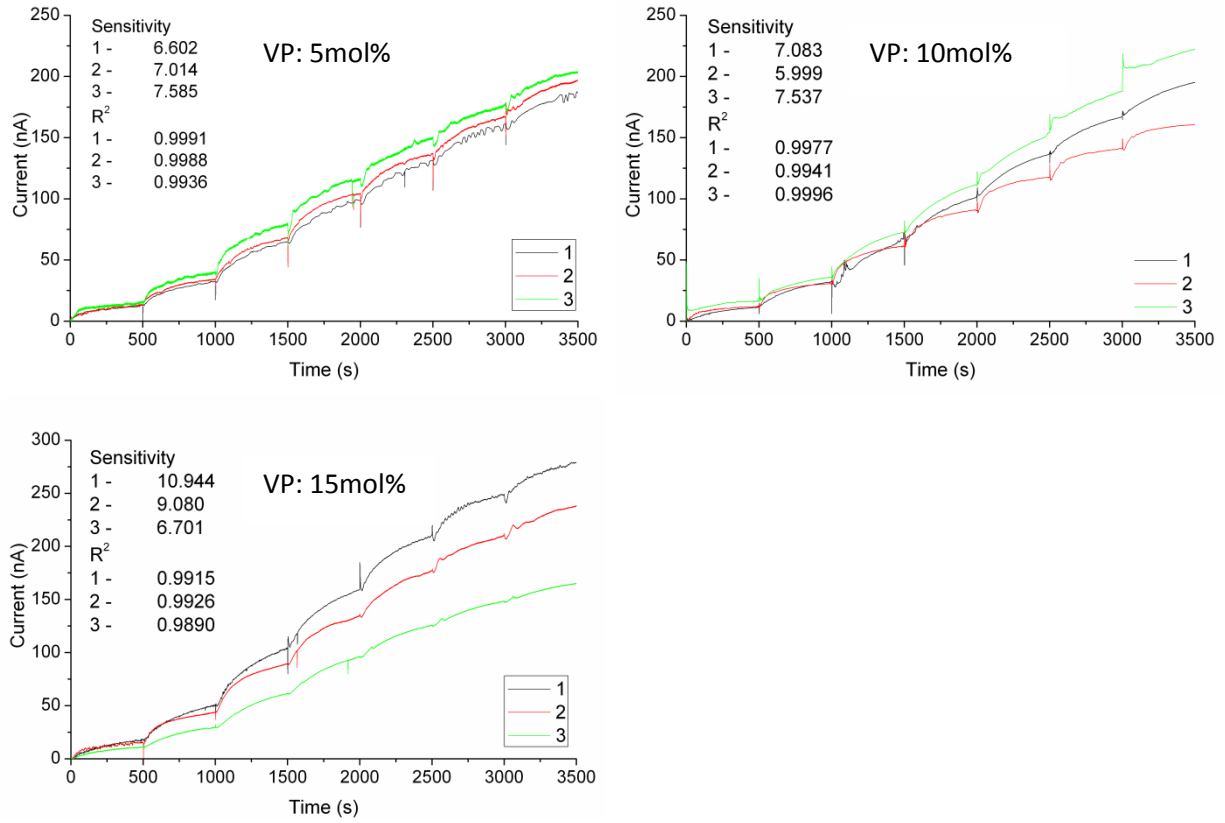

Figure 27: Current response to a stepwise glucose concentration increase for three sets of sensors. Each set was coated with hydrogel membrane having different NVP concentration. The molar ratio between HEMA to DHPMA for all four hydrogels was kept constant at 1:1 and EGDMA concentration for this series was kept at 2.5 mole%

As seen in Figure 27, with increasing concentration of NVP the sensor to sensor variation amplifies which can be observed especially at high glucose concentrations. Sensors coated with hydrogels containing 5 mol% of NVP exhibit very similar response to change in glucose concentration. With increased molar ratio of NVP to 10, sensors response becomes diverse and with 15 mol% concentration of NVP further variation can be observed. Since increased concentration of NVP improves the porosity which is beneficial for *in vivo* performance of these sensors, hydrogels containing 10 mol% of this monomer were chosen for further study.

Long term sensor performance

To evaluate long term performance of sensors coated with hydrogel membrane sensors were prepared as described in section 2.10. The chemical composition of permselective membrane was chosen based on the results from section 4.1. Hydrogels containing 10 mol% of NVP, 43.75 mol% HEMA, 43.75 mol% DHPMA and 2.5 mol% of EGDMA were used.

Figure 28 shows a typical calibration curve in response to step increase of glucose concentration (0-30mM) for three sensors coated with a hydrogel membrane, measured 60 days after fabrication. The sensors respond to changes in glucose concentration in a nearly identical way having very similar response times (4min 20s ±3s, n=3) and sensitivity (25.2±1.5 nA/mM, n=3). The linearity of the sensors was acceptable (R^2 = 0.997) for glucose concentrations varying from 0-30mM which meets the requirement for *in vivo* glucose monitoring [16].

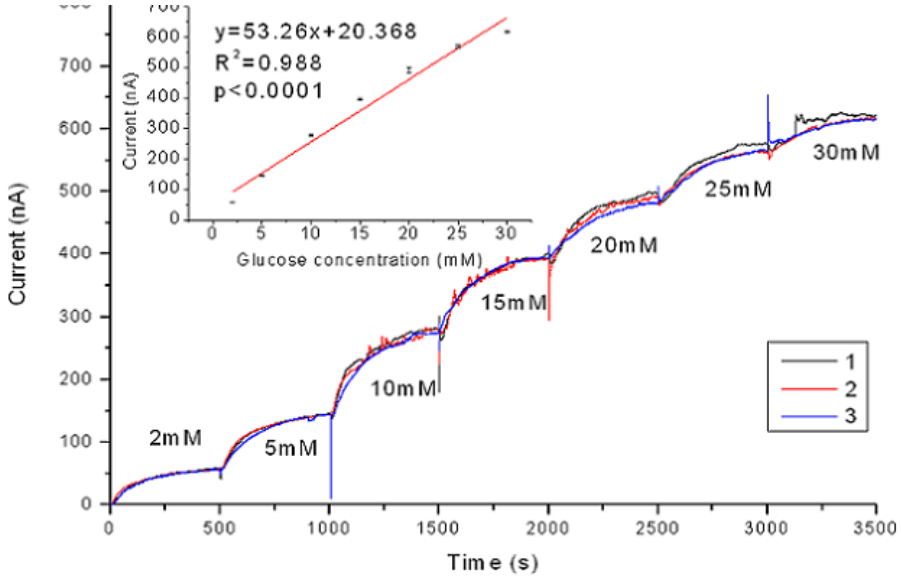

Figure 28: Current response to a stepwise glucose concentration increase for three sensors coated with hydrogel which acts as a semi-permeable membrane (and the calibration curve in insert). The measurements were done 60 days after sensor fabrication. R^2 = 0.997 in glucose concentration varying from 0-30mM.

Two types (hydrogel and epoxy-PU) of sensors were compared in order to determine their reproducibility. To quantify the variations, each sensor was calibrated with step increases of glucose concentration (0-30mM). Subsequently the data was fitted with a linear equation and the slope was determined for each sensor. For the hydrogel coated sensor, 60 days after fabrication the slope was 20.37 ±0.18 nA/mM (n=3, see Figure 28) and for the sensors coated with epoxy – PU membrane 5.70±7.15 nA/mM (n=3, see Figure 25).

To further evaluate the long term performance, four sensors were kept in 5mM glucose solution for 60 days. At day 2, 5, 11 and 60 all sensors were calibrated to determine the sensitivity for each sensor. As seen in Figure 29 the sensitivity significantly increases from day 2 to 11 and remains

stable up to day 60. The increase of the sensitivity in the first 12 days can be attributed to the BSA matrix needing time to fully hydrate, which in the case of a hydrogel membrane is quicker than with a PU membrane(21 days, [67]).

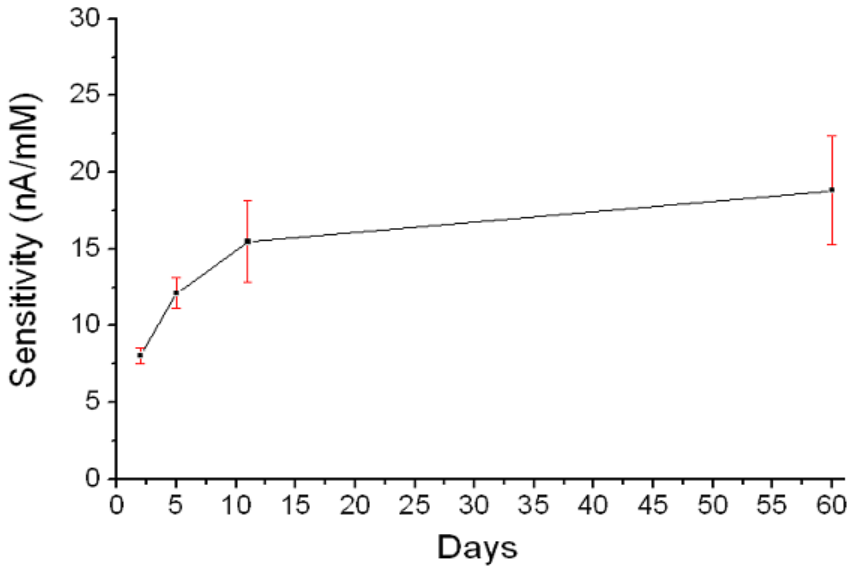

Figure 29: Long term sensor stability testing. Four sensors were kept in PBS with 5mM glucose concentration for 60 days. The graph represents an average sensitivity at day 2, 5, 11 and 60. The variation observed is probably due to mechanical damage of the membranes as the sensors tested just once 60 days after fabrication do not exhibit such deviations

4.2.5 Characterisation of the hydrogel membrane

Following the functional efficacy testing of sensor responses in PBS, and ascertaining that the hydrogel membrane functioned as a permselective membrane, the hydrogel was further characterized to elucidate structure-function relationships.

Characterisation of the hydrogel membrane coated on the sensors

To allow easier observation of transparent hydrogels under the optical microscope, the sensors were stained with H&E as described in section2.10.5. Visual examination confirmed that the sensing elements are fully coated with the hydrogel and no enzyme is directly exposed to the surrounding environment. To measure the thickness of hydrogel membrane the sensors were glued to a glass slide and sectioned perpendicularly to the working electrode coil in order to expose all layers as presented in Figure 30. The uniformly dispersed hydrogel membrane was interconnected with underlying GOx/BSA layer and had a thickness of 41.4 ±9.8 µm.

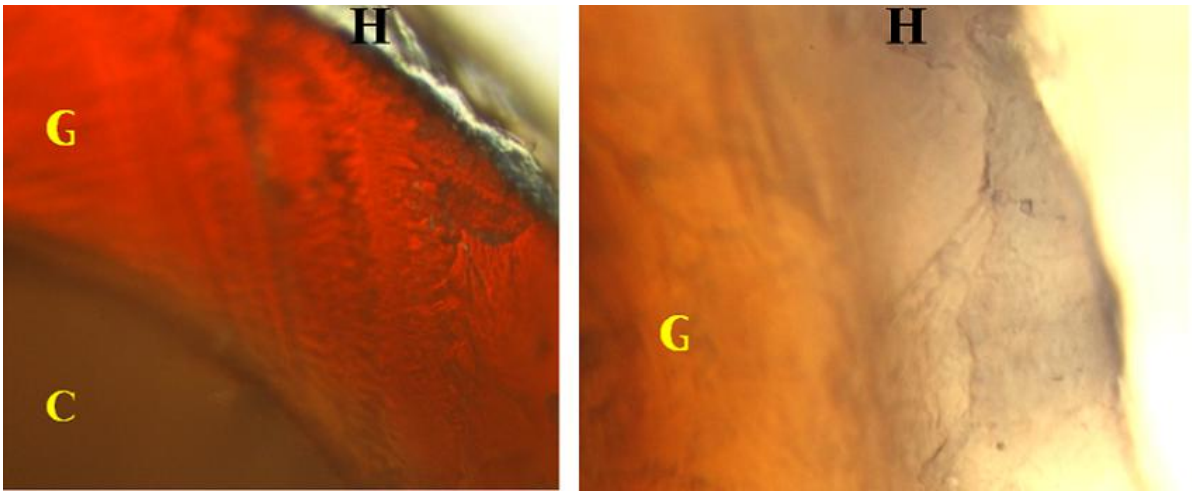

Figure 30: Optical micrograph of the sensor. Magnification 50x (left) and 100x (right). The hydrogel has a blue-purple colour due to a staining with hematoxylin. C- Cotton; G- Glucose oxidase and BSA crosslinked with GA; H - Hydrogel coating

Symmetric cross-section morphology

The hydrogels were fabricated by a phase separation process, thus their structural properties depend on the water uptake during the polymerisation[206]. To investigate this phenomenon Scanning Electron Microscopy was used as stated in section 2.9.3. Three types of samples were prepared, all having the same chemical composition as membranes (10 mol% of NVP, 43.75 mol% HEMA, 43.75 mol% DHPMA and 2.5 mol% of EGDMA). The specimens were polymerised at 90%, 50% and 0% humidity at room temperature. After washing with DI water, the samples were stored for one week at room temperature in PBS (changed daily) to hydrate and freeze-dried for SEM imaging.

As seen in Figure 31 the hydrogel membrane is composed of two very distinct layers. The inner layer has a uniform, apparently non porous structure and its main function is to limit the diffusion of

glucose. The outer (skin) layer has a very porous and uniform structure whose main function is to promote cell ingrowth. As it is seen from SEM images both layers are very well organised which contributes significantly to the reproducibility of the sensors.

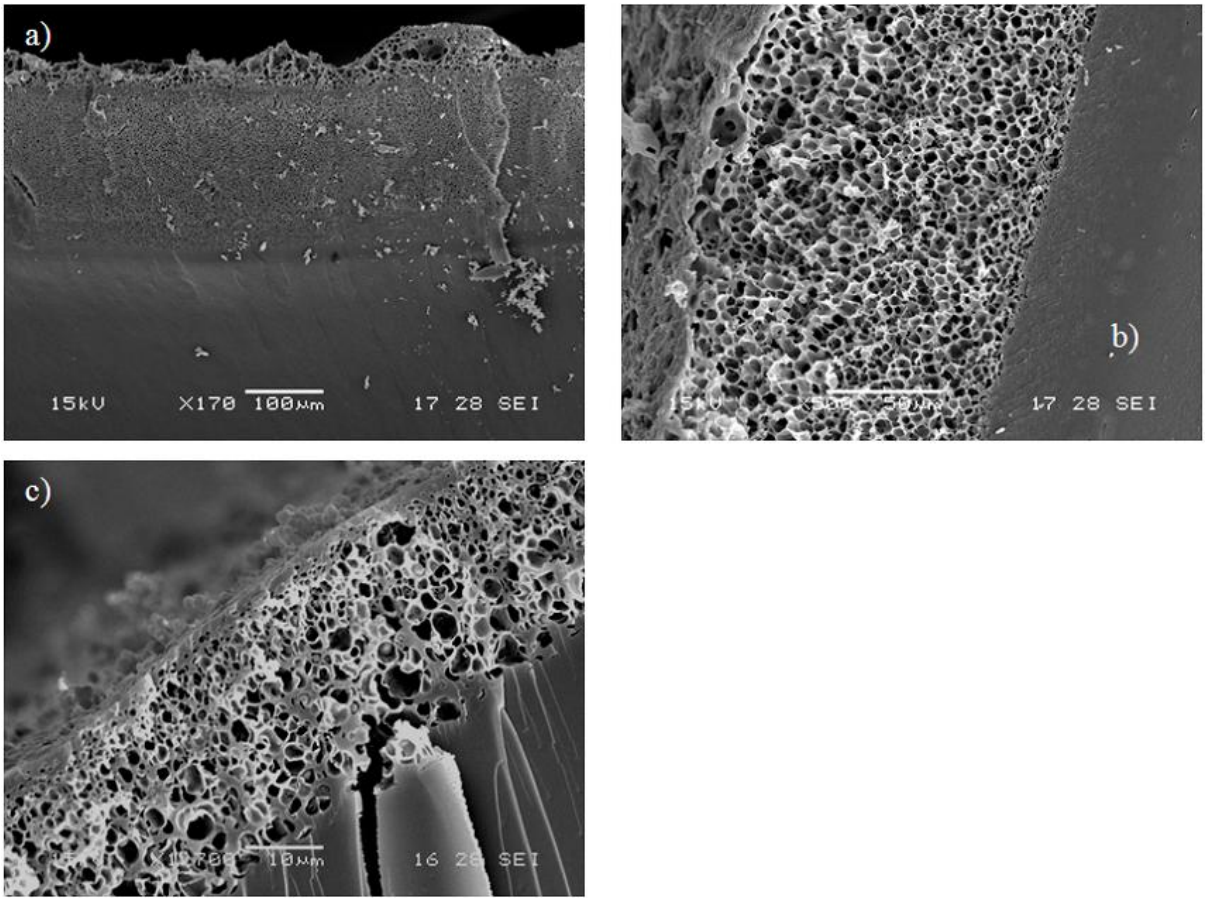

Figure 31: SEM pictures of membranes skin layer. Hydrogels were polymerised at room temperature in a) 90% humidity (scale bar 100µm), b) 50% humidity (scale bar 50µm) and c) nitrogen atmosphere (0% humidity, scale bar 10µm). The thicknesses of porous skin layer are 230±4 µm, 137±3 µm and 26±1 µm, respectively

The influence of humidity on hydrogel structural properties was investigated. As seen in Figure 31 the thickness of skin layer decreases with reduced humidity. This can be attributed to a relatively high crosslinker concentration and higher water accumulation at the surface of the hydrogel during

the polymerisation (which in dry environment can be minimised). The permselective behaviour of the hydrogel relied on the solubility of glucose and oxygen in the membrane and controls the reactant flux to the enzyme.

Chemical composition of skin and bottom layer of hydrogel

To determine whether there were differences in chemical composition between the skin and bottom layer of hydrogel, FTIR was used. IR spectra were recorded at room temperature in the mid-infrared range (4000–650 cm^{-1}) as described in section 2.9.1. The membranes were fabricated as described above (see 'Symmetric cross-section morphology') with 90% humidity as this produced membrane with a thick skin layer. After hydration the two layers were separated with a scalpel blade and freeze-dried prior to FTIR characterisation.

As presented on Figure 32, the FTIR spectra representing the chemical composition of both morphologically different hydrogel layers appears to be matching. Since the chemical composition is very similar, the permselectivity of the membrane mainly depends on the inner layers morphological properties as the outer layer appears too porous to be a diffusion barrier for glucose/oxygen.

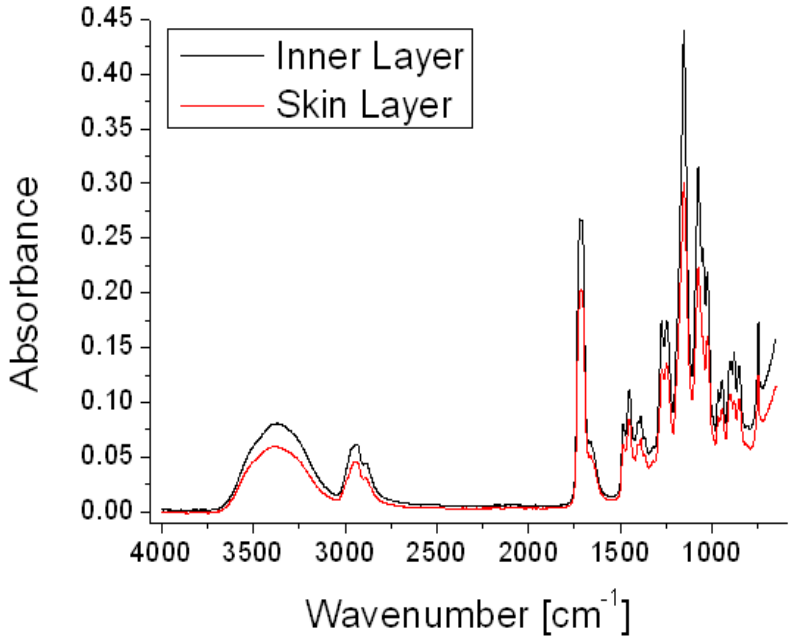

Figure 32: FTIR spectra of outer (skin) and inner layer of the hydrogel membrane

4.2.6 Scanning Electrochemical Microscopy (SECM) experiments

Scanning Electrochemical Microscopy was used in order to map the enzyme activity on the planer sensors. This technique involved measuring hydrogen peroxide concentration within close proximity to the sensor surface. As hydrogen peroxide is a direct product of the GOx enzymatic reaction, it can be used as an indicator of the rate at which glucose is converted. Thus, the glucose diffusion can be assessed by mapping the hydrogen peroxide concentration at the surface of a sensor.

For the SECM experiments, sensor mock-ups were prepared as described in section 2.12.1. Hydrogel composition was kept the same as described in previous section (10 mol% of NVP, 43.75 mol% HEMA, 43.75 mol% DHPMA and 2.5 mol% of EGDMA). Such prepared samples were scanned using optical profilometer to ensure their flatness. An example of such measurements is presented in Figure 33.

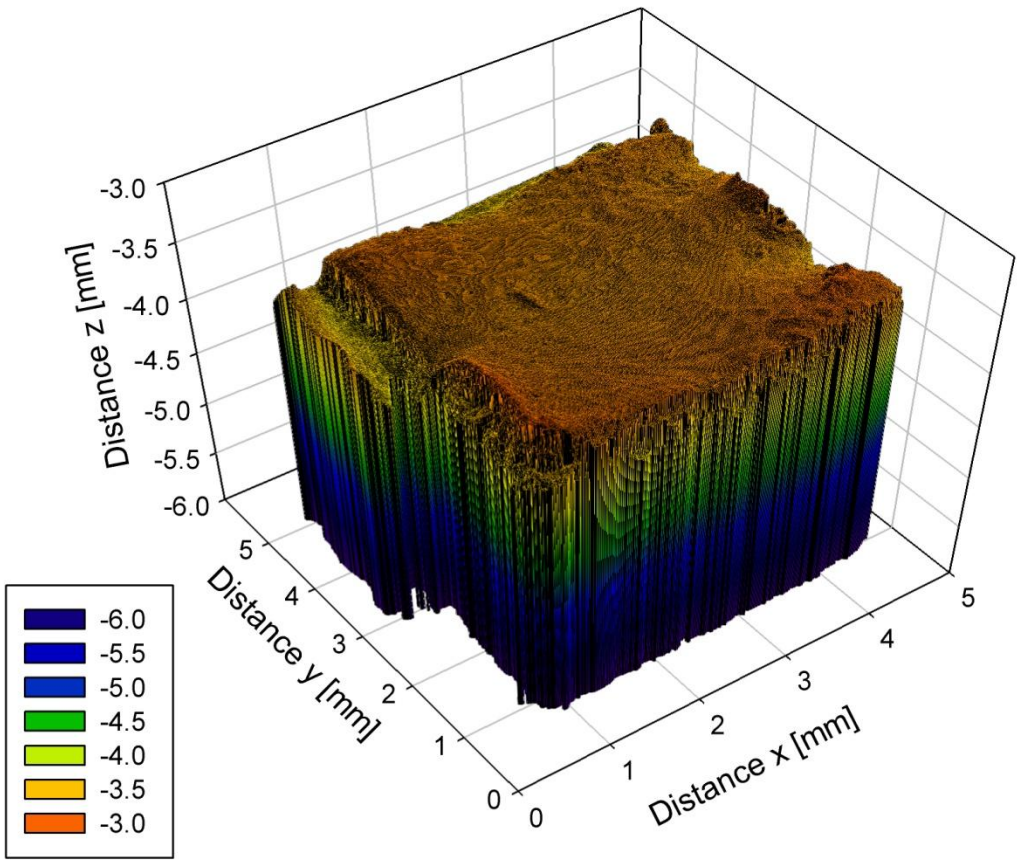

Figure 33: An example of image taken using optical profilometer which indicates that the variation on the sample surface is less than 0.5mm. Such samples were further analyzed using SECM

After cleaning the UME, PVA films coated with either hydrogel or epoxy-PU membrane were placed at the middle of the SECM cell filled with 50mM glucose dissolved in PBS. To determine the positioning of a sample in the SECM cell, couple of line scans were conducted in both x and y direction. The UME was operating at 0.7V to measure the hydrogen peroxide which was synthesized by the immobilised enzyme on PVA film. An example of such scan is presented on Figure 34.

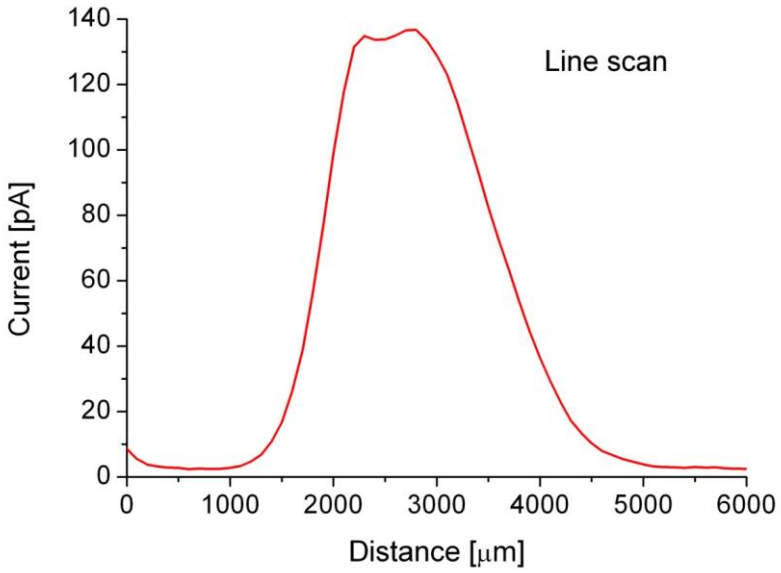

Figure 34: A typical line scan conducted on PVA sheet comprised of GOx, BSA and crosslinked with GA and coated with hydrogel permselective membrane immersed in 50mM glucose/PBS solution. The scan was conducted in x direction with UME measuring current every 100µm.

Based on the line scans UME was positioned directly above the sample. In order to determine the exact distance from the sensor mock-ups, an approach curve was performed. The UME was lowered in z direction until a peak was observed as illustrated on Figure 35.

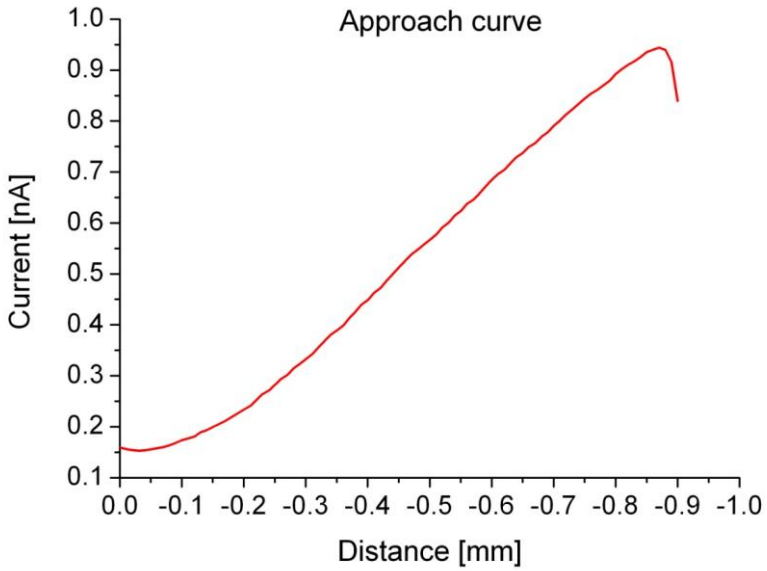

Figure 35: An approach curve experiment where the UME working at 0.7V against Ag/AgCl and Pt reference and counter electrodes, respectively, was lowered to a close proximity to the sample

The peak current observed in the figure above represents the minimum distance from the sensor at which the diffusion of hydrogen peroxide is not hindered. The decrease of current observed after the maximum current is reached indicates that the distance between the UME and the sample is small enough to limit the feedback. After conducting an approach curve, which allowed accurately measuring the distance of UME from the sample, the SECM tip was positioned 50µm above the point where the maximum current was noted.

After determining the edges of the sample with line scan experiments and adjusting the height of UME by approach curve experiments the area of approximately 36mm^2 was scanned as described in section 2.12.2. A comparison between samples coated with epoxy-PU and hydrogel membrane is presented in Figure 36.

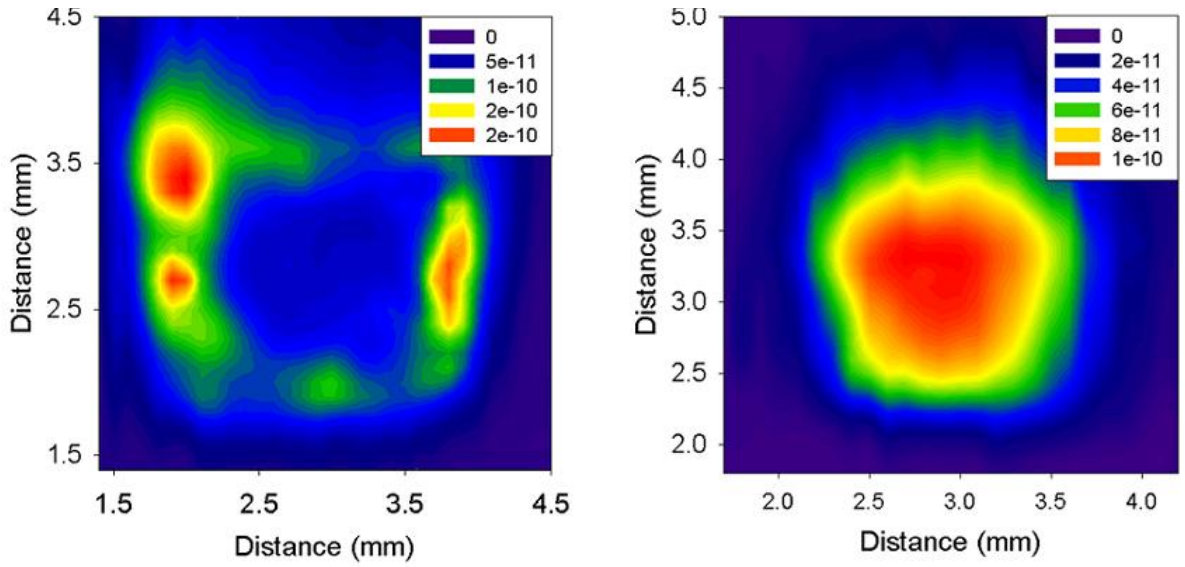

Figure 36: SECM images of hydrogen peroxide diffusion through epoxy-PU (left) and hydrogel (right) membranes coated on GOx immobilised on BSA by GA crosslinking, assembled on polyvinyl alcohol sheets (current is presented in colour gradient scale - see inserts).

SECM results indicate that the epoxy-PU membranes do not have uniform lateral transport properties, which may be the cause of the lack of reproducibility of the sensors. The membrane shows higher hydrogen peroxide permeability at the sides of the mock-up sensor and virtually none in the centre. On the other hand, hydrogel coated sensors show uniform hydrogen peroxide diffusion, which indicates consistent glucose conversion at the interface between the hydrogel and the enzyme.

4.2.7 Conclusion

In this section a novel hydrogel based mass transport limiting membrane for enzymatic glucose biosensors is presented. The membrane was characterised in terms of morphology and chemical

composition, which revealed it comprises of two chemically very similar but morphologically distinct layers. Sensors coated with such membranes exhibit analogous response to the change of glucose concentration, which was confirmed by electrochemical measurements (presented in Figure 28). SECM microscopy was used to explore this phenomenon further. The results indicate that the diffusion of glucose through hydrogel membrane is much more uniform than that through commonly used epoxy – PU membranes.

4.3 Summary

To conclude, the hydrogel coatings are good candidates to replace the commonly used permselective membranes as they allow fabrication of reliable and reproducible sensors, whose efficacy is not affected by the preparation conditions. It was demonstrated that the chemical composition of the hydrogel can be tailored to the application, i.e. it is considered that the increase of NVP concentration to 15% in hydrogel membrane (which, as demonstrated in Figure 27, has higher sensitivity but affects the reproducibility *in vitro*) can be beneficial for sensors used *in vitro* where, due to biofouling effect, the signal reduces with time. Also, a novel method for coating the sensors was developed. The temperature measurements were used as an indicator of polymerisation progress, which allowed precisely controlled sensor coating. The electrochemical characterisation of hydrogel coated sensors was performed, which allowed further optimization of membrane chemical composition. Also a long term study of the sensor response revealed that the performance did not vary much over a 60 day period. Furthermore, the hydrogel permselective membrane was further characterised in order to correlate its structure to functional performance. The sensors were stained and examined under light microscope which revealed that the hydrogel is

uniformly coats and is interconnected with the underlying GOx layer. SEM experiments indicated that the outer layer of hydrogel is porous and does not act as a selective barrier for glucose, however, it is speculated that this could be beneficial for the *in vivo* cell attachment. Finally SECM was used to compare epoxy-PU and hydrogel coated sensor surrogates. The results clearly show that the diffusion of hydrogen peroxide (which is produced by the enzyme catalyzing the oxidation of glucose) is much more uniform in mock-up sensors coated with hydrogel membrane.

Chapter 5

Conclusion and recommendation for future studies

We present the steps taken to investigate novel technologies for glucose sensing applications. In the first part of this work, a detailed description of the microspike based platform for minimally invasive glucose sensing was presented. In contrast, second part contains a methodology for the development of sophisticated permselective membrane to address the reproducibility issues in coil-type implantable biosensors. The aim for this chapter is to summarise the research findings presented, and to indicate possible future directions for these studies.

5.1 Conclusion

The goal for this work was to design glucose biosensors having the potential, in combination with an insulin pump, to provide the patient with a CGMS. To address this, in the first part of this work a detailed description of a method to fabricate and functionalise microspikes to act as glucose biosensors is presented.

The unique abilities of microspikes, namely their ability to painlessly penetrate the skin layer and access ISF, makes them good candidates for minimally invasive biosensors. The microspikes were fabricated using lithographic techniques and sputtered with gold to serve as electrodes for electrochemical biosensors. The gold surface was functionalised with glucose oxidise using EDC/NHS chemistry. To protect the enzyme layer and to increase the linear working range of such modified sensors, two types of coatings were tested, namely Nafion and epoxy – PU permselective membranes both containing TTF mediator. Functional testing of biosensors revealed that the Nafion membrane allows determining glucose in 0 to 10mM concentration range, which is insufficient for sensing in ISF. Epoxy – PU membranes improved the linear detection range (to 0-25mM, R^2=0.989), which was confirmed by calculated apparent Michaelis-Menten constant, thus was selected for further studies.

To further characterise microspike based biosensors and eliminate the noise from the measurements (which were caused by stirring the solution during functional testing) the sensors were incorporated into a microfluidics platform. The data from this study indicate that the sensor

response is flow rate dependent in the initial stage and independent of flow rate thereafter, due to a slow mixing of the glucose containing solution in the microfluidics chamber.

In conclusion, it was presented that the microspikes can be functionalised to act as biosensors and with an appropriate coating sense the glucose concentration within clinically relevant range. A microfluidics platform proved to be useful in further characterisation of such sensors.

In addition, we have concentrated on improving the coil-type invasive biosensors; specifically we attempt to address the issues related to batch to batch variability in sensor response, which is presented in the second part of this work. Hydrogels, which are well known for their biocompatibility, served as a basis for our study. It was hypothesised that these materials, if fabricated using high enough concentration of the crosslinker, can serve as permselective membranes. Since the final morphology of hydrogels does not depend on the polymerisation conditions, it was also assumed that such membranes will improve sensors reproducibility.

Chemical characterisation of hydrogels using FTIR revealed the optimal concentration of monomers for the hydrogel fabrication. It was concluded that the maximum concentration of the EGDMA crosslinker is 2.5mol% and that the NVP monomer, which allows adjusting hydrogel pore size and distribution, can be varied from 0 to 45mol%. However, tuning of the final concentration of monomers in hydrogel had to be done trough functional testing.

To evaluate the hydrogel based permselective membrane performance, a novel method of sensor coating technique was developed. The hydrogel membrane polymerisation progress (induced using APS/SMS free radical initiators) was monitored by measuring the temperature of the monomer solution, which was used as an indicator for sensor coating. This was followed by the functional

performance tests, based on which the optimal concentration of the monomers was determined. The goal of fabricating sensors with an exceptional reproducibility (hydrogel coated sensors calibration curve slope was 20.37 ±0.18 nA/mM compared to an epoxy – PU coated sensors 5.70±7.15 nA/mM) was achieved. The sensors also exhibit a stable long term performance, which was confirmed by testing the response to a change in glucose concentration for 60 days.

Characterisation of hydrogel coated on the coil-type sensors using optical microscope and H&E staining revealed that the membrane is interconnected with the underlying GOx/BSA/GA layer. Furthermore, based on the SEM images of hydrogel fabricated when varying humidity, it was concluded that the membrane is composed of two morphologically different layers: an outer (skin) layer and an inner layer. The skin layer appeared highly porous whereas the inner layer structure was compact, which indicates that the permselectivity of the membrane is mainly dependent on the latter. An FTIR study of both layers was conducted to determine whether the morphological differences reflected an underlying difference in composition, no difference in chemical composition was seen between the layers.

To determine the transport of glucose through the hydrogel membrane a novel technique was developed. Based on SECM measurements the diffusion of glucose into the mock-up sensors was correlated to the diffusion of hydrogen peroxide outside the sensor. Based on these results a map of hydrogen peroxide diffusion patterns through the sensor membrane was constructed, based on which it was concluded that the hydrogel membranes have evenly distributed transport properties across their surface unlike the epoxy – PU ones and this, in turn, is postulated to have an effect on their reproducibility.

To conclude, a novel hydrogel membrane for coil-type amperometric glucose sensors is presented. It was characterised using various techniques in terms of its morphology and chemical composition as well as its functional performance. A novel technique, based on the SECM, was developed to map the diffusion of the substrate through such membrane.

5.2 Recommendation for future studies

Based on this work, future development should concentrate on *in vivo* studies for both types of biosensors. It was shown in our group and by others [49, 50] that microspikes can penetrate the skin layer and access ISF and, with appropriate functionalization presented in this work, act as glucose sensors. However, to our knowledge, the effects of the physical puncturing of skin by the microspike device on the microspikes and their outer coatings are not known. Such data would allow determining whether any additional modifications are required to maintain the device integrity.

It was also shown within our group that microspikes can be functionalised to act as lactate biosensors. This idea can be further exploited to design a multi-analyte detecting platform. However, for that a different design of microspikes is needed where each spike would be individually addressed. Furthermore, the functionalization of microspikes with an enzyme would have to be modified to allow attaching an enzyme to an individual spike.

For the coil-type invasive biosensors, it is also proposed to concentrate on *in vivo* studies. Hydrogel membrane developed in this work has a potential to improve the *in vivo* sensor life time, as the most outer layer is designed to be highly porous, which should promote cells attachment. Moreover, being able to fabricate reproducible sensors, it is suggested to research whether it is feasible to

correlate the response of implanted sensor with those tested *in vitro*, which could reduce (or eliminate) the amount of calibrations required.

Finally, it is suggested to further optimise the SECM technology for measuring the diffusion of a substrate through the membrane. More accurate measurements, in nanoscale resolution, could be done when combining SECM with an AFM system and operating at the constant distance from the sample surface. In this case AFM tip can serve as an electrode, minimising the issues associated with the UME R/G ratio.

Appendix 1

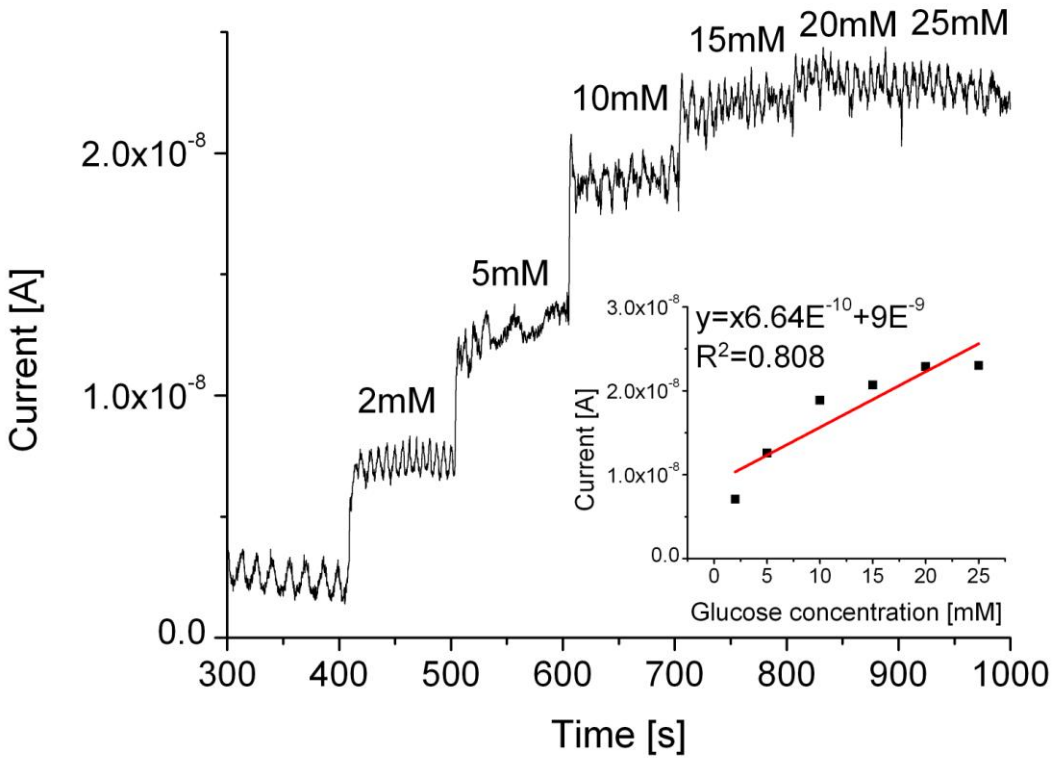

Figure 37 An example of current response to a stepwise glucose concentration increase for microspike sensors coated with Nafion permselective membrane and the calibration curve in insert. The operating potential was 150mV vs. SCE.

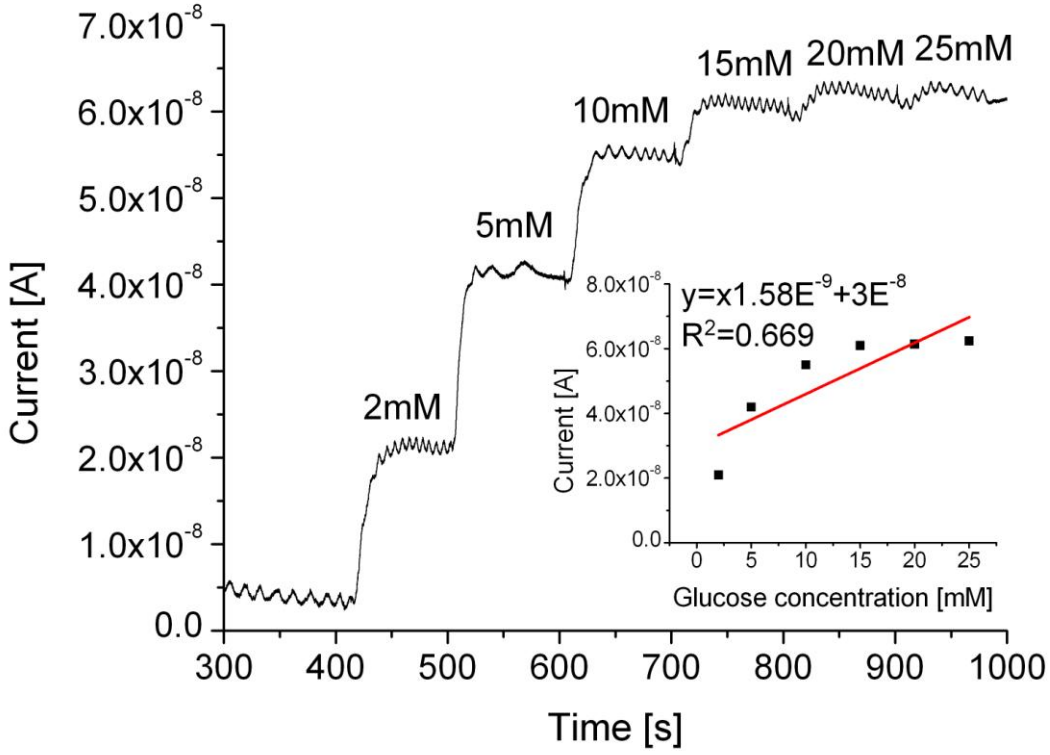

Figure 38 An example of current response to a stepwise glucose concentration increase for microspike sensors coated with Nafion permselective membrane and the calibration curve in insert. The operating potential was 150mV vs. SCE.

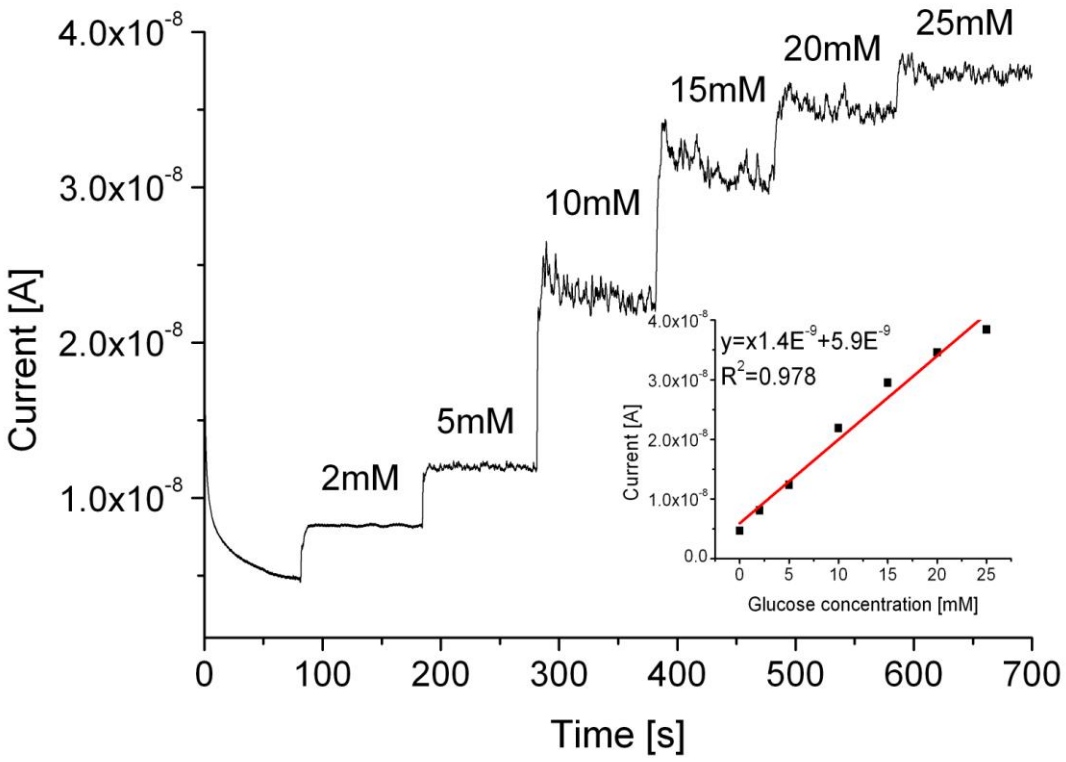

Figure 39 An example of current response to a stepwise glucose concentration increase for microspike sensors coated with epoxy-PU permselective membrane and the calibration curve in insert. The operating potential was 150mV vs. Ag/AgCl reference and counter electrode.

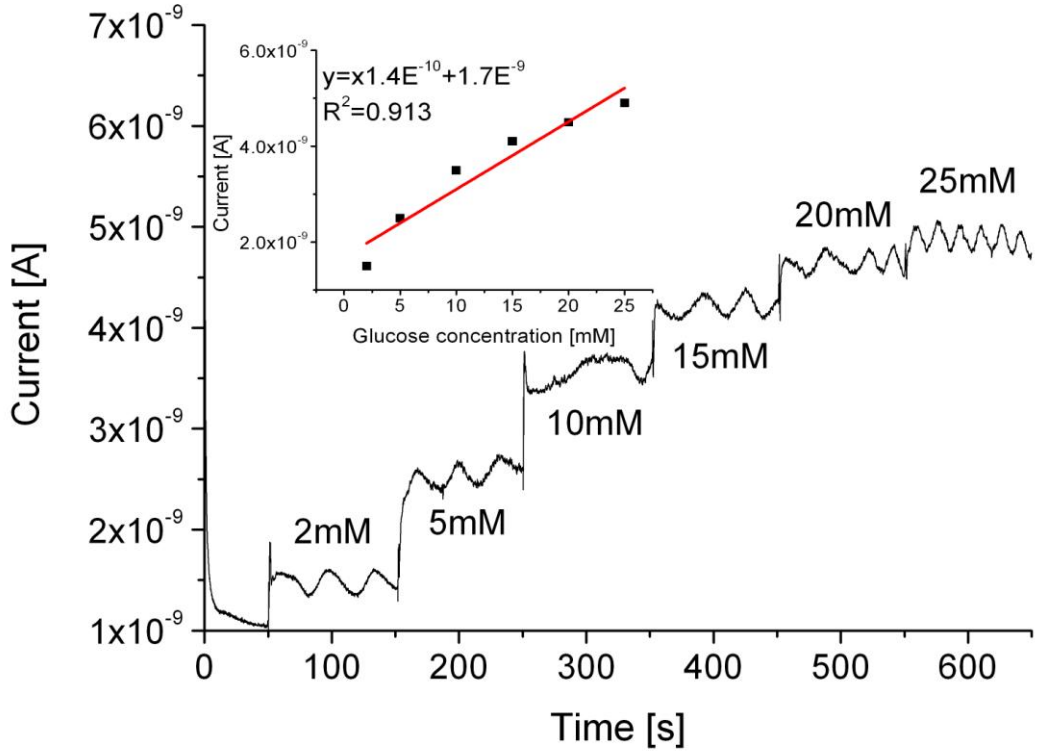

Figure 40 An example of current response to a stepwise glucose concentration increase for microspike sensors coated with epoxy-PU permselective membrane and the calibration curve in insert. The operating potential was 150mV vs. Ag/AgCl reference and counter electrode.

Appendix 2

Microfluid Nanofluid
DOI 10.1007/s10404-010-0740-y

ORIGINAL PAPER

An integrated silicon sensor with microfluidic chip for monitoring potassium and pH

Sanjiv Sharma · Anna Radomska-Botelho Moniz · Iasonas Triantis · Kostis Michelakis · Jakub Trzebinski · Alireza Azarbadegan · Benjamin Field · Chris Toumazou · Ian Eames · Anthony Cass

Received: 17 June 2010 / Accepted: 4 November 2010

Abstract We present ion-sensitive field effect transistor-based sensors, integrated with a microfluidic chip, for monitoring pH and potassium cations. The sensor is strategically located at the base of a well so that the response time of the device depends both on the mean flow through the device and the diffusion coefficient of the analyte being monitored. This would enable monitoring of ions in the presence of larger molecules. The dependence of the device response time on diffusive transport of analytes was examined through a numerical study of the flow field and the passive diffusion of a chemical species. The predicted device response time was compared with the experimental measurements and reasonable agreement found. The general dependence of device response time on geometry, flow rate, and analyte diffusion coefficient was derived. These devices can be used with biological fluids where monitoring of pH and cations provide vital information about the well-being of patients.

S. Sharma (✉) · A. R.-B. Moniz · I. Triantis · K. Michelakis · J. Trzebinski · C. Toumazou · A. Cass
Institute of Biomedical Engineering, Imperial College London, South Kensington Campus, Exhibition Road, London SW7 2AZ, UK
e-mail: s.sharma@imperial.ac.uk

B. Field
Department of Investigative Medicine, Imperial College London, Hammersmith Campus, Du Cane Road, London W12 0NN, UK

J. Trzebinski
Brunel Institute for Bioengineering, Brunel University, Uxbridge, West London UB8 3PH, UK

A. Azarbadegan · I. Eames
Mechanical Engineering Department, University College London, Torrington Place, London WC1E 7JE, UK

Published online: 01 December 2010

Keywords Microfluidic · ISFET · ChemFET · Computational fluid dynamics

1 Introduction

Since their introduction in 1970 by Bergveld (1972) as sensors for measuring ion concentration around nerve tissues (Bergveld 2003), ion-sensitive field effect transistors (ISFET) today are used in wide range of sensing applications in the fields of clinical medicine, biotechnology, and the environment (Schning 2002). Their attractive features, such as small size, fast response time, low cost, and multiple integration of various kinds of biologically active materials (e.g., enzymes, antibodies, DNA, and cells), make them well suited for Micro Total Analytical Systems (μTAS) or Lab-on-Chip devices (Reyes et al. 2002; Auroux et al. 2002). Integrating field effect devices with microfluidic platform allow manipulation of low volume samples and the realisation of high-performance detection systems with reduced size. Together they offer cheap and portable devices for real-time monitoring that could be used for various biomedical and point of care diagnostic applications.

The first attempt towards integrating microfluidics and field effect transistors was reported in 1999, referred to as flowFETs. These devices were used as controlling and switching elements in microfluidic networks (Schasfoort et al. 1999). Sharma et al. (2006) have reported silicon on insulator-based microfluidic device with monolithically integrated FETs for microTAS applications. An extended gate field effect transistor (EGFET)-based biosensor integrated with a silicon microfluidic channel for the electronic detection of streptavidin–biotin protein complexes has been reported by Kim et al. In this instance, gold was used

as the extended gate coated with self-assembled monolayers of thiols, on to which the biotin avidin complex was immobilized (Kim et al. 2006).

Truman et al. (2006) reported the use of silicon-based ISFETs for monitoring transport and chemical properties of liquids in microfluidic systems. Reliable, time-resolved ion, and molecular transport sensing in chemoreceptive neurons in microfluidic channels using transistors has been demonstrated by Jacquot et al. (2007). Tetraphenylborate derivatives have been used to modify ISFETs on polymeric microfluidic devices for sensing cationic surfactants in dental rinses (Masadome et al. 2006). In another instance, a microfluidic chip was used for cell culture and a large transistor-based sensor array chip for direct extracellular imaging (Milgrew et al. 2005). Literature survey does not reveal any solid state sensors integrated microfluidic device that could be used for simultaneous determination of cations.

In this study, the authors report on a novel design for a microfluidic device integrated with ISFET sensor. The novel aspect of the device design is that the device response time is sensitive to the diffusivity of the analyte species, thereby enabling it to exploit differences in diffusion coefficient between large and small molecules. This is achieved by locating the sensor at the base of a well which is placed below a hexagonal fluid chamber—the combination of these two aspects means that the flow above the sensor is sufficiently slow and hence the response time is largely controlled by diffusion. The authors present simulation studies of the fluid flowing through the channel, governed by the diffusion of the cations to the sensor surface, and look at the sensor response. The results from a detailed numerical study were compared with experiments involving different solutions (pH and potassium cations) at different concentrations and interpreted using a mathematical model. The results are then put into a general context in the conclusion.

2 Experimental and theoretical methodology

2.1 Fabrication

The ISFETs were obtained commercially from Sentron Europe. The devices are encapsulated, thereby exposing only the sensitive area of the ISFET, as seen in Fig. 1 (inset).

The multilayered microfluidic platform comprises a polydimethylsiloxane (PDMS) microfluidic chip, planar electrodes, and the sensing layer (Fig. 1). The PDMS chip was fabricated using a standard moulding technique as described earlier (Hofmann 2005) (Duffy et al. 1998). Sylguard 184 monomer and the curing agent (ratio 10:1)

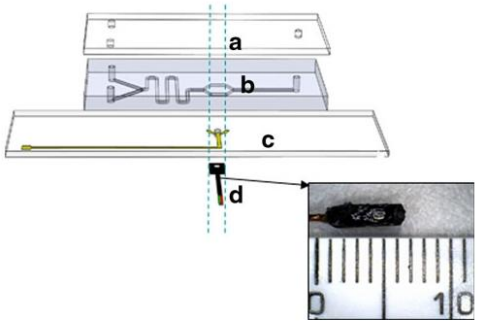

Fig. 1 Exploded view of the microfluidic. The device comprises **a** a glass cover plate for tubings, **b** a PDMS microchip, **c** a planar electrode with Au/Ti electrode on a glass slide with 1-mm hole for access to sensitive area of the ISFET, and **d** an ISFET sensor. The separation between the *vertical lines* in the inset is 1 mm. The *inset* shows an encapsulated ISFET and the geometry used in the computational study. As can be seen, the *black* encapsulation layer insulates the ISFET only exposing the sensitive gate surface

were poured into a photo-lithographically pre-fabricated SU-8 mould and left to cure overnight. The PDMS was the cut and peeled off the mould. This chip has two inlets with meanders leading to hexagonal chamber and finally terminates with an outlet. The microchannels are 1.0-mm wide and 1.0-mm deep.

The gold planar reference electrode on glass used for pH sensing was fabricated by standard photolithography and liftoff. AZ5214 photoresist was spun on a glass slide. Using a mask aligner and a photo mask, the areas where the gold electrodes are desired, were exposed and developed. The slide was then placed in an evaporator and 10 nm of Titanium and 40 nm of gold were deposited. The photoresist was stripped-off using acetone leaving the desired planar patterned gold electrode on the glass slide. For potassium sensing, the silver planar electrodes were fabricated in the same manner as described before with silver evaporated and later modified using $FeCl_3$ to obtain Ag/AgCl reference electrode.

The ISFET readout circuit used for these experiments was based on the circuit described by Bergveld (1972). The top amplifier, connected as a buffer, makes sure that the ISFET drain current and drain source voltage were fixed at 100 μA and 500 mV, respectively. In this so-called drain follower configuration, with the remote gate voltage grounded (reference electrode to ground), the voltage across the resistor R is equal to the source drain voltage V_{DS}. Since the current source is fixed and the V_{DS} was constant, the current sink determines the drain current and the source voltage can be sensed and fed to the output through the bottom amplifier. Thus, the source voltage is used to trace the gate potential variations due to the ionic concentration changes.

K^+ChemFETs were obtained by solvent casting of a conventional plasticized carboxylated polyvinyl chloride membrane (PVC-COOH) (66% w/w), containing valinomycin (1% w/w) and plasticiser (33% w/w) on the ISFET sensing membrane, after appropriately adapting existing protocol (Chudy et al. 2001).

The glass and PDMS layers were aligned and bonded together after their exposure to oxygen plasma for 1 min at a pressure of 0.8 mBar using an oxygen plasma instrument (Diener Technologies). The encapsulated ISFET and K^+ChemFET were attached to the microfluidic system using Araldite instant clear epoxy adhesive. These K^+ChemFETs were found to be stable for 1 week and could be stripped off the microfluidic platform using a surgical blade and replaced by new ones.

2.2 Numerical simulation of fluid flow and ion diffusion

The purpose of the computational study was to examine the influence of flow rate and ion diffusivity on the response of the device to changes in ion concentration.

These transport process were analysed using a commercially available software package (ANSYS CFX 5.0). The flow was assumed to be incompressible, isothermal and to consist of water at 25°C whose properties are (dynamic viscosity 8.9×10^{-4} kg/ms and density 997 kg/m^3). The transport of ions (H^+ and K^+) was modelled based on the realistic assumption that they were passive (and did not affect the fluid properties), whose evolution could be described by a linear advection diffusion equation with a diffusivity which is independent of the ion concentration. These assumptions are realistic for this problem. The characteristic Reynolds number of the flow $Re = Q/hw$ was low ($\sim$1–10) so that the flow is steady and symmetric about a mid vertical plane. To reduce computation burden, reflectional symmetry was employed and after discretising the domain gave a mixed grid with 223756 elements. The diffusive transport process was analysed by initialising the whole concentration field with $\hat{C} = 1$ and placing an inlet condition of $\hat{C} = 0$. The sweeping of material from the well provided a clear indication of how the flow rate and diffusivity affected changes in concentration at the base of the well ($\hat{C}_S$). The flow in the computational model was defined in terms of an inlet (top-hat) flow field normal to the inlet plane and a zero gauge pressure on the outlet plane.

2.3 Device operation

A schematic of the integrated device is shown in Fig. 1. The platform consists of a top glass cover plate that allows interfacing with a peristaltic/syringe pumps via tubings. Below the glass cover plate is the PDMS microfluidic chip. The central hexagonal part of the microfluidic chip (of width $w_H = 5$ mm) provides the necessary chamber volume and sits above the planar reference electrode and the active gate area of the ISFET. The solution in the microfluidic chip comes in contact with the sensitive area of the ISFET through the 1-mm hole drilled on the glass slide.

2.4 Measurements

The functioning of the chemical sensor was demonstrated by testing the H^+ ion detection properties. Potential hydrogen (pH) measurements were studied using three standard buffer solutions (pH 4.0, 7.0, and 10.0). All the measurements were performed at a constant temperature (20°C) in a beaker, against both Au, and Ag/AgCl reference electrodes.

The K^+ChemFETs were obtained by modifying ISFETs as described before. These K^+ChemFETs were used for titrations with solutions in the range of 10^{-4} to 10^{-1} M. Titrations were done in pure DI water and PBS saline solutions. All potentials were measured against an Ag/AgCl reference electrode. The K^+ChemFET s was operated at constant drain current, $I_{DS} = 100$ μA and constant drain-source voltage, $V_{DS} = 500$ mV.

The ISFET-based microfluidic device was connected to a syringe pump. Different pH solutions were pumped through the device at flow rates of $Q = 100$, 250, and 500 μl/min. Devices with K^+ChemFET were connected to syringe pumps and KCl salt solutions pumped in the device in the range of 1 μM–1 M potassium concentration at flow rates of 100, 125, and 250 μl/min. A National Instruments data acquisition module was used with LabView program to collect data at 100 Hz. The measured time-series enabled the response time of the device t_D corresponding to the time its takes for the voltage (or pH) to reach 90% of its final value. This time is proportional to the (e^{-1}) response time of the normalised concentration ($\hat{C}_S$), where $t_D \sim 4t_R$.

3 Results and discussion

The main objective of this study is to demonstrate functional integration of encapsulated ISFET-based sensors with microfluidic platforms. In the process, the authors have introduced a device design comprising a sensor that is located orthogonal to the microchannel. The fluid flows perpendicular to the sensor and the cation diffuse through a 1-mm diameter, 1-mm deep cylindrical well.

3.1 Solid state sensors integrated to microfluidic chip

The potentiometric response of the microfluidic device with ISFET sensor for flow rates of 100, 250, and 500 µl/min for the three pH solutions is depicted in Fig. 2. The sensitivity values measured are 49.67, 48.83, and 34.72 mV/pH unit, respectively. The microfluidic device with ISFET sensor shows a good response for different pH solutions at flow rates of 100 and 250 µl/min. Higher flow rates affect the sensor performance as evident from the response time data for 500 µl/min. This could be attributed to a diffusion limiting step because of a shorter residence time of the fluid in the chamber.

The K^+ChemFET sensor showed a good potentiometric response to manual as well as syringe-based injections of various potassium concentrations varying from 10^{-2} to 10^{-6} M. Above a KCl concentration of 10^{-2} M, the device is weakly dependent on concentration because at higher concentrations the sensor surface gets saturated with potassium ions making detection difficult.

The characteristic response time of the device for different flow rates was estimated from the response curves by examining the time taken for the measured potentiometric response to reach a steady value following a change in species concentration. Figure 3 shows the variation of the response time with flow rate.

3.2 Simulation of fluid dynamics

Transient simulations were undertaken using the same geometry as the experiments and flow rates of $Q = 50$, 100, 250, and 500 µl/min for H^+ (or K^+). The ions were treated as passive material whose spreading is described by a linear advection–diffusion equation characterised by a constant diffusion coefficient. A concentration C_∞ of ions was injected into the device with had an initial concentration of C_0; the normalised concentration $\hat{C} = (C - C_0)/(C_\infty - C_0)$, which takes values between 0 and 1 was calculated as a function of time and position. The concentration field at the base of the sensor well, C_S, was calculated, and from this the pH $\mathrm{pH} = -\log_{10} C$.

Figure 4 shows a table of the concentration field $\hat{C}$ for H^+ in water for contrasting times and volume flow rates. The normalised concentration field at the midpoint of the base of the well $\hat{C}_S$ was calculated as a function of time and is taken as a proxy measure of the concentration at the sensor surface. Figure 5a illustrates the typical variation of $\hat{C}_S$ (for protons) with time for different flow rates, which confirmed the exponential decay in $\hat{C}_S$ with time. Lines of best fit, of the form $\hat{C}_S = \exp(-(t - t_0)/t_R)$, where t_0 is the time the normalised concentration starts to decay, were calculated for the period after which the concentration field

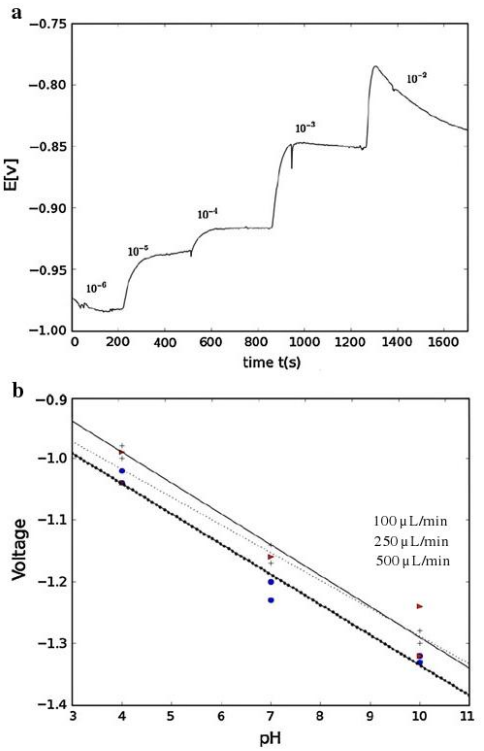

Fig. 2 **a** Potentiometric response of microfluidic devices for fixed flow rates $Q = 100$ µl/min, for K^+ChemFET. The concentration of KCl in M is given in the graph. **b** This shows the calculation curve for the pH sensor for different flow rates, the *red triangles* represent flow rate of 500 µl/min; the *blue circle* represents 250 µl/min; while the *crosses* represent flow rate of 100 µl/min. The trend lines for 100, 250, and 500 µl/min are shown by the *dotted*, *straight*, and *thick dotted lines*

began to decay. Figure 5bi and bii together shows the difference between how the ion concentration and pH approach saturated values, with the response time of the pH curve being approximately four times longer than the concentration curve. Figure 3 also shows the variation of the calculated response time t_R as function of flow rate and species type as predicted by numerical studies.

To understand the effect of diffusion on the transport from the top of the well to the sensor, the authors first consider diffusive transport described by $\partial\hat{C}/\partial t = D\partial^2\hat{C}/\partial y^2$, where y is in the vertical direction and D is the diffusion coefficient. For long time, the solution takes the form $\hat{C} \sim \exp(-t/t_R)f(y)$, where the slowest decaying solution has the form $1/t_R = (\pi/2)D/h_w^2$, where h_w is the

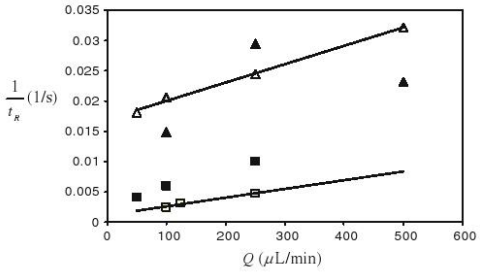

Fig. 3 A comparison between the difference response times in the ion concentration are plotted for the experiments and numerical calculations. The *fully shaded symbols* represent experimental measurements, while the *unshaded symbols* represent numerical simulations. *Triangles* represent potassium cation, while *squares* represent pH measurements

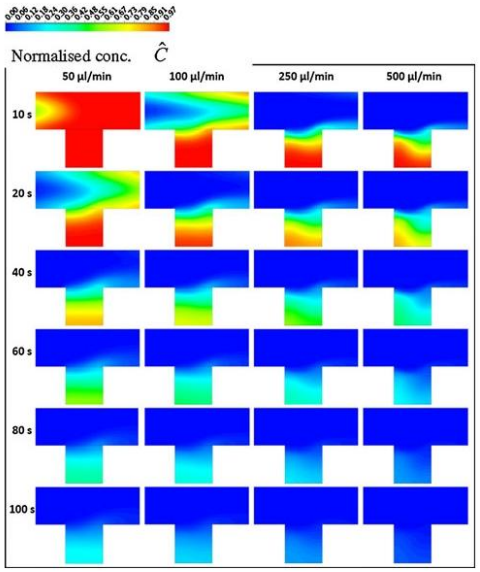

Fig. 4 Matrix of solutions showing the normalised concentration field ($\hat{C}$) in a midplane through the well at different times and flow rates

depth of the well. The effect of advection is to increase the rate of material being transported from the region above the well to the sensor head. The channel widening in the hexagonal chamber (from a channel width w to w_H, where $w_H/w = 5$) decreases the mean flow above the well head from $\bar{U} = Q/wh$ (where $h = 1$ mm is the channel depth) to $(w/w_H)\bar{U}$. The characteristic velocity within the well is a fraction of this, $\lambda(w/w_H)\bar{U} = \lambda Q/w_H h$. Since the flow in the well is driven by the shear stress at the top of the well where the flow adjusts from non-slip to slip, $\lambda \ll 1$, which gives a characteristic advective timescale, $h_W w_H h/\lambda Q$. A harmonic mean of the two characteristic timescales based on advection and diffusion provides an appropriate estimate of the response of the device to changes in the concentration. In total, this gives,

$$\frac{1}{t_R} = \frac{\pi D}{2h_W^2} + \frac{\lambda Q}{h_W w_H h}. \quad (1)$$

Equation 1 enables the responsiveness of the device to be expressed in terms of the geometry of the device, flow rate and diffusivity of the species. Figure 3b shows the variation of $1/t_R$ with Q and confirms, for the numerical calculations, the linear increase of increase response time with flow rate. The gradient of the linear fits for the pH and KCl simulations are the quite similar ($1.7 \times 10^6 Q$ (for pH) and $1.8 \times 10^6 Q$ (for KCl)). This suggests that $\lambda \sim 10^{-2}$. The intercept with the vertical axis provides an indication of pure diffusive transport. The authors estimated the values as $D = 1.5 \times 10^{-9}$ m^2/s (KCl) and $D = 10^{-8}$ m^2/s (pH), giving predicted intercepts (from 1) of 2.3×10^{-3} and 0.016, which compares well with the intercepts from the numerical results of 2.8×10^{-3} and 0.017, respectively. The discrepancy between experimental and numerical values appears to be greater for the protons. A plausible reason might be that protons diffuse by Grotthuss mechanism which might not be accurately reflected by the diffusion coefficient value used for the numerical studies.

4 Conclusions

We have developed a novel integrated microfluidic device which through its design is both sensitive and capable of discriminating between large and smaller ions with different diffusivities. The advection effect is substantially reduced as a consequence of both the divergent hexagonal section above the 1-mm diameter well head and the sensor located at the base of a well. Both of these design features ensure that the primary mode by which ions reach the sensors is dominated by diffusion. The novel feature is that recording a time series of the potentiometric response can enable suitably calibrated devices to discriminate between different species injected, mainly because the sensor response time is much faster than the ability of molecules to be introduced to the sensor surface.

The detailed computational study has shown that the ion concentration at the sensor surface has an exponential decay with a characteristic response time t_R whose dependence on device geometry was analysed and this is broadly confirmed by analysis of the potentiometric data.

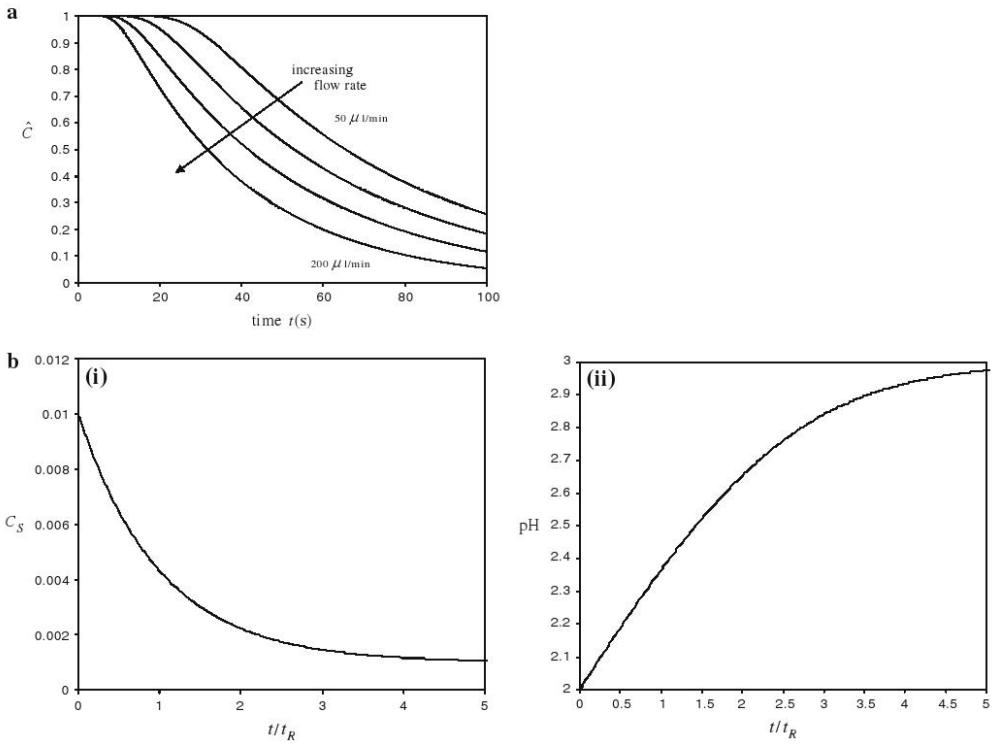

Fig. 5 **a** The variation of the normalised concentration $\hat{C}_S$ at the base of the well with time, for contrasting flow rates ($Q = 50$, 100, 250, and 500 μl/min). A log-linear plot confirms the exponential decay for large time, of the form $A\exp(-t/t_R)$ the ion concentration at the base of the well is plotted for dimensionless time in (**bi**) for the case when ions with concentration 10^{-2} are displaced by ions of concentration 10^{-3}. The corresponding change in pH is shown in (**bii**). In both the cases the flow rate is 100 μl/min

This supports the view that other physical processes might be important, such as density effects, which can be important over the long response times measured.

Although the response time of the silicon-based sensors increases when integrated to the microfluidic platform, this configuration possesses some major advantages. The ISFETs with Au reference electrode show an increased sensitivity (49.67 mV/pH unit) when integrated into a microfluidic platform compared to when used in bulk (33.27 mV/pH unit).This could be attributed to the efficient mass transport, in this case through the 1-mm diameter cavity between the microfluidic system and the sensor surface. With highly sensitive potentiostats capable of detecting 0.5 mV changes this would enable measurement of change in $\sim$0.01 unit of pH to be resolved. Moreover, this device enables the measurement of potassium cations in the range of 10^{-3} M to 10^{-6} M. The ability of the device to facilitate differential migration of analytes based on diffusion coefficients can allow measurement of cations in biological fluids without the need for major sample pre-treatments for larger molecules.

Acknowledgments The authors wish to acknowledge Vlady Bystrykivskyy for the designing of the device schematic and Suresh Vishwanathan Chettiar for help with clean-room fabrications. The authors acknowledge the use of the UCL *Legion* High Performance Computing Facility, and associated support services, in the completion of the computational aspect of this study.

References

Auroux PA, Iossifidis D, Reyes DR, Manz A (2002) Micro total analysis systems. 2. Analytical standard operations and applications. Anal Chem 74(12):2637–2652. doi:10.1021/Ac020239t

Bergveld P (1972) Development, operation, and application of the ion-sensitive field-effect transistor as a tool for electrophysiology. IEEE Trans Biomed Eng 19(5):342–351

Bergveld P (2003) Thirty years of isfetology—what happened in the past 30 years and what may happen in the next 30 years. Sens Actuator B 88(1):1–20

Chudy M, Wróblewski W, Dybko A, Brzózka Z (2001) Multi-ion analysis based on versatile sensor head. Sens Actuators B 78(1–3):320–325

Duffy DC, McDonald JC, Schueller OJA, Whitesides GM (1998) Rapid prototyping of microfluidic systems in poly(dimethylsiloxane). Anal Chem 70(23):4974–4984

Hofmann O (2005) Towards microalbuminuria determination on a disposable diagnostic microchip with integrated fluorescence detection based on thin-film organic light emitting diodes. Lab Chip 5(8):863–868

Jacquot BC, Lee C, Shen YN, Kan EC (2007) Time-resolved charge transport sensing by chemoreceptive neuron mos transistors (cvmos) with microfluidic channels. IEEE Sens J 7(9–10):1429–1434

Kim SM, Sommer GJ, Burns MA, Hasselbrink EF (2006) Low-power concentration and separation using temperature gradient focusing via joule heating. Anal Chem 78(23):8028–8035

Masadome T, Yada K, Wakida SI (2006) Microfluidic polymer chip integrated with an ISFET detector for cationic surfactant assay in dental rinses. Anal Sci 22(8):1065–1069

Milgrew MJ, Riehle MO, Cumming DRS (2005) A large transistor-based sensor array chip for direct extracellular imaging. Sens Actuator B 111:347–353

Reyes DR, Iossifidis D, Auroux PA, Manz A (2002) Micro total analysis systems. 1. Introduction, theory, and technology. Anal Chem 74(12):2623–2636. doi:10.1021/Ac0202435

Schasfoort RBM, Schlautmann S, Hendrikse L, van den Berg A (1999) Field-effect flow control for microfabricated fluidic networks. Science 286(5441):942–945

Schning M (2002) Recent advances in biologically sensitive field-effect transistors (biofets). Analyst 127(9):1137–1151

Sharma S, Buchholz K, Luber SM, Rant U, Tornow M, Abstreiter G (2006) Silicon-on-insulator microfluidic device with monolithic sensor integration for Mu-TAS applications. J Microelectromech Syst 15(2):308–313

Truman P, Uhlmann P, Stamm M (2006) Monitoring liquid transport and chemical composition in lab on a chip systems using ion sensitive FET devices. Lab Chip 6(9):1220–1228

Appendix 3

Full Paper **ELECTROANALYSIS**

Hydrogel Membrane Improves Batch-to-Batch Reproducibility of an Enzymatic Glucose Biosensor

Jakub Trzebinski,[*a, b] *Anna Radomska-Botelho Moniz*,[a] *Sanjiv Sharma*,[a] *Krishna Burugapalli*,[b] *Francis Moussy*,[b] *Anthony E. G. Cass*[a]

[a] Department of Chemistry and Institute of Biomedical Engineering, Imperial College London, South Kensington Campus, Exhibition Road, London SW72AZ, UK
[b] Brunel Institute for Bioengineering, Brunel University, Uxbridge, West London, UB83PH, UK
*e-mail: jtrzebin@imperial.ac.uk

Received: May 24, 2011
Accepted: September 13, 2011

Abstract
A permselective membrane is a critical component that defines the linear detection limits, the sensitivity, and thus the ultimate efficacy of an enzymatic biosensor. Although membranes like epoxy-polyurethane (epoxy-PU) and Nafion are widely used and provide the desired glucose detection limits of 2 to 30 mM, both the within batch and batch-to-batch variability of sensors that use these materials is a concern. The hypothesis for this study was that a crosslinked hydrogel would have a sufficiently uniform porosity and hydrophilicity to address the variability in sensor sensitivity. The hydrogel was prepared by crosslinking di-hydroxyethyl methacrylate, hydroxyethyl methacrylate and *N*-vinyl pyrrolidone with 2.5 mol% ethylene glycol dimethacrylate using water soluble initiators – ammonium persulfate and sodium metabisulfite under a nitrogen atmosphere. The hydrogel was applied to the sensor by dip coating during polymerisation. Electrochemical measurements revealed that the response characteristics of sensors coated with this membrane are highly consistent. Scanning electrochemical microscopy (SECM) was used to spatially resolve glucose diffusion through the membrane by measuring the consequent H_2O_2 release and compared with an epoxy-PU membrane. Hydrogen peroxide measurements using SECM revealed that the epoxy-PU membranes had uneven lateral diffusion profiles compared to the uniform profile of the hydrogel membranes. The uneven diffusion profiles of epoxy-PU membranes are attributed to a fabrication method that results in uneven membrane properties, while the uniform diffusion profiles of the hydrogel membranes are primarily dictated by their uniform pore size.

Keywords: Glucose biosensor, SECM, Hydrogel, Permselective membrane

DOI: 10.1002/elan.201100286

Supporting Information for this article is available on the WWW under http://dx.doi.org/10.1002/elan.201100286.

1 Introduction

A continuous glucose monitoring platform together with closed loop insulin delivery could significantly reduce the risk of complications in diabetes, as it would reduce the need for patient compliance [1]. Among the non-invasive, minimally invasive and invasive approaches being developed for such a platform [2], so far, it is the subcutaneously implanted amperometric sensors that are available for commercial use. The advantage of such sensors, based on enzymes, is that they can provide reliable glucose measurements for a relatively long period of time in vitro. For example, Yu et al. reported a coil-type sensor, coated with excess enzyme, to function in vitro for $\geq$3 months under constant polarisation [3]. However, as soon as such sensors are implanted in the body, they start losing their sensitivity due to biofouling and immune responses triggered by implantation injury, and these ultimately lead to the sensors' failure [3,4]. Several attempts were made to minimise these effects and the most recent of which include the use of hydrogel [5], collagen [6] or polylactic acid [7] as a protective coating, the suppression of immune responses using corticosteroids [8] or the promotion of neovascularisation using growth factors [9]. Most such approaches increase the in vivo sensing life of the sensors, but often, only one of many ostensibly identical sensors functions longer than a few weeks [7].

The host influence could be also assessed when having a validated process for fabricating reproducible sensors and studying their in vivo response compared with that in vitro. The continuous drift in sensitivity of implanted sensors necessitates frequent sensor recalibration.

The disadvantage of not having reproducible sensors is that there is a need for frequent recalibration before and while implanted in the host tissue [10]. As previous reports suggest [11] this could be overcome by using two sensors fabricated the same way, one with and one without the enzyme. As both sensors will experience very similar environmental effects after implantation the response for the sensor without the enzyme can be correlated to background current and extracted from glucose measure-

ments. Such set up allows measuring current caused by known (e.g. l-ascorbic acid, acetaminophen or uric acid) [12] as well as any unknown interfering agents.

The lack of reproducibility was often correlated with the fact that both needle-type and coil-type sensors are partially handmade which leaves a lot of room for variation [12]. It was also reported that the performance of the sensors (e.g. sensitivity or time response) is mainly dictated by the semi-permeable membrane coated on the sensor surface [12]. Both conclusions were based on the current response of sensors coated with Nafion or Polyurethane (PU) based membranes [13,14]. These polymers seems to be good materials for permselective membranes as they block interfering agents from reacting with the enzyme and significantly reduce glucose diffusion rates thus extending the sensors' linear range. A major disadvantage with permselective membranes for biosensors based on Nafion and PU is that small variations in curing time, humidity, or temperature during their polymerisation can cause significant variation in porosity, leading to high variability in sensor performance [15].

In this paper we present a novel hydrogel coating for a coil-type amperometric glucose sensor which acts as a permselective membrane making the sensors more reproducible. The hydrogel is based on hydroxyethyl methacrylate (HEMA), 2,3-dihydroxypropyl methacrylate (DHPMA) and *N*-vinyl 2-pyrrolidinone (N-VP) crosslinked with ethyleneglycol dimethacrylate (EGDMA). Similar hydrogels were developed for contact lenses and are widely acknowledged as a biocompatible [5]. In this case, however, the hydrogel is used as a permselective membrane. The advantage of hydrogel over Nafion or PU based membranes is that its properties are much less dependent on environmental changes (e.g. temperature, humidity or curing time) during the polymerisation, meaning that the final alignment and compactness of the polymer chains (which in turn dictates the material properties) are mainly determined by the chemical composition and not by conditions at which the polymerisation has occurred. The hydrogels having a high degree of crosslinking and uniform porosity can function as permselective membranes for biosensors, improving their performance and reproducibility.

2 Experimental

2.1 Materials

Bovine serum albumin (BSA), glutaraldehyde (GA), glucose oxidase (GOD, from *Aspergillus niger,* 155.6 units/mg), ATACS5104 epoxy adhesive, polyurethane (PU), polyethylene glycol dodecyl ether (Brij 30), tetrahydrofuran (THF), ammonium peroxodisulfate (APS), sodium metabisulfite (SMS), 2-hydroxyethyl methacrylate (HEMA), 1-vinyl-2-pyrrolidone (NVP), ethylene glycol dimethacrylate (EGDMA), polyethylenimine (M_w 25,000) branched (PEI), phosphate buffer saline (PBS) tablets and eosin were obtained from Sigma-Aldrich, UK. HEMA, NVP and EGDMA were purified by vacuum distillation before use. 2 mm thick polyvinyl acetate (PVA) sheets were purchased from Ceiba Technologies (Chandler, AZ, USA). 2,3-dihydroxypropyl methacrylate (DHPMA) was purchased from Polysciences Inc. (Warrington, PA, USA). Teflon coated Platinum–Iridium (Pt-Ir, 9:1 weight ratio, ∅ = 0.125 mm) and Silver (Ag, ∅ =

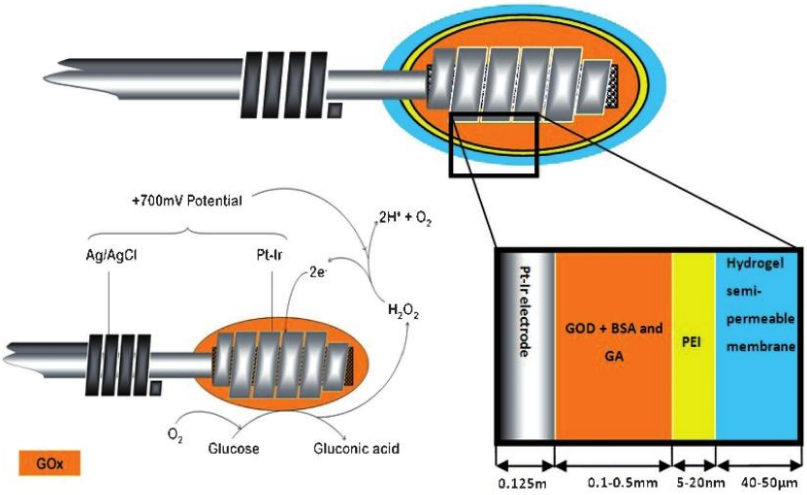

Fig. 1. Schematic representation of hydrogel coated sensor with a description of each layer and a diagram presenting enzyme based amperometric sensor working principle.

0.125 mm) wires were obtained from Medwire (Mt. Vermon, NY, USA).

2.2 Preparation of Glucose Biosensor

The sensors were prepared in a similar fashion to that previously described [5,12]. The sensor is a two electrode system containing a coil-type Pt-Ir anode as the working electrode and silver/silver chloride (Ag/AgCl) as the reference electrode.

2.2.1 Working Electrode

1 cm of Teflon coating was stripped from each end of 7 cm long Teflon coated Pt–Ir wire. One end was carefully wound around a 30 gauge 1/2 inch hypodermic needle to obtain a coil end (8 windings) of the sensor. The coil chamber was reinforced with cotton to ensure stability of immobilised enzyme gel and prevention of air bubble formation. The cotton reinforced Pt-Ir coils were then sonicated in distilled water for 30 min followed by 20 min wash in absolute ethanol to remove any impurities and dried at 60 °C for 20 min.

2.2.2 Enzyme Loading

About 2.5 μL of enzyme loading solution (12 mg of BSA, 2.5 mg GOD and 5 μL of GA dissolved in 300 μL of deionised (DI) water) was applied on the cotton reinforced Pt-Ir coil and air dried at room temperature for about 1 h. This procedure was repeated three times and the resulting enzyme gels on sensor coils were allowed to crosslink overnight.

2.2.3 Reference Electrode

1 cm of Teflon coating was stripped from each end of a 6 cm long Teflon coated silver wire. One end was carefully wound around a 30 gauge 1/2 inch hypodermic needle to obtain a coil end (8 windings) of the sensor. The Ag-coil was treated with ammonia solution for 30 s followed by 6 M nitric acid for 10 s. The coil was then washed in DI water and oxidised in 0.01 M HCl at a constant current of 0.1 mA using a galvanostat (263A, Princeton Applied Research, TN, US) overnight. The resulting Ag/AgCl reference electrode coils were rinsed with DI water. The sensors were assembled by passing the free-end of the Pt-Ir working electrode wire through the Ag/AgCl reference electrode coil. The Teflon coated Ag and Pt-Ir wires were wound up such that the Ag/AgCl coil is separated from the enzyme loaded Pt-Ir coil by a distance of about 5 mm.

2.3 Sensor Coatings

2.3.1 Epoxy - Polyurethane Membrane

The epoxy-polyurethane loading solution was prepared by dissolving 26.7 mg of PU in 4 mL of THF and 1 mg Brij 30, 17.8 mg each of Part A and Part B of epoxy adhesive as previously described [5]. The sensors were coated by applying 1–1.5 μL of the loading solution and air dried at room temperature for 30 min following by 20 min curing in oven at 80 °C. The sensors were then cooled to room temperature, followed by storage immersed in PBS (pH 7.4) at 4 °C until further use.

2.3.2 Hydrogel Membrane

In order to increase the affinity of the polymer chains of hydrogel for the enzyme surface, the sensor assembly including the enzyme coated Pt-Ir coil and Ag/AgCl reference coil were dipped in a 0.1 M PEI (MW=25kDa, branched polycation) solution under continuous stirring for 30 min followed by 30 min washing in DI water.

For the preparation of hydrogel coatings, the monomer mixture was prepared by mixing 5 mol% VP, 46.25 mol% HEMA, 46.25 mol% DHPMA and 2.5 mol% EGDMA and diluted 1:1 with DI water. The monomer mixing ratio was chosen based on previous report [5], with the exception of the crosslinker concentration. The solubility of the crosslinker EGDMA reached saturation above 2.5 mol% when the monomer solution was diluted at 1:1 ratio with water. At the high crosslinking concentration (2.5 mol%), the hydrogels were expected to have very low porosity allowing it to function as a mass-transport limiting membrane for the sensors. The main hydrophilic components for the hydrogel, HEMA and DHPMA were kept at 1:1 ratio, while that of VP was 5 mol% of total monomer content.

To coat the sensors with hydrogel, a vertically aligned 3 ml disposable syringe with plunger removed and nitrogen supply attached to the needle end was used. The monomer mixture was poured into the syringe, and held within the syringe by nitrogen gas flow. The solution was deoxygenated for at least 5 min with N_2 gas bubbling. For the free-radical polymerization, 1.5 mol% SMS was added to monomer mixture and allowed to mix uniformly (assisted by N_2 gas bubbling). After about 5 min 1.5 mol% APS was added drop-wise to initiate the polymerization. The temperature of the reaction was constantly monitored using an Apollo 4000 temperature microsensor (World Precision Instruments, Inc. Sarasota, FL). Three or four sensors were firstly immersed in the reaction mixture and then raised above the reaction mixture before the reaction gel point was reached. A rapid increase of 5–10 °C in the temperature was used as the indication for removing the sensors from the reaction mixture. The sensors were left in the N_2 atmosphere within the syringe, but above the reaction mixture, for about 20 min after the gel point was reached. Care was taken to prevent the sensors touching the syringe walls. Thereafter,

the sensors were suspended vertically in air at room temperature for an additional 2 h, then transferred to PBS and stored at 4 °C until further use. The schematic representation of the hydrogel coated sensor and its working principle is shown in Figure 1 and a photograph of the assembled sensor in Figure S1 in the Supporting Information.

The integrity and nature of the hydrogel coating on the sensor was tested by hematoxylin-eosin staining. The hydrogel coated sensors were stained in hematoxylin solution for 20 min, washed in running tap water for 10 min, stained in eosin for 20 min, washed in running tap water for 10 min and finally washed in DI water. The stained sensor was examined visually for staining under a Nikon Eclipse optical microscope. The cross-section of the sensor coatings was also observed using an optical microscope. The sensor was glued vertically on a glass slide and the coatings at the tip of the sensor were manually cut using a scalpel blade to expose coating cross-section for microscopic observation.

2.4 Electrochemical Measurements of the Sensor Response

The electrochemical measurements were performed using Apollo 4000 Amperometric Analyzer (World Precision Instruments Inc., Sarasota FL). Before measurements the sensors were polarized at 0.7 V vs. Ag/AgCl electrode until a stable current was observed. Calibration plots were obtained by measuring the current while increasing the glucose concentration from 0–30 mM (stepwise). The response time was calculated as 90 % of the maximum response time after increasing the glucose concentration from 5 to 15 mM. The sensitivity (S) of each sensor was calculated from the following formula:

$$S = (I_{15mM} - I_{5mM})/10$$

where I_{15mM} and I_{5mM} are the steady state currents for 15 and 5 mM glucose concentration respectively.

2.5 Characterisation of the Hydrogels

Following the functional efficacy testing of sensor responses in PBS pH 7.4, and ascertaining that the hydrogel membrane functioned as a mass-transport limiting membrane, the hydrogel was further characterized to elucidate structure-function relationships.

2.5.1 Symmetric Cross-Section Morphology

The hydrogels were fabricated by a phase separation process, thus their structural properties depend on the water uptake during the polymerisation [16]. To investigate this phenomenon Scanning Electron Microscopy (Variable Pressure SEM JEOL JSM 5610 LV) was used. Three types of samples were prepared, all having the same chemical composition as membranes (see above). The specimens were polymerised at 90 %, 50 % and 0 % humidity at room temperature. After washing with DI water, the samples were stored for one week at room temperature in PBS (changed daily) to hydrate the samples and freeze-dried for SEM imaging.

2.5.2 Fourier Transform Infrared Spectroscopy (FTIR)

To determine the differences in chemical composition between the skin and bottom layer of hydrogel, FTIR was used. IR spectra were recorded at room temperature in the mid-infrared range (4000–650 cm^{-1}) using attenuated total reflectance Fourier Transform Infrared (ATR-FTIR) Spectrometer (FTIR-8300, Shimadzu Europe Ltd., Duisburg, Germany). The membranes were fabricated as described above (see 'Symmetric cross-section morphology') with 90 % humidity as this produced membrane with a thick skin layer. After hydration the two layers were separated with a scalpel blade and freeze-dried prior to FTIR characterisation.

2.6 Scanning Electrochemical Microscope (SECM) Experiments

SECM is a commonly used technique to analyse and map the enzyme activity of surfaces [17–19]. In this study we demonstrate that SECM is also a feasible method to characterise membrane functional performance and permeability to the substrate. The constant height, generation – collection imaging mode was used as in presence of glucose the GOD enzyme produces a redox–active substrate (H_2O_2) which than can be directly correlated to the consumption of glucose by the enzyme.

2.6.1 Sample Preparation

In order to analyze the membrane properties, epoxy–PU and hydrogel coated sensor surrogates were prepared. 1 mm thick PVA film was glued to a glass microscope cover slip. Care was taken in order to ensure that the film is laid flat on the glass slide. Next, the samples were coated with glucose oxidase and either the epoxy–PU or hydrogel membrane was deposited in the same manner as for the sensors. Subsequently the samples were scanned using an Optical Profilometer (Xyris 4000 CL, TaiCaan Technologies, Southampton, UK) in order to assess their flatness. The surrogate sensors were stored in PBS at +4 °C.

2.6.2 SECM Measurements

SECM measurements were done using a 10 μm diameter Ultramicroelectrode (UME) and an SECM M370 (Uniscan Instruments Ltd, Buxton, UK). Ag/AgCl and platinum were used as reference and counter electrodes respectively. In all experiments a potential of +0.7 V was used as cyclic voltammetry confirmed this is suitable for hydrogen peroxide detection at the UME. The samples

were tested in 50 mM glucose/PBS solution. The sample was positioned in the middle of the SECM three-electrode cell and an approach curve was measured in order to obtain exact information about the distance from the sample. Subsequently the UME was then positioned 100 μm above the sample surface and an area of 36 cm^2 was scanned. The measurements were taken at 100 μm intervals in both x and y direction with a10 μm/s scan velocity and a 1 s sample predelay.

3 Results and Discussion

3.1 Hydrogel Membrane

The sensors were stained with H&E in order to allow easier observation of transparent hydrogels under the optical microscope. Visual examination of the sensors confirmed that the sensing elements are fully coated with the hydrogel and no enzyme is directly exposed to the surrounding environment. To measure the thickness of hydrogel membrane the sensing elements were glued to a glass slide and sectioned perpendicularly to the working electrode coil in order to expose all layers (see Figure S2 in the Supporting Information). The uniformly dispersed hydrogel membrane was interconnected with underlying GOD/BSA layer and had a thickness of 41.4 ± 9.8 μm.

3.2 Response Characteristics of the Sensor

As previously reported [12] the response of coil type amperometric glucose sensors is mainly determined by the permselective membrane properties (morphology and pore structure) and their distribution across the sensor surface. Although not widely acknowledged in the scientific literature, the reproducibility of such sensors is often quite poor. Here we present a hydrogel mass-transport limiting membrane, which, while polymerising, is less susceptible to environmental changes, and when handled with care can be uniformly dispersed on top of a sensor surface. Figure 2 shows a typical calibration curve in re-

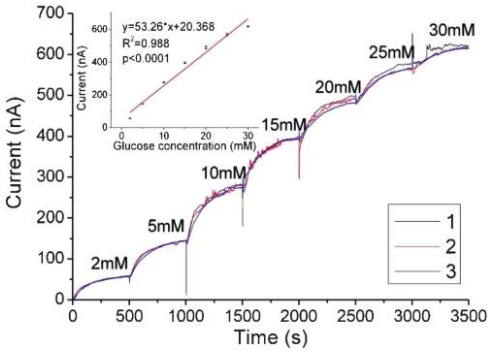

Fig. 2. Current response to a stepwise glucose concentration increase for three sensors (1, 2 and 3) coated with hydrogel which acts as a semi-permeable membrane (and the calibration curve in inset). The measurements were done 60 days after sensor fabrication. $R^2 = 0.997 \pm 2\%$ in glucose concentration varying from 0–30 mM.

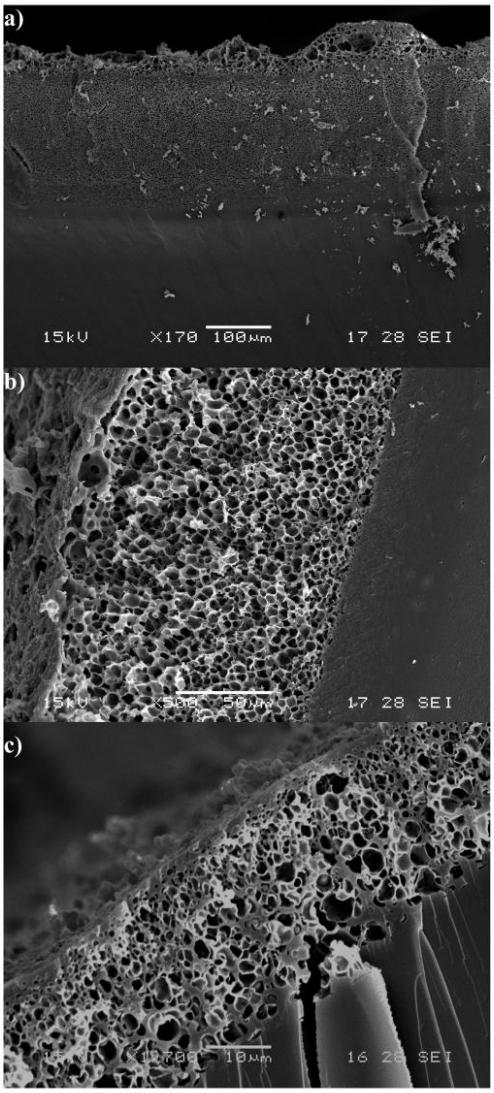

Fig. 3. SEM pictures of membranes skin layer. Hydrogels were polymerised at room temperature in a) 90% humidity (scale bar 100 μm), b) 50% humidity (scale bar 50 μm) and c) nitrogen atmosphere (0% humidity, scale bar 10 μm). The thicknesses of porous skin layer are 230 ± 4 μm, 137 ± 3 μm and 26 ± 1 μm respectively.

sponse to step increase of glucose concentration (0–30 mM) of three sensors coated with such a hydrogel membrane, measured 60 days after the sensors were fabricated. The sensors respond to changes in glucose concentration in a nearly identical way having very similar response times (4 min 20 s ± 3 s, $n=3$) and sensitivity (25.2 nA/mM ± 6%, $n=3$). The linearity of the sensors was acceptable ($r^2=0.997\pm2\%$) for glucose concentrations varying from 0–30 mM which meets the requirement for in vivo glucose monitoring [2]. Two types (hydrogel and epoxy-PU) of sensors were compared in order to determine their reproducibility. To quantify the variations, each sensor was calibrated with step increases of glucose concentration (0–30 mM). Subsequently the data was fitted to a linear equation and the slope was determined for each sensor. For the hydrogel coated sensor, 60 days after fabrication the slope was 20.37 ± 0.18 ($n=4$) and for the sensors coated with epoxy–PU membrane 5.70 ± 7.15 ($n=4$).

To evaluate the long-term performance, four sensors were kept in 5 mM glucose solution for 60 days. At day 2, 5, 11 and 60 all sensors were calibrated and the sensitivity of each sensor was calculated. The sensitivity of the sensors significantly increases from day 2 to 11 and remains stable up to day 60 (see Figure S3 in the Supporting Information). The increase of the sensitivity in the first couple of days can be attributed to the BSA matrix needing time to fully hydrate, which in the case of a hydrogel membrane is quicker than with a PU membrane (21 days, [3]).

3.3 Characterisation of the Hydrogels

3.3.1 Symmetric Cross-Section Morphology

As seen in Figure 3 the hydrogel membrane is composed of two very distinct layers. The inner layer has a uniform, non-porous structure and its main function is to limit the diffusion of glucose. The outer (skin) layer has a very porous and uniform structure whose main function is to promote cell in growth. As it is seen from SEM pictures both layers are very well organised which contributes significantly to the reproducibility of the sensors.

The influence of humidity on hydrogel structural properties was investigated. As seen in Figure 3 the thickness of skin layer decreases with reduced humidity. This can be attributed to a relatively high crosslinker concentration and higher water accumulation at the surface of the hydrogel during the polymerisation (which in dry environment can be minimised). The permselective behaviour of the hydrogel relied on the solubility of glucose and oxygen in the membrane and controls the reactant flux to the enzyme.

3.3.2 Fourier Transform Infrared Spectroscopy (FTIR)

The chemical composition of both morphologically different hydrogel layers appears to be the same based on their FTIR spectra (see Figure S3 in the Supporting Information). This confirms that the permselectivity of the membrane mainly depends on the inner layer's morphological properties, as the outer layer appears too porous to be a diffusion barrier for glucose/oxygen.

3.4 Scanning Electrochemical Microscopy (SECM) Experiments

Scanning Electrochemical Microscopy was used in order to map the enzyme activity on the planer sensors. This technique involved measuring hydrogen peroxide concentration within close proximity to the sensor surface. As hydrogen peroxide is a direct product of the enzyme reaction it can be used as an indicator of the rate at which glucose is converted. Thus, mapping the H_2O_2 concentration on top of a sensor, as seen in Figure 4, can assess the

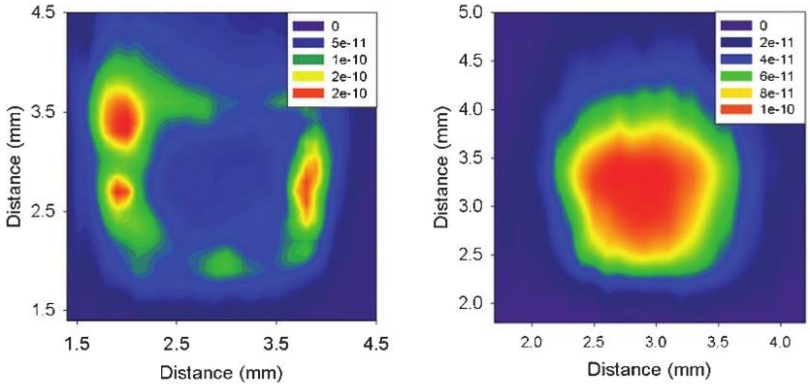

Fig. 4. SECM images of H_2O_2 diffusion through epoxy-PU (left) and hydrogel (right) membranes coated on GOD immobilised on BSA by GA crosslinking, assembled on polyvinyl alcohol sheets.

glucose diffusion. SECM results clearly show that the epoxy-PU membranes do not have uniform lateral transport properties which will have an effect on the reproducibility of the sensors. The membrane shows higher permeability at the sides and virtually none in the centre. On the other hand, hydrogel coated sensors show uniform H_2O_2 transport which indicates consistent glucose conversion at the interface between the hydrogel and the enzyme.

4 Conclusions

We have presented a novel hydrogel based mass transport limiting membrane for enzymatic glucose biosensors. The membrane was characterised in terms of morphology and chemical composition, which revealed it comprises of two chemically very similar but morphologically distinct layers. Sensors coated with such membranes had nearly identical response to the change of glucose concentration which was confirmed by electrochemical measurements (presented in Figure 2). SECM microscopy was used to explore this phenomenon further. The results indicate that the diffusion of glucose through hydrogel membrane is much more uniform than that through commonly used PU based membranes. To conclude, the hydrogel coatings are good candidates to replace the commonly used permselective membranes as they allow fabrication of reliable and reproducible sensors, whose efficacy is not affected by the preparation conditions.

References

[1] H. D. H. Shamoon, N. Engl, *J. Med.* **1993**, *329*, 977.
[2] N. S. Oliver, C. Toumazou, A. E. Cass, D. G. Johnston, *Diabet. Med.* **2009**, *26*, 197.
[3] B. Yu, Y. Ju, L. West, Y. Moussy, F. Moussy, *Diabetes Technol. Ther.* **2007**, *9*, 265.
[4] N. Wisniewski, F. Moussy, W. M. Reichert, *Fresenius J. Anal. Chem.* **2000**, *366*, 611.
[5] B. Yu, C. Wang, Y. M. Ju, L. West, J. Harmon, Y. Moussy, F. Moussy, *Biosens. Bioelectron.* **2008**, *23*, 1278.
[6] Y. M. Ju, B. Yu, L. West, Y. Moussy, F. Moussy, *J. Biomed. Mater. Res. A* **2010**, *92*, 650.
[7] H. E. Koschwanez, F. Y. Yap, B. Klitzman, W. M. Reichert, *J. Biomed. Mater. Res. A* **2008**, *87*, 792.
[8] Y. M. Ju, B. Yu, L. West, Y. Moussy, F. Moussy, *J. Biomed. Mater. Res. A* **2010**, *93*, 200.
[9] W. K. Ward, M. J. Quinn, M. D. Wood, K. L. Tiekotter, S. Pidikiti, J. A. Gallagher, *Biosens. Bioelectron.* **2003**, *19*, 155.
[10] J. Wang, *Talanta* **2008**, *75*, 636.
[11] R. A. Jeong, J. Y. Hwang, S. Joo, T. D. Chung, S. Park, S. K. Kang, W. Y. Lee, H. C. Kim, *Biosens. Bioelectron.* **2003**, *19*, 313.
[12] B. Yu, N. Long, Y. Moussy, F. Moussy, *Biosens. Bioelectron.* **2006**, *21*, 2275.
[13] R. C. Mercado, F. Moussy, *Biosens. Bioelectron.* **1998**, *13*, 133.
[14] B. Yu, Y. Moussy, F. Moussy, *Front. Biosci.* **2005**, *10*, 512.
[15] G. M. S. Brzezinski, T. Nowak, H. Schmidt, D. Marcinkowska, A. Kaleta, *Fibres and Textiles in Eastern Europe* **2005**, *13*, 54.
[16] M. Ulbricht, *Polymer* **2006**, *47*, 2217.
[17] J. L. Fernandez, C. Hurth, A. J. Bard, *J. Phys. Chem. B* **2005**, *109*, 9532.
[18] G. Wittstock, *Fresenius J. Anal. Chem.* **2001**, *370*, 303.
[19] T. Wilhelm, G. Wittstock, R. Szargan, *Fresenius J. Anal. Chem.* **1999**, *365*, 163.

Appendix 4

Lab on a Chip

Dynamic Article Links

Cite this: DOI: 10.1039/c1lc20885c

www.rsc.org/loc

PAPER

Microfluidic device to investigate factors affecting performance in biosensors designed for transdermal applications

Jakub Trzebinski,*[ab] Sanjiv Sharma,[a] Anna Radomska,[a] Kostis Michelakis,[a] Yangyang Zhang[a] and Anthony E. G. Cass[a]

Received 14th September 2011, Accepted 8th November 2011
DOI: 10.1039/c1lc20885c

In this work we demonstrate a novel microfluidic based platform to investigate the performance of 3D out-of-plane microspike array based glucose and lactate biosensors. The microspike array was bonded with a glass slide and modified with glucose oxidase or lactate oxidase using covalent coupling chemistry. An epoxy-polyurethane based membrane was used to extend the linear working range (from 0 to 25mM of substrate) of these biosensors. Both lactate and glucose sensors performed well in the clinically relevant substrate concentration range. Glucose microspikes were further investigated with respect to the effects of substrate transfer by incorporation into a microfluidic system. Data from the microfluidic system revealed that the sensor response is mainly dependent on enzyme kinetics rather than membrane permeability to glucose. The robustness of the sensors was demonstrated by its consistency in performance extending over 48 h.

Introduction

The response of amperometric biosensors can be limited either by enzymatic kinetics or mass transport effects.[1] Although these phenomena have been investigated for simple planar sensor designs[2] there is not enough evidence for more complex electrode geometries such as out-of-plane three dimensional electrodes. We present a microfluidic based system to study mass transport of glucose and lactate microspikes based sensors. These studies are useful in understanding and optimizing the physical and chemical aspects of a biosensor to ensure high performance prior to *in vivo* studies.

Microfluidics systems have been extended to various fields such as point of care diagnostic devices,[3] microreactor systems,[4] cell culture assays[5] and combinatorial chemistry and drug discovery systems.[6] Microfluidic based *in vivo*-surrogate assay platform for cell-based studies [7] and microscale cell culture analogue system[8] have been also described before. In this study, we attempt to mimic the behaviour of sensors monitoring the transdermal substrate concentration using a simple microfluidic system incorporated with a functionalised set of microspikes.

The use of micron sized structures for delivery of drug molecules and vaccines[9] has become popular over the last decade because it is minimally invasive and painless.[10–17] These hollow, micron sized structures are referred to as "microneedles".[18,19] Polymer and silicon based microneedles have been used for transdermal drug delivery of small molecules such as insulin.[20] These approaches of using such structures as biosensor platforms are based on sampling the interstitial fluid (ISF) followed by offline analysis.

We refer to our structures as "microspikes" as they are not hollow and the substrate material is a smart material that acts as a sensor surface. In this specific application it was also more beneficial to use microspikes as they exhibit extensive robustness and eliminate the problem of clogging associated with hollow microneedles. Compared to planar electrochemical sensors, the three dimensional structure of the microspikes provides larger surface area which results in an increased current hence greater signal to noise ratio. It also allows higher enzyme loading which in turn leads to longer time performance of the biosensor.

Monitoring of glucose and lactate concentrations in blood or interstitial fluid is vital towards understanding the physiological state. Abnormal blood glucose levels (lower than 3.6 or greater than 5.8 mM[21]) are indicative of conditions such as diabetes and are also useful in understanding the course of treatment administered. Similarly, monitoring lactate in blood or interstitial fluid is useful in conditions such as sepsis and muscle fatigue. In both cases a significant improvement is observed when the measurements are done continuously and the treatment is adjusted accordingly. Various approaches have been described for continuous monitoring of glucose in biofluids. These include optical, microprobe, intravenous implantable, microdialysis or subcutaneously implanted sensors.[21,22] Minimally invasive transdermal sensors would offer advantage over these and when

[a]*Institute of Biomedical Engineering & Department of Chemistry, Imperial College London, South Kensington Campus, Exhibition Road, London, SW7 2AZ, UK. E-mail: jtrzebin@imperial.ac.uk*
[b]*Brunel Institute for Bioengineering, Brunel University, Uxbridge, West London, UB8 3PH, UK*

ART ■ C1LC20885C

combined with an insulin pump have a great potential for glucose closed loop therapy.

Materials and methods

Chemicals

All chemicals were purchased from Sigma-Aldrich, unless otherwise stated.

Microspikes fabrication

The polymer based microspikes were fabricated using the method reported by Kim *et al.*[23] and were subsequently conformally metallised with gold (see Fig. 1). The microspike arrays were spin coated with a photoresist to isolate the individual spikes. Prior to the functionalization, the microspike array was glued onto a glass slide patterned with planar silver electrodes. Photoresist from a part of the array platform (see Fig. 2) was dissolved using acetone to expose the metal layer. This region was then connected to the silver electrode contact pads using silver epoxy resin. A separate silver pattern was modified with 0.1M $FeCl_3$ as described earlier[24] to serve as both reference and counter electrode. For measurements in bulk solution an external Ag/AgCl reference electrode was used.

Microspike functionalization

The microspikes were cleaned with 0.5M H_2SO_4 and electroplated with gold using full bright cyanide free gold plating solution (Gold ECF 60, 10g l^{-1} of Au, pH = 9) in order to lower the resistance of the obtained material. A standard three electrode cell comprising of a working, reference and counter electrodes consisting of microspikes, Ag/AgCl and platinum gauze respectively was used. Only the gold coated part of the microspikes was exposed to the electroplating solution. Gold metallization was conducted using eight cycles of three potential sequences (0.3V for 20s, −0.6V for 0.1s and −0.5V for 800s). These samples were tested using cyclic voltammetry (0–0.4V at 50mV s^{-1} scan rate) in 0.1M PBS solution containing 1mM

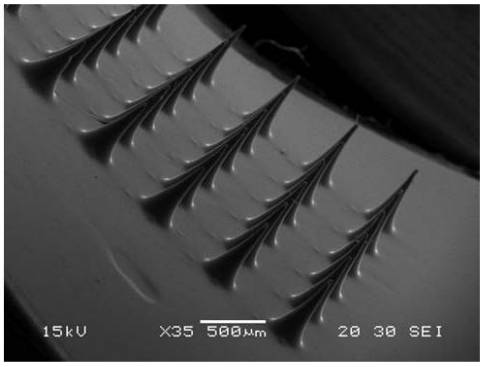

Fig. 1 SEM picture of a microspike array before functionalization to biosensor.

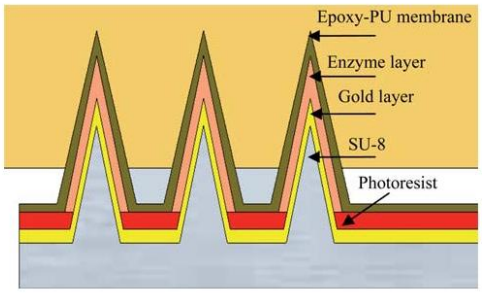

Fig. 2 Schematic representation of a microspike based skin patch for glucose/lactate detection.

potassium ferricyanide to confirm the proper gold attachment to the underlying microspikes. After an additional cleaning with 0.5M H_2SO_4 microspikes were functionalised with 0.4M thiomalic acid (TMA) for 1h at room temperature. Subsequently 2mM of ethyl-dimethyl-aminopropylcarbodiimide (EDC) and 5mM and N-hydroxy-succinimide (NHS) were used to activate TMA's carboxyl groups by incubating the microspikes at room temperature for 2h. Next, the microspikes were immersed in 0.1M PBS, 0.001% poly-l-lysine and 10mg L^{-1} of glucose oxide (GOD, from *Aspergillus niger*, lyophilized, powder, ~200 units/mg) or lactate oxidase (LOD from *Pediococcus* sp. lyophilized powder, ≥20 units/mg) enzyme overnight at 4 °C. An electron transfer mediator, tetrathiafulvalene (TTF) was incorporated into an epoxy-polyurethane (PU) by dissolving 0.5 M TTF, 17.8 mg each of Part A and Part B of epoxy adhesive and 26.7 mg of PU in 4 ml of THF and 1 ml of Brij 30. 1µL of such membrane was deposited onto the microspikes and left for drying in room temperature for 20min. The membrane proved to be much more reliable than previously used outer membranes [25] showing greater reduction of sensors' sensitivity. This prolongs the linear working range and increases resistance to interfering agents such as dopamine, ascorbic acid, acetaminophen, or uric acid.[26] A schematic representation of sensor design is presented in Fig. 2. When not in use the sensors were stored in PBS at 4 °C.

Electrochemical measurements of sensor response

The electrochemical measurements were performed using a Ivium potentiostat (CompactStat mobile potentiostat/galvanostat, Gloucestershire, UK). All measurements were conducted with the microspikes as working electrode and Ag/AgCl as both reference and counter electrode. Calibration plots were obtained by measuring the current while increasing the substrate (glucose or L-lactate) concentration from 0 to 25mM (stepwise). The apparent Michaelis–Menten constant, was calculated using Lineweaver–Burk type equation:[2]

$$\frac{1}{i} = \left(\frac{K_M^{app}}{i_{max}}\right)\left(\frac{1}{C}\right) + \frac{1}{i_{max}} \quad (1)$$

where C is a substrate concentration, i is steady state current, i_{max} is maximum steady state current, and K_M^{app} is an apparent Michaelis–Menten constant.[27]

ART ■ C1LC20885C

Incorporation of microspikes into a microfluidics platform

As shown in Fig. 3, the microfluidic platform comprises of a polydimethylsiloxane (PDMS) microfluidic chip, and the 4 × 4 microspike array layer. Sylguard 184 monomer and the curing agent (ratio 10 : 1) were poured into a pre-fabricated SU-8 mould and left to cure overnight. The PDMS was the cut and peeled off the mould. This chip design has 2 inlets with meanders leading to hexagonal chamber which finally terminates into an outlet. The microchannels are 1.0 mm wide and 1.0 mm deep. The microfluidic chip was bonded with a glass slide consisting of the microspike array using Oxygen plasma treatment (Diener Technologies) at 60% flow rate and by exposing for 120 s was used to bond the PDMS chip to a glass slide.

Electrochemical response of microspikes incorporated into a microfluidics platform

Both glucose and lactate sensors are based on the same working principle involving catalysis of an enzyme driven reaction and electron transfer using TTF as a mediator to the gold electrode. Cyclic voltammetry measurements revealed that the optimal potential for TTF oxidation is 150 mV and that further increase of voltage results in irreversible oxidation of the mediator and permanent damage of the sensor, thus this potential was used throughout the experiments.

Glucose sensor was chosen as a representative for these studies. The sensors were tested using two syringe pumps connected to two inlets. To determine the response to the change of glucose concentration, the sensor was first stabilised with PBS flowing at a constant rate until a stable current was observed. The flow was stopped and a 5mM glucose solution was introduced through the second inlet keeping the same flow rate. The experiment was continued until the steady state current was reached. To evaluate the sensor performance 50, 100 and 200μL min^{-1} flow rates were used. The device lifetime was determined by repeating experiments with the same sensor over several days.

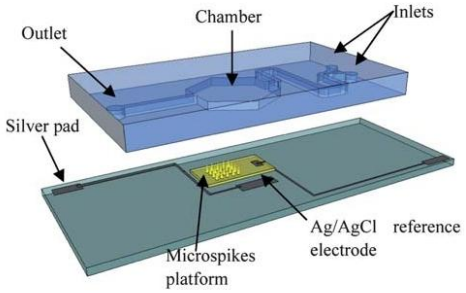

Fig. 3 A schematic representation of microfluidics based system to study mass transport phenomena in biosensors.

Results and discussion

Electrochemical response of glucose and lactate sensors

Various immobilisation techniques have been described for glucose and lactate sensors.[21,28,29] The self assembling method proved to be the most appropriate one for uniformly coating a three-dimensional structure. This technique offers the advantage of yielding a consistent layer of enzyme deposited onto complex electrode geometry in a well controlled manner. As seen in Fig. 4, such an approach is applicable for both lactate and glucose biosensors. In case of glucose biosensors coated with epoxy-PU membrane the performance was optimum ($R^2 = 0.976$, response time 15 ± 9s). The lactate sensor showed performance within the acceptable range ($R^2 = 0.855$, response time 21 ± 6s). The lower value can be attributed to the fact that lactate oxidise enzyme (20 units/mg) is less reactive than glucose oxidise (100 units/mg), thus has lower maximum limiting current (LOD I_{max} = 4.8nA; GOD I_{max} = 24.6nA) and reaches saturation at lower substrate concentrations.

The electrochemical response of both types of sensors can be described by the apparent Michaelis–Menten constant, K_M^{app}, which expresses a specific characteristic of the electrode–enzyme system. In case of GOD sensors, the apparent constant K_M^{app} = 51.8mM is much higher than LOD K_M^{app} = 2.2mM. Since the sensors are composed of a membrane and a mediator (which affect the K_M^{app} values) the results cannot be compared to the literature values for saturated enzymes. However, high K_M^{app} for the GOD sensors confirms that these sensors can work in much higher substrate concentration range than the LOD sensors. Moreover these results indicate that the LOD sensors are more sensitive at the lower substrate concentrations that the GOD sensors.

Nevertheless, both sensors cover the clinically relevant range which makes them viable for further investigation. The sensors were stable over 48h even when stored at room temperature and in 10mM glucose solution which meets the requirements for a minimally invasive system.

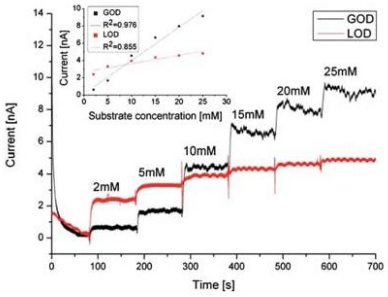

Fig. 4 Non-flow cell experiment. Lactate (LOD) and glucose (GOD) biosensors calibration curves (stepwise substrate increase in a stationary solution) and determination of K_M^{app} for the GOD and LOD sensors (insert).

ART ■ C1LC20885C

Electrochemical response of glucose sensing microspikes incorporated into a microfluidics platform

To characterise the biosensor performance we incorporated the modified microspike array into a microfluidics platform (see Fig. 3). As shown in Fig. 5 the sensor response is dependent on the flow rate in the initial stage. As discussed below this is a consequence of the design of the flow chamber resulting in a period during which the concentration reaches a constant value. Once this chamber concentration has stabilised the plateau current is independent of flow rate. This implies that once the steady state is reached the current is limited either by the enzyme kinetics or membrane diffusion and not by external mass transport. In other words, the unstirred layer at the membrane surface is sufficiently thin at all flow rates studied for diffusion across this layer not to be rate limiting.

The time required for the sensor to reach equilibrium is much longer when incorporated into a microfluidic platform than in bulk measurements. The main reason for that is the relatively slow mixing in the microfluidic chamber which has been described earlier.[30] It has been reported that in a hexagonal chamber reaching concentration equilibrium takes several minutes. The sensor response for two different measurements at 100 μL min^{-1} flow rate indicates the reproducibility of the device.

It is important to determine whether there are any membrane defects as they could lead to a mediator leakage which affects the senor performance and can lead to loss of functionality. Incorporating microspikes into a microfluidics platform proved to be a very useful technique to study this phenomenon, as it provides us with a very stable, well controlled system where any release of the mediator from the sensor can be measured. Thus, during the experiments described above the flow-through solution was collected and analyzed for TTF by voltammetry. Based on these results (not shown) it was concluded that the epoxy-PU membrane was not damaged or cracked and there was no detectable leakage of TTF as the current was stable before, during and after the experiment.

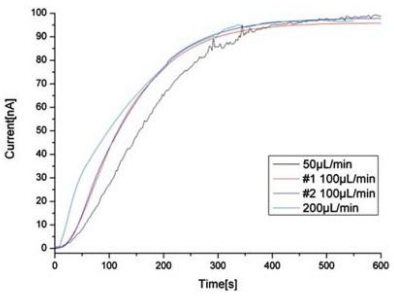

Fig. 5 Electrochemical response of glucose sensing microspikes incorporated into a microfluidics platform. The increase of glucose concentration from 0 to 5mM is presented. Two sensor responses at a flow rate of 100μL min^{-1} are shown to present the stability and reproducibility of the method.

Conclusions

We have demonstrated that a microfluidics system can be used in conjunction with a unique microspike array to provide the basis for a biosensor. The non-flow cell set-up allowed for the determination of the working range and time response of sensors for glucose and lactate. It was concluded that both types of sensors can operate in clinically relevant range with quick response time (less than 20s for both sensors). Glucose sensors exhibit much higher working range due to a higher enzyme activity than lactate which was confirmed by the calculated apparent Michaelis–Menten constant.

Microfluidics experiments involving out-of-plane microspikes revealed that the sensor response is flow rate dependent in the initial stage and independent of flow rate thereafter. The glucose sensors show a long response time in the microfluidic platform. This can be attributed to the slow mixing of the solutions in the hexagonal chamber. The parabolic flow profile due to the syringe pumps coupled with laminar flow and backpressure[30] in the hexagonal chamber explain the high response time. This is further compounded by the use of two syringe pumps in sequence which leads to backpressure near the inlets. The microfluidic platform described here provides valuable information on the kinetic processes which affect the sensor performance.

Transdermal biosensors can potentially be used as disposable devices for measuring glucose or lactate concentration in interstitial fluid (ISF). The device design presented here can be further modified. Modifications such as having two differently subsets of functionalised microspikes incorporated into the microfluidic platform will enable simultaneous measurements of glucose and lactate concentrations.

Acknowledgements

The authors acknowledge the Imperial College Biomedical Research Centre (BRC) for funding the project. Thanks are also due to Katerina Tsagaraki (FORTH, Greece) for facilitating the SEM images.

References

1 J. F. Castner and L. B. Wingard, Jr., *Biochemistry*, 1984, **23**, 2203–2210.
2 S. R. Mikkelsen and R. B. Lennox, *Anal. Biochem.*, 1991, **195**, 358–363.
3 V. Srinivasan, V. K. Pamula and R. B. Fair, *Lab Chip*, 2004, **4**, 310–315.
4 M. Brivio, W. Verboom and D. N. Reinhoudt, *Lab Chip*, 2006, **6**, 329–344.
5 M. H. Wu, S. B. Huang and G. B. Lee, *Lab Chip*, 2010, **10**, 939–956.
6 R. F. Winkle, J. M. Nagy, A. E. G. Cass and S. Sharma, *Expert Opin. Drug Discovery*, 2008, **3**, 1281–1292.
7 G. T. Baxter, *Atla-Alternatives to Laboratory Animals*, 2009, **37**, 11–18.
8 T. H. Park and M. L. Shuler, *Biotechnol. Prog.*, 2003, **19**, 243–253.
9 M. L. Crichton, A. Ansaldo, X. F. Chen, T. W. Prow, G. J. P. Fernando and M. A. F. Kendall, *Biomaterials*, 2010, **31**, 4562–4572.
10 D. Bodhale, A. Nisar and N. Afzulpurkar, *Microfluid. Nanofluid.*, 2010, **8**, 373–392.
11 B. J. Kim, H. J. Kim, S. M. Jung, J. K. Sung and H. H. Lee, *Biochip Journal*, 2009, **3**, 281–286.
12 H. B. Zhou, G. Li, X. N. Sun, Z. H. Zhu, B. J. Xu, Q. H. Jin, J. L. Zhao and Q. S. Ren, *Sens. Actuators, A*, 2009, **150**, 296–301.

ART ■ C1LC20885C

13 A. Arora, M. R. Prausnitz and S. Mitragotri, *Int. J. Pharm.*, 2008, **364**, 227–236.
14 M. Matteucci, M. Casella, M. Bedoni, E. Donetti, M. Fanetti, F. De Angelis, F. Gramatica and E. Di Fabrizio, *Microelectron. Eng.*, 2008, **85**, 1066–1073.
15 J. W. Lee, J. H. Park and M. R. Prausnitz, *Biomaterials*, 2008, **29**, 2113–2124.
16 J. H. Park, M. G. Allen and M. R. Prausnitz, *J. Controlled Release*, 2005, **104**, 51–66.
17 S. Rajaraman and H. T. Henderson, *Sens. Actuators, B*, 2005, **105**, 443–448.
18 H. J. G. E. Gardeniers, R. Luttge, E. J. W. Berenschot, M. J. de Boer, S. Y. Yeshurun, M. Hefetz, R. van't Oever and A. van den Berg, *J. Microelectromech. Syst.*, 2003, **12**, 855–862.
19 S. Chandrasekaran, J. D. Brazzle and A. B. Frazier, *J. Microelectromech. Syst.*, 2003, **12**, 281–288.
20 Y. W. Noh, T. H. Kim, J. S. Baek, H. H. Park, S. S. Lee, M. Han, S. C. Shin and C. W. Cho, *Int. J. Pharm.*, 2010, **397**, 201–205.
21 N. S. Oliver, C. Toumazou, A. E. Cass and D. G. Johnston, *Diabetic Med.*, 2009, **26**, 197–210.
22 M. Frost and M. E. Meyerhoff, *Anal. Chem.*, 2006, **78**, 7370–7377.
23 K. Kim, D. S. Park, H. M. Lu, W. Che, K. Kim, J. B. Lee and C. H. Ahn, *J. Micromech. Microeng.*, 2004, **14**, 597–603.
24 J. Ho Shim, H. Do and Y. Lee, *Electroanalysis*, 2010, **22**, 359–366.
25 B. Yu, N. Long, Y. Moussy and F. Moussy, *Biosens. Bioelectron.*, 2006, **21**, 2275–2282.
26 B. Yu, Y. Ju, L. West, Y. Moussy and F. Moussy, *Diabetes Technol. Ther.*, 2007, **9**, 265–275.
27 L. Doretti, D. Ferrara, S. Lora, F. Schiavon and F. M. Veronese, *Enzyme Microb. Technol.*, 2000, **27**, 279–285.
28 M. H. Gil, J. P. Sardinha, M. T. Vieira, M. Vivan, D. Costa, C. Rodrigues, F. M. Matysik and A. M. Oliveira Brett, *Biotechnol. Tech.*, 1999, **13**, 595–599.
29 J. Wang, *Chem. Rev.*, 2008, **108**, 814–825.
30 A. Mustafic, H. M. Huang, E. A. Theodorakis and M. A. Haidekker, *J. Fluoresc.*, 2010, **20**, 1087–1098.

ART ■ C1LC20885C

Appendix 5

LETTER TO EDITOR

Minimally Invasive Enzyme Microprobes: An Alternative Approach for Continuous Glucose Monitoring

Anna Radomska Bothelo Moniz, Ph.D.,[1] Kostis Michelakis, Ph.D.,[1] Jakub Trzebinski, B.Eng.,[1,2] Sanjiv Sharma, Ph.D.,[1] Desmond G. Johnston, F.Med.Sci.,[3] Nick Oliver, M.R.C.P.,[3] and Anthony Cass, D.Phil., FRSC[1]

Continuous glucose monitoring has been shown to improve glycemia in diabetes.[1,2] To minimize the pain, inconvenience, and discomfort associated with long-term implanted sensors, minimally invasive technologies are being developed, including microneedles that remove small volumes of subcutaneous interstitial fluid (ISF).[3] We describe here an alternative approach for continuous monitoring of glucose in ISF that involves using solid microprobes that access the interstitium in a minimally invasive and less painful manner than using a lancet to draw capillary blood. The glucose sensor is a small (~1 cm^2) wearable patch covered with arrays of solid microprobes, which penetrate the stratum corneum and monitor glucose in ISF within the epidermis. Unlike microneedles, solid microprobes are not susceptible to clogging and their minimally invasive nature may be less traumatic than existing subcutaneous sensors, reducing the risk of sensor drift and protein adsorption that degrades performance.[4,5]

The microprobes were made by photolithography using backside illumination[6] adapted to create 500–750 μm long structures with tip diameters of 10 μm. Sensitivity to glucose was achieved by assembling glucose oxidase (GOx; EC 1.1.3.4) on the gold-coated microprobes using 1-Ethyl-3-(3-dimethylaminopropyl) carbodiimide/N-hydroxysuccinimide coupling followed by a Nafion membrane incorporating tetrathiafulvalene (TTF) as an electron transfer mediator. *In vitro* studies with these devices have demonstrated that they perform well in the clinically relevant range (2–20 mM; **Figure 1**), with a linear response to increasing glucose and measured currents in the microampere domain.

Data are presented for glucose measurement, but the platform may be employed with other enzymes such as lactate oxidase or beta-hydroxybutyrate dehydrogenase. It is also possible to partition the microprobe array and immobilize different enzymes across multiple subarrays for continuous multianalyte sensing. Partitioning may also allow multiple sensors to be used in a "voting" system for the same analyte, thus improving sensor reliability.

Author Affiliations: [1]Institute of Biomedical Engineering, Department of Chemistry, Imperial College London, South Kensington Campus, London, United Kingdom; [2]Brunel Institute for Bioengineering, Brunel University, Uxbridge, West London, United Kingdom; and [3]Diabetes, Endocrinology, and Metabolic Medicine, Imperial College London, St. Mary's Campus, London, United Kingdom

Abbreviations: (GOx) glucose oxidase, (ISF) interstitial fluid, (TTF) tetrathiafulvalene

Keywords: continuous glucose monitor, diabetes, electrochemistry, glucose monitoring

Corresponding Author: Anthony Cass, D.Phil., FRSC, Institute of Biomedical Engineering, Department of Chemistry, Imperial College London, South Kensington Campus, Exhibition Road, London SW7 2AZ; email address t.cass@imperial.ac.uk

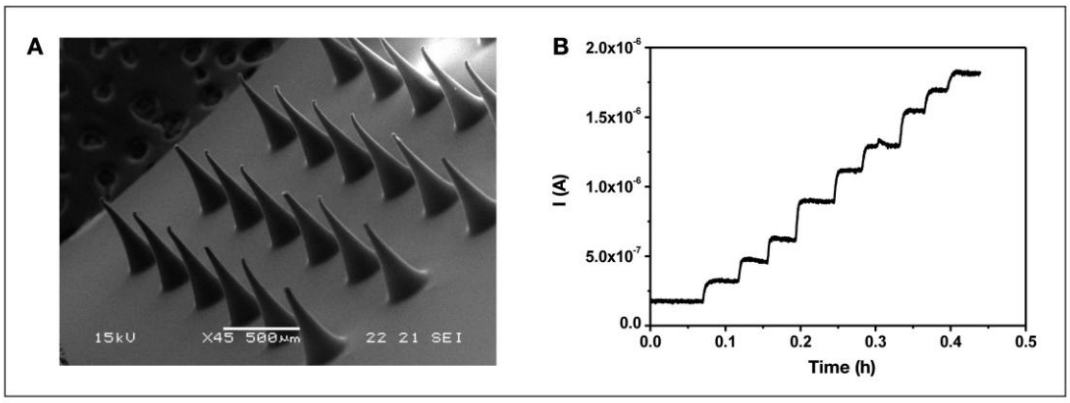

Figure 1. (A) Scanning electron microscope image showing 600 µm high microprobe array. **(B)** Calibration of TTF/GOx-modified gold microprobes performed in 0.1 M phosphate-buffered saline pH 7.4 background solution; each step represents an increase of 2 mM in glucose concentration.

Funding:

This work was funded by the Imperial College Biomedical Research Committee Fund and Imperial Innovations.

References:

1. Juvenile Diabetes Research Foundation Continuous Glucose Monitoring Study Group, Tamborlane WV, Beck RW, Bode BW, Buckingham B, Chase HP, Clemons R, Fiallo-Scharer R, Fox LA, Gilliam LK, Hirsch IB, Huang ES, Kollman C, Kowalski AJ, Laffel L, Lawrence JM, Lee J, Mauras N, O'Grady M, Ruedy KJ, Tansey M, Tsalikian E, Weinzimer S, Wilson DM, Wolpert H, Wysocki T, Xing D. Continuous glucose monitoring and intensive treatment of type 1 diabetes. N Engl J Med. 2008;359(14):1464–76.
2. Juvenile Diabetes Research Foundation Continuous Glucose Monitoring Study Group, Beck RW, Hirsch IB, Laffel L, Tamborlane WV, Bode BW, Buckingham B, Chase P, Clemons R, Fiallo-Scharer R, Fox LA, Gilliam LK, Huang ES, Kollman C, Kowalski AJ, Lawrence JM, Lee J, Mauras N, O'Grady M, Ruedy KJ, Tansey M, Tsalikian E, Weinzimer SA, Wilson DM, Wolpert H, Wysocki T, Xing D. The effect of continuous glucose monitoring in well-controlled type 1 diabetes. Diabetes Care. 2009;32(8):1378–83.
3. Mukerjee EV, Collins SD, Isseroff RR, Smith RL. Microneedle array for transdermal biological fluid extraction and in situ analysis. Sens Actuat A Phys. 2004;114(2-3):267–75.
4. Noh YW, Kim TH, Baek JS, Park HH, Lee SS, Han M, Shin SC, Cho CW. *In vitro* characterization of the invasiveness of polymer microneedle against skin. Int J Pharm. 2010;397(1-2):201–5.
5. Oliver NS, Toumazou C, Cass AE, Johnston DG. Glucose sensors: a review of current and emerging technology. Diabet Med. 2009;26(3):197–210.
6. Kim K, Park DS, Lu HM, Che W, Kim K, Lee JB, Ahn CH. A tapered hollow metallic microneedle array using backside exposure of su-8. J Micromech Microeng. 2004;14(4):597–603.

Bibliography

1. Wang, J., *Analytical electrochemistry*. 2nd ed. 2000, New York: Wiley-VCH. xvi, 209 p.
2. Nicholson, R.S., *Theory and Application of Cyclic Voltammetry for Measurement of Electrode Reaction Kinetics.* Analytical Chemistry, 1965. **37**(11): p. 1351-1355.
3. Bard, A.J., et al., *Scanning Electrochemical Microscopy - Introduction and Principles.* Analytical Chemistry, 1989. **61**(2): p. 132-138.
4. Kwak, J. and A.J. Bard, *Scanning electrochemical microscopy. Theory of the feedback mode.* Analytical Chemistry, 1989. **61**(11): p. 1221-1227.
5. Bugg, T., *Introduction to enzyme and coenzyme chemistry*. 2004, GB: Blackwell Publishing.
6. D'Costa, E.J., I.J. Higgins, and A.P.F. Turner, *Quinoprotein glucose dehydrogenase and its application in an amperometric glucose sensor.* Biosensors, 1986. **2**(2): p. 71-87.
7. Wohlfahrt, G., et al., *1.8 and 1.9 angstrom resolution structures of the Penicillium amagasakiense and Aspergillus niger glucose oxidases as a basis for modelling substrate complexes.* Acta Crystallographica Section D-Biological Crystallography, 1999. **55**: p. 969-977.
8. Witt, S., et al., *Conserved arginine-516 of Penicillium amagasakiense glucose oxidase is essential for the efficient binding of beta-D-glucose.* Biochemical Journal, 2000. **347**: p. 553-559.
9. Bhethanabotla, M.K.R.a.V.R., *Sensors for Chemical and Biological Applications*. 2010: Boca Raton, Fla. : Taylor & Francis.
10. Daniels, J.S. and N. Pourmand, *Label-Free Impedance Biosensors: Opportunities and Challenges.* Electroanalysis, 2007. **19**(12): p. 1239-1257.
11. Cass, A.E.G., et al., *Ferrocene-mediated enzyme electrode for amperometric determination of glucose.* Analytical Chemistry, 1984. **56**(4): p. 667-671.
12. *Facts sheets: Diabeties; Fact sheet N°312*. January 2011 [cited 2011; Available from: http://www.who.int/mediacentre/factsheets/fs312/en/.
13. Roglic, G., et al., *The burden of mortality attributable to diabetes: realistic estimates for the year 2000.* Diabetes Care, 2005. **28**(9): p. 2130-5.
14. Krynski, I.A. and J.E. Logan, *Dextrostix as a quantitative test for glucose in whole blood.* Can Med Assoc J, 1967. **97**(17): p. 1006-11.
15. Peterson, C.M., et al., *FEASIBILITY OF TIGHT CONTROL OF JUVENILE DIABETES THROUGH PATIENT MONITORED GLUCOSE DETERMINATIONS.* Diabetes, 1978. **27**: p. 437-437.
16. Oliver, N.S., et al., *Glucose sensors: a review of current and emerging technology.* Diabet Med, 2009. **26**(3): p. 197-210.

17. Albareda-Sirvent, M., A. Merkoçi, and S. Alegret, *Configurations used in the design of screen-printed enzymatic biosensors. A review.* Sensors and Actuators B: Chemical, 2000. **69**(1-2): p. 153-163.
18. Hirsch, I.B., et al., *Clinical application of emerging sensor technologies in diabetes management: consensus guidelines for continuous glucose monitoring (CGM).* Diabetes Technol Ther, 2008. **10**(4): p. 232-44; quiz 245-6.
19. Instruments, G. *Portable Blood Glucose Monitor*. March 2011]; Available from: http://www.groveinstruments.com/.
20. Saiga, N. and K. Matsuda, *Spectroscopic measurement of glucose content in a solution involving the water molecule clusters downsized by ultrasonic cavitations.* Optical Review, 2009. **16**(4): p. 461-465.
21. Khalil, O.S., *Non-invasive glucose measurement technologies: an update from 1999 to the dawn of the new millennium.* Diabetes Technol Ther, 2004. **6**(5): p. 660-97.
22. Nelson, L.A., et al., *Development and validation of a multiwavelength spatial domain near-infrared oximeter to detect cerebral hypoxia-ischemia.* Journal of Biomedical Optics, 2006. **11**(6): p. 064022.
23. Burmeister, J.J., M.A. Arnold, and G.W. Small, *Noninvasive blood glucose measurements by near-infrared transmission spectroscopy across human tongues.* Diabetes Technol Ther, 2000. **2**(1): p. 5-16.
24. Heinemann, L., et al., *Noninvasive glucose measurement by monitoring of scattering coefficient during oral glucose tolerance tests. Non-Invasive Task Force.* Diabetes Technol Ther, 2000. **2**(2): p. 211-20.
25. Malchoff, C.D., et al., *A Novel Noninvasive Blood Glucose Monitor.* Diabetes Care, 2002. **25**(12): p. 2268-2275.
26. Dieringer, J.A., et al., *Surface enhanced Raman spectroscopy: new materials, concepts, characterization tools, and applications.* Faraday Discuss, 2006. **132**: p. 9-26.
27. Lambert, J.L., et al., *Measurement of aqueous glucose in a model anterior chamber using Raman spectroscopy.* Journal of Raman Spectroscopy, 2002. **33**(7): p. 524-529.
28. Malik, B.H. and G.L. Cote, *Real-time, closed-loop dual-wavelength optical polarimetry for glucose monitoring.* J Biomed Opt, 2010. **15**(1): p. 017002.
29. Cameron, B.D. and H. Anumula, *Development of a Real-Time Corneal Birefringence Compensated Glucose Sensing Polarimeter.* Diabetes Technology & Therapeutics, 2006. **8**(2): p. 156-164.
30. Cameron, B.D., J.S. Baba, and G.L. Cote, *Measurement of the glucose transport time delay between the blood and aqueous humor of the eye for the eventual development of a noninvasive glucose sensor.* Diabetes Technol Ther, 2001. **3**(2): p. 201-7.
31. Larin, K.V., et al., *Noninvasive Blood Glucose Monitoring With Optical Coherence Tomography.* Diabetes Care, 2002. **25**(12): p. 2263-2267.
32. Sapozhnikova, V.V., et al., *Effect on blood glucose monitoring of skin pressure exerted by an optical coherence tomography probe.* Journal of Biomedical Optics, 2008. **13**(2): p. 021112.
33. Gabbay, R.A. and S. Sivarajah, *Optical Coherence Tomography-Based Continuous Noninvasive Glucose Monitoring in Patients with Diabetes.* Diabetes Technology & Therapeutics, 2008. **10**(3): p. 188-193.
34. MacKenzie, H.A., et al., *Advances in Photoacoustic Noninvasive Glucose Testing.* Clin Chem, 1999. **45**(9): p. 1587-1595.

35. Weiss, R., et al., *Noninvasive Continuous Glucose Monitoring Using Photoacoustic Technologyâ€"Results from the First 62 Subjects.* Diabetes Technology & Therapeutics, 2007. **9**(1): p. 68-74.
36. Stein, E.W., S. Singh, and M.J. McShane, *Microscale Enzymatic Optical Biosensors Using Mass Transport Limiting Nanofilms. 2. Response Modulation by Varying Analyte Transport Properties.* Analytical Chemistry, 2008. **80**(5): p. 1408-1417.
37. Srivastava, R., et al., *"Smart tattoo" glucose biosensors and effect of coencapsulated anti-inflammatory agents.* J Diabetes Sci Technol. **5**(1): p. 76-85.
38. Badugu, R., J.R. Lakowicz, and C.D. Geddes, *A glucose-sensing contact lens: from bench top to patient.* Current Opinion in Biotechnology, 2005. **16**(1): p. 100-107.
39. Kovatchev, B.P., D. Shields, and M. Breton, *Graphical and numerical evaluation of continuous glucose sensing time lag.* Diabetes Technol Ther, 2009. **11**(3): p. 139-43.
40. Boyne, M.S., et al., *Timing of Changes in Interstitial and Venous Blood Glucose Measured With a Continuous Subcutaneous Glucose Sensor.* Diabetes, 2003. **52**(11): p. 2790-2794.
41. Ching, T.S. and P. Connolly, *Simultaneous transdermal extraction of glucose and lactate from human subjects by reverse iontophoresis.* Int J Nanomedicine, 2008. **3**(2): p. 211-23.
42. Tierney, M.J., et al., *Design of a Biosensor for Continual, Transdermal Glucose Monitoring.* Clin Chem, 1999. **45**(9): p. 1681-1683.
43. Tierney, M.J., et al., *Clinical evaluation of the GlucoWatch® biographer: a continual, non-invasive glucose monitor for patients with diabetes.* Biosensors and Bioelectronics, 2001. **16**(9-12): p. 621-629.
44. Yoo, E.-H. and S.-Y. Lee, *Glucose Biosensors: An Overview of Use in Clinical Practice.* Sensors, 2010. **10**(5): p. 4558-4576.
45. Mitragotri, S. and J. Kost, *Low-frequency sonophoresis: A review.* Advanced Drug Delivery Reviews, 2004. **56**(5): p. 589-601.
46. Kost, J., et al., *Transdermal monitoring of glucose and other analytes using ultrasound.* Nat Med, 2000. **6**(3): p. 347-350.
47. Amaral, C.E.F. and B. Wolf. *Effects of glucose in blood and skin impedance spectroscopy*. in *AFRICON 2007*. 2007.
48. Pfutzner, A., et al., *Impact of Posture and Fixation Technique on Impedance Spectroscopy Used for Continuous and Noninvasive Glucose Monitoring.* Diabetes Technology & Therapeutics, 2004. **6**(4): p. 435-441.
49. Kaushik, S., et al., *Lack of Pain Associated with Microfabricated Microneedles.* Anesthesia & Analgesia, 2001. **92**(2): p. 502-504.
50. Smart, W.H. and K. Subramanian, *The Use of Silicon Microfabrication Technology in Painless Blood Glucose Monitoring.* Diabetes Technology & Therapeutics, 2000. **2**(4): p. 549-559.
51. Prausnitz, M.R., *Microneedles for transdermal drug delivery.* Advanced Drug Delivery Reviews, 2004. **56**(5): p. 581-587.
52. Hashmi, S., et al., *Genetic transformation of nematodes using arrays of micromechanical piercing structures.* Biotechniques, 1995. **19**(5): p. 766-70.
53. McAllister, D.V., et al., *Microfabricated needles for transdermal delivery of macromolecules and nanoparticles: Fabrication methods and transport studies.* Proceedings of the National Academy of Sciences of the United States of America, 2003. **100**(24): p. 13755-13760.
54. Kabseog, K. and et al., *A tapered hollow metallic microneedle array using backside exposure of SU-8.* Journal of Micromechanics and Microengineering, 2004. **14**(4): p. 597.

55. Wang, P.M., M. Cornwell, and M.R. Prausnitz, *Minimally Invasive Extraction of Dermal Interstitial Fluid for Glucose Monitoring Using Microneedles.* Diabetes Technology & Therapeutics, 2005. **7**(1): p. 131-141.
56. Schoonen, A.J.M., et al., *Development of a potentially wearable glucose sensor for patients with diabetes mellitus: design and in-vitro evaluation.* Biosensors and Bioelectronics, 1990. **5**(1): p. 37-46.
57. Heinemann, L., *Continuous Glucose Monitoring by Means of the Microdialysis Technique: Underlying Fundamental Aspects.* Diabetes Technology & Therapeutics, 2003. **5**(4): p. 545-561.
58. Zahn, J.D., D. Trebotich, and D. Liepmann, *Microdialysis Microneedles for Continuous Medical Monitoring.* Biomedical Microdevices, 2005. **7**(1): p. 59-69.
59. Henry, S., et al., *Microfabricated microneedles: A novel approach to transdermal drug delivery.* J Pharm Sci, 1999. **88**(9): p. 948.
60. Henry, S., et al., *Microfabricated microneedles: a novel approach to transdermal drug delivery.* J Pharm Sci, 1998. **87**(8): p. 922-5.
61. Matriano, J.A., et al., *Macroflux® Microprojection Array Patch Technology: A New and Efficient Approach for Intracutaneous Immunization.* Pharmaceutical Research, 2002. **19**(1): p. 63-70.
62. Tiessen, R.G., et al., *Slow ultrafiltration for continuous in vivo sampling: application for glucose and lactate in man.* Analytica Chimica Acta, 1999. **379**(3): p. 327-335.
63. Schoemaker, M., et al., *The SCGM1 System: Subcutaneous Continuous Glucose Monitoring Based on Microdialysis Technique.* Diabetes Technology & Therapeutics, 2003. **5**(4): p. 599-608.
64. Heller, A. and B. Feldman, *Electrochemical Glucose Sensors and Their Applications in Diabetes Management.* Chemical Reviews, 2008. **108**(7): p. 2482-2505.
65. Rossetti, P., et al., *Evaluation of the Accuracy of a Microdialysis-Based Glucose Sensor During Insulin-Induced Hypoglycemia, Its Recovery, and Post-Hypoglycemic Hyperglycemia in Humans.* Diabetes Technology & Therapeutics, 2006. **8**(3): p. 326-337.
66. Wisniewski, N., F. Moussy, and W.M. Reichert, *Characterization of implantable biosensor membrane biofouling.* Fresenius J Anal Chem, 2000. **366**(6-7): p. 611-21.
67. Yu, B., et al., *An investigation of long-term performance of minimally invasive glucose biosensors.* Diabetes Technol Ther, 2007. **9**(3): p. 265-75.
68. Gough, D.A., et al., *Function of an Implanted Tissue Glucose Sensor for More than 1 Year in Animals.* Science Translational Medicine, 2010. **2**(42): p. 42ra53.
69. Yu, B., et al., *Use of hydrogel coating to improve the performance of implanted glucose sensors.* Biosens Bioelectron, 2008. **23**(8): p. 1278-84.
70. Ju, Y.M., et al., *A dexamethasone-loaded PLGA microspheres/collagen scaffold composite for implantable glucose sensors.* J Biomed Mater Res A, 2009.
71. Ju, Y.M., et al., *A novel porous collagen scaffold around an implantable biosensor for improving biocompatibility. II. Long-term in vitro/in vivo sensitivity characteristics of sensors with NDGA- or GA-crosslinked collagen scaffolds.* J Biomed Mater Res A, 2009.
72. Ward, W.K., et al., *Vascularizing the tissue surrounding a model biosensor: how localized is the effect of a subcutaneous infusion of vascular endothelial growth factor (VEGF)?* Biosens Bioelectron, 2003. **19**(3): p. 155-63.

73. Koschwanez, H.E., et al., *In vitro and in vivo characterization of porous poly-L-lactic acid coatings for subcutaneously implanted glucose sensors.* J Biomed Mater Res A, 2008. **87**(3): p. 792-807.
74. Mang, A., et al., *Biocompatibility of an electrochemical sensor for continuous glucose monitoring in subcutaneous tissue.* Diabetes Technol Ther, 2005. **7**(1): p. 163-73.
75. Updike, S.J. and G.P. Hicks, *The Enzyme Electrode.* Nature, 1967. **214**(5092): p. 986-988.
76. Guilbault, G.G. and G.J. Lubrano, *An enzyme electrode for the amperometric determination of glucose.* Analytica Chimica Acta, 1973. **64**(3): p. 439-455.
77. Wang, J., *Electrochemical glucose biosensors.* Chem Rev, 2008. **108**(2): p. 814-25.
78. Yu, B., Y. Moussy, and F. Moussy, *Coil-type implantable glucose biosensor with excess enzyme loading.* Front Biosci, 2005. **10**: p. 512-20.
79. Li, Q., et al., *Amperometric Detection of Glucose with Glucose Oxidase Absorbed on Porous Nanocrystalline TiO2 Film.* Electroanalysis, 2001. **13**(5): p. 413-416.
80. Saha, S., et al., *Nanoporous cerium oxide thin film for glucose biosensor.* Biosensors and Bioelectronics, 2009. **24**(7): p. 2040-2045.
81. Olea, D., O. Viratelle, and C. Faure, *Polypyrrole-glucose oxidase biosensor: Effect of enzyme encapsulation in multilamellar vesicles on analytical properties.* Biosensors and Bioelectronics, 2008. **23**(6): p. 788-794.
82. Sasso, S.V., et al., *Electropolymerized 1,2-diaminobenzene as a means to prevent interferences and fouling and to stabilize immobilized enzyme in electrochemical biosensors.* Analytical Chemistry, 1990. **62**(11): p. 1111-1117.
83. Gooding, J.J., et al., *Amperometric biosensor with enzyme amplification fabricated using self-assembled monolayers of alkanethiols: the influence of the spatial distribution of the enzymes.* Electrochemistry Communications, 2000. **2**(4): p. 217-221.
84. Gooding, J.J., et al., *Parameters Important in Fabricating Enzyme Electrodes Using Self-Assembled Monolayers of Alkanethiols.* Analytical Sciences, 2001. **17**(1): p. 3-9.
85. Masson, J.-F., et al., *Improved sensitivity and stability of amperometric enzyme microbiosensors by covalent attachment to gold electrodes.* Biosensors and Bioelectronics, 2007. **23**(3): p. 355-361.
86. Sirkar, K., A. Revzin, and M.V. Pishko, *Glucose and Lactate Biosensors Based on Redox Polymer/Oxidoreductase Nanocomposite Thin Films.* Analytical Chemistry, 2000. **72**(13): p. 2930-2936.
87. Degani, Y. and A. Heller, *Direct electrical communication between chemically modified enzymes and metal electrodes. I. Electron transfer from glucose oxidase to metal electrodes via electron relays, bound covalently to the enzyme.* The Journal of Physical Chemistry, 1987. **91**(6): p. 1285-1289.
88. Xiao, Y., et al., *"Plugging into Enzymes": Nanowiring of Redox Enzymes by a Gold Nanoparticle.* Science, 2003. **299**(5614): p. 1877-1881.
89. Liu, J., et al., *Achieving Direct Electrical Connection to Glucose Oxidase Using Aligned Single Walled Carbon Nanotube Arrays.* Electroanalysis, 2005. **17**(1): p. 38-46.
90. Chaubey, A. and B.D. Malhotra, *Mediated biosensors.* Biosensors and Bioelectronics, 2002. **17**(6-7): p. 441-456.
91. McDonald, T.A., S. Waidyanatha, and S.M. Rappaport, *Measurement of adducts of benzoquinone with hemoglobin and albumin.* Carcinogenesis, 1993. **14**(9): p. 1927-1932.
92. Turner, A.P.F., *Biosensors : fundamentals and applications* 1987: Oxford University Press,.

93. Kulys, J., et al., *Glucose Oxidase Electrode Based on Graphite and Methylthio Tetrathiafulvalene as Mediator.* Analytical Letters, 1993. **26**(12): p. 2535 - 2542.
94. Palleschi, G. and A.P.F. Turner, *Amperometric tetrathiafulvalene-mediated lactate electrode using lactate oxidase absorbed on carbon foil.* Analytica Chimica Acta, 1990. **234**: p. 459-463.
95. Kulys, J., V. Simkeviciene, and I.J. Higgins, *Concerning the toxicity of two compounds used as mediators in biosensor devices: 7,7,8,8-tetracyanoquinodimethane (TCNQ) and tetrathiafulvalene (TTF).* Biosensors and Bioelectronics, 1992. **7**(7): p. 495-501.
96. Zakeeruddin, S.M., et al., *Towards mediator design: Characterization of tris-(4,4'-substituted-2,2'-bipyridine) complexes of iron(II), ruthenium(II) and osmium(II) as mediators for glucose oxidase of Aspergillus niger and other redox proteins.* Journal of Electroanalytical Chemistry, 1992. **337**(1-2): p. 253-283.
97. Lee, S.-H., et al., *Electrochemical study on screen-printed carbon electrodes with modification by iron nanoparticles in Fe(CN)6 4−/3− redox system.* Analytical and Bioanalytical Chemistry, 2005. **383**(3): p. 532-538.
98. Jaffari, S.A. and A.P.F. Turner, *Novel hexacyanoferrate(III) modified graphite disc electrodes and their application in enzyme electrodes--Part I.* Biosensors and Bioelectronics, 1997. **12**(1): p. 1-7.
99. *Exactech Blood Glucose Meter.* Diabetic Medicine, 1995. **12**(5): p. 450-450.
100. Cai, C. and J. Chen, *Direct electron transfer of glucose oxidase promoted by carbon nanotubes.* Analytical Biochemistry, 2004. **332**(1): p. 75-83.
101. Ivnitski, D., et al., *Entrapment of Enzymes and Carbon Nanotubes in Biologically Synthesized Silica: Glucose Oxidase-Catalyzed Direct Electron Transfer.* Small, 2008. **4**(3): p. 357-364.
102. Zhao, H.-Z., et al., *Direct electron transfer and conformational change of glucose oxidase on carbon nanotube-based electrodes.* Carbon. **48**(5): p. 1508-1514.
103. Zhao, S., et al., *Glucose oxidase/colloidal gold nanoparticles immobilized in Nafion film on glassy carbon electrode: Direct electron transfer and electrocatalysis.* Bioelectrochemistry, 2006. **69**(2): p. 158-163.
104. Bahshi, L., et al., *Following the Biocatalytic Activities of Glucose Oxidase by Electrochemically Cross-Linked Enzymeâˆ’Pt Nanoparticles Composite Electrodes.* Analytical Chemistry, 2008. **80**(21): p. 8253-8259.
105. Ma, S., et al., *Inhibition and enhancement of glucose oxidase activity in a chitosan-based electrode filled with silver nanoparticles.* Colloids and Surfaces A: Physicochemical and Engineering Aspects, 2008. **324**(1-3): p. 9-13.
106. Zou, Y.J., et al., *Glucose biosensor based on electrodeposition of platinum nanoparticles onto carbon nanotubes and immobilizing enzyme with chitosan-SiO2 sol-gel.* Biosensors & Bioelectronics, 2008. **23**(7): p. 1010-1016.
107. Shan, D., et al., *Colloidal laponite nanoparticles: Extended application in direct electrochemistry of glucose oxidase and reagentless glucose biosensing.* Biosensors and Bioelectronics. **25**(6): p. 1427-1433.
108. German, N., et al., *Glucose biosensor based on graphite electrodes modified with glucose oxidase and colloidal gold nanoparticles.* Microchimica Acta. **168**(3): p. 221-229.
109. Heller, A., *Plugging metal connectors into enzymes.* Nat Biotech, 2003. **21**(6): p. 631-632.
110. Katz, E., et al., *Glucose oxidase electrodes via reconstitution of the apo-enzyme: tailoring of novel glucose biosensors.* Analytica Chimica Acta, 1999. **385**(1-3): p. 45-58.

111. Shults, M.C., C.C. Capelli, and S.J. Updike, *Biological fluid measuring device*, U.S.P. Office, Editor. 1991: US Patent: 4994167.
112. Updike, S.J., M. Shults, and B. Ekman, *Implanting the glucose enzyme electrode: problems, progress, and alternative solutions.* Diabetes Care, 1982. **5**(3): p. 207-12.
113. Mercado, R.C. and F. Moussy, *In vitro and in vivo mineralization of Nafion membrane used for implantable glucose sensors.* Biosens Bioelectron, 1998. **13**(2): p. 133-145.
114. Ward, W.K., et al., *A new amperometric glucose microsensor: in vitro and short-term in vivo evaluation.* Biosens Bioelectron, 2002. **17**(3): p. 181-189.
115. Linke, B., et al., *Amperometric biosensor for in vivo glucose sensing based on glucose oxidase immobilized in a redox hydrogel.* Biosens Bioelectron, 1994. **9**(2): p. 151-158.
116. Matsumoto, T., et al., *A long-term lifetime amperometric glucose sensor with a perfluorocarbon polymer coating.* Biosens Bioelectron, 2001. **16**(4-5): p. 271-276.
117. Matsumoto, T., et al., *A micro-planar amperometric glucose sensor unsusceptible to interference species.* Sensor Actuat B-Chem, 1998. **49**(1-2): p. 68-72.
118. Madaras, M.B., et al., *Microfabricated amperometric creatine and creatinine biosensors.* Anal Chim Acta, 1996. **319**(3): p. 335-345.
119. Reddy, S.M. and P. Vadgama, *Entrapment of glucose oxidase in non-porous poly(vinyl chloride).* Anal Chim Acta, 2002. **461**(1): p. 57-64.
120. Chung, T.D., *In vitro evaluation of the continuous monitoring glucose sensors with perfluorinated tetrafluoroethylene coatings.* Bull Korean Chem Soc, 2002. **24**(4): p. 514-516.
121. Heller, A. and M.V. Pishko, *Subcutaneous glucose electrode*, U.P. Office, Editor. 2001: US Patent: 6514718.
122. Yu, B., Y. Moussy, and F. Moussy, *Lifetime Improvement of Glucose Biosensor by Epoxy-Enhanced PVC Membrane.* Electroanal, 2005. **17**(19): p. 1771-1779.
123. Adiga, S.P., et al., *Nanoporous membranes for medical and biological applications.* WIREs Nanomed Nanobiotechnol, 2009. **1**(5): p. 568-581.
124. Harrison, D.J., R.F. Turner, and H.P. Baltes, *Characterization of perfluorosulfonic acid polymer coated enzyme electrodes and a miniaturized integrated potentiostat for glucose analysis in whole blood.* Anal Chem, 1988. **60**(19): p. 2002-7.
125. Bruck, S.D., *Blood Compatible Synthetic Polymers*. 1974, Charles C. Thomas: Springfield, IL. p. 94-96.
126. Moussy, F., D.J. Harrison, and R.V. Rajotte, *A miniaturized Nafion-based glucose sensor: in vitro and in vivo evaluation in dogs.* Int J Artif Organs, 1994. **17**(2): p. 88-94.
127. Moussy, F., et al., *In vitro and in vivo performance and lifetime of perfluorinated ionomer-coated glucose sensors after high-temperature curing.* Anal Chem, 1994. **66**(22): p. 3882-8.
128. Mercado, R.C. and F. Moussy, *In vitro and in vivo mineralization of Nafion membrane used for implantable glucose sensors.* Biosens Bioelectron, 1998. **13**(2): p. 133-45.
129. Valdes, T.I. and F. Moussy, *A ferric chloride pre-treatment to prevent calcification of Nafion membrane used for implantable biosensors.* Biosens Bioelectron, 1999. **14**(6): p. 579-85.
130. Galeska, I., et al., *Calcification-resistant Nafion/Fe3+ assemblies for implantable biosensors.* Biomacromolecules, 2000. **1**(2): p. 202-7.
131. Yu, B., et al., *A long-term flexible minimally-invasive implantable glucose biosensor based on an epoxy-enhanced polyurethane membrane.* Biosens Bioelectron, 2006. **21**(12): p. 2275-82.

132. Chen, C.Y., et al., *Multifunctional biocompatible membrane and its application to fabricate a miniaturized glucose sensor with potential for use in vivo.* Biomed Microdevices, 1999. **1**(2): p. 155-66.
133. Galeska, I., et al., *Characterization and biocompatibility studies of novel humic acids based films as membrane material for an implantable glucose sensor.* Biomacromolecules, 2001. **2**(4): p. 1249-55.
134. Tipnis, R., et al., *Layer-by-layer assembled semipermeable membrane for amperometric glucose sensors.* J Diabetes Sci Technol, 2007. **1**(2): p. 193-200.
135. Stein, E.W., S. Singh, and M.J. McShane, *Microscale Enzymatic Optical Biosensors Using Mass Transport Limiting Nanofilms. 2. Response Modulation by Varying Analyte Transport Properties.* Anal Chem, 2008. **80**(5): p. 1408-1417.
136. Stein, E.W., et al., *Microscale Enzymatic Optical Biosensors Using Mass Transport Limiting Nanofilms. 1. Fabrication and Characterization Using Glucose as a Model Analyte.* Anal Chem, 2007. **79**(4): p. 1339-1348.
137. Uehara, H., et al., *Size-selective diffusion in nanoporous but flexible membranes for glucose sensors.* ACS Nano, 2009. **3**(4): p. 924-32.
138. Chu, M., et al., *A soft and flexible biosensor using a phospholipid polymer for continuous glucose monitoring.* Biomed Microdevices, 2009. **11**(4): p. 837-42.
139. Li, Q., et al., *Amperometric Detection of Glucose with Glucose Oxidase Absorbed on Porous Nanocrystalline TiO2 Film.* Electroanal, 2001. **13**(5): p. 413-416.
140. Singh, S.P., et al., *Cholesterol biosensor based on rf sputtered zinc oxide nanoporous thin film.* Appl Phy Lett, 2007. **91**(6): p. 063901.
141. Saha, S., et al., *Nanoporous cerium oxide thin film for glucose biosensor.* Biosens Bioelectron, 2009. **24**(7): p. 2040-5.
142. Saha, S., et al., *Zinc oxide-potassium ferricyanide composite thin film matrix for biosensing applications.* Anal Chim Acta, 2009. **653**(2): p. 212-6.
143. Liu, H. and N. Hu, *Study on Direct Electrochemistry of Glucose Oxidase Stabilized by Cross-Linking and Immobilized in Silica Nanoparticle Films.* Electroanal, 2007. **19**(7-8): p. 884-892.
144. Yu, J., S. Liu, and H. Ju, *Glucose sensor for flow injection analysis of serum glucose based on immobilization of glucose oxidase in titania sol-gel membrane.* Biosens Bioelectron, 2003. **19**(4): p. 401-409.
145. Malitesta, C., et al., *Glucose Fast-Response Amperometric Sensor Based on Glucose-Oxidase Immobilized in an Electropolymerized Poly(Ortho-Phenylenediamine) Film.* Anal Chem, 1990. **62**(24): p. 2735-2740.
146. Netchiporouk, L.I., et al., *In Vivo Brain Glucose Measurements:â€‰ Differential Normal Pulse Voltammetry with Enzyme-Modified Carbon Fiber Microelectrodes.* Anal Chem, 1996. **68**(24): p. 4358-4364.
147. Cosnier, S., *Biomolecule immobilization on electrode surfaces by entrapment or attachment to electrochemically polymerized films. A review.* Biosens Bioelectron, 1999. **14**(5): p. 443-456.
148. Pandey, P.C., S. Upadhyay, and H.C. Pathak, *A new glucose sensor based on encapsulated glucose oxidase within organically modified sol-gel glass.* Sensor Actuat B-Chem, 1999. **60**(2-3): p. 83-89.
149. Tatsu, Y., et al., *Entrapment of Glucose Oxidase in Silica Gel by the Sol-Gel Method and Its Application to Glucose Sensor.* Chem Lett, 1992. **21**(8): p. 1615-1618.

150. Ansari, A.A., P.R. Solanki, and B.D. Malhotra, *Sol-gel derived nanostructured cerium oxide film for glucose sensor.* Appl Phy Lett, 2008. **92**(26): p. 263901-263901-3.
151. Sasso, S.V., et al., *Electropolymerized 1,2-Diaminobenzene as a Means to Prevent Interferences and Fouling and to Stabilize Immobilized Enzyme in Electrochemical Biosensors.* Anal Chem, 1990. **62**(11): p. 1111-1117.
152. Palmisano, F., et al., *An Interference-Free Biosensor Based on Glucose-Oxidase Electrochemically Immobilized in a Nonconducting Poly(Pyrrole) Film for Continuous Subcutaneous Monitoring of Glucose through Microdialysis Sampling.* Biosensors & Bioelectronics, 1993. **8**(9-10): p. 393-399.
153. Lukachova, L.V., et al., *Electrosynthesis of poly-o-diaminobenzene on the Prussian Blue modified electrodes for improvement of hydrogen peroxide transducer characteristics.* Bioelectrochem, 2002. **55**(1-2): p. 145-148.
154. Zhang, Z., H. Liu, and J. Deng, *A Glucose Biosensor Based on Immobilization of Glucose Oxidase in Electropolymerized o-Aminophenol Film on Platinized Glassy Carbon Electrode.* Anal Chem, 1996. **68**(9): p. 1632-1638.
155. Chen, X., et al., *Electrochemically Mediated Electrodeposition/Electropolymerization To Yield a Glucose Microbiosensor with Improved Characteristics.* Anal Chem, 2002. **74**(2): p. 368-372.
156. Murphy, L.J., *Reduction of Interference Response at a Hydrogen Peroxide Detecting Electrode Using Electropolymerized Films of Substituted Naphthalenes.* Anal Chem, 1998. **70**(14): p. 2928-2935.
157. Emr, S.A. and A.M. Yacynych, *Use of Polymer-Films in Amperometric Biosensors.* Electroanal, 1995. **7**(10): p. 913-923.
158. Jia, W.-Z., K. Wang, and X.-H. Xia, *Elimination of electrochemical interferences in glucose biosensors.* TrAC Trends Anal Chem, 2010. **29**(4): p. 306-318.
159. Sternberg, R., et al., *Covalent Enzyme Coupling on Cellulose-Acetate Membranes for Glucose Sensor Development.* Anal Chem, 1988. **60**(24): p. 2781-2786.
160. Muguruma, H., A. Hiratsuka, and I. Karube, *Thin-film glucose biosensor based on plasma-polymerized film: A simple design for mass production.* Anal Chem, 2000. **72**(11): p. 2671-2675.
161. Jung, S.-K. and G.S. Wilson, *Polymeric Mercaptosilane-Modified Platinum Electrodes for Elimination of Interferants in Glucose Biosensors.* Anal Chem, 1996. **68**(4): p. 591-596.
162. Wang, J. and H. Wu, *Permselective Lipid Poly(O-Phenylenediamine) Coatings for Amperometric Biosensing of Glucose.* Anal Chim Acta, 1993. **283**(2): p. 683-688.
163. Zhang, Y.N., et al., *Elimination of the Acetaminophen Interference in an Implantable Glucose Sensor.* Anal Chem, 1994. **66**(7): p. 1183-1188.
164. Vaidya, R., P. Atanasov, and E. Wilkins, *Effect of interference on the performance of glucose enzyme electrodes using Nafion® coatings.* Med Eng Phys, 1995. **17**(6): p. 416-424.
165. Rodríguez, M. and G. Rivas, *Assembly of Glucose Oxidase and Different Polyelectrolytes by Means of Electrostatic Layer-by-Layer Adsorption on Thiolated Gold Surface.* Electroanal, 2004. **16**(20): p. 1717-1722.
166. Gardeniers, H.J.G.E., et al., *Silicon micromachined hollow microneedles for transdermal liquid transport.* Journal of Microelectromechanical Systems, 2003. **12**(6): p. 855-862.
167. Chandrasekaran, S., J.D. Brazzle, and A.B. Frazier, *Surface micromachined metallic microneedles.* Journal of Microelectromechanical Systems, 2003. **12**(3): p. 281-288.

168. Crichton, M.L., et al., *The effect of strain rate on the precision of penetration of short densely-packed microprojection array patches coated with vaccine.* Biomaterials, 2010. **31**(16): p. 4562-4572.
169. Bodhale, D., A. Nisar, and N. Afzulpurkar, *Structural and microfluidic analysis of hollow side-open polymeric microneedles for transdermal drug delivery applications.* Microfluidics and Nanofluidics, 2010. **8**(3): p. 373-392.
170. Kim, B.J., et al., *Fabrication of Microneedle Using Laser Written PDMS Mold for Molecule Transport into Plant Skin.* Biochip Journal, 2009. **3**(4): p. 281-286.
171. Zhou, H.B., et al., *A new process for fabricating tip-shaped polymer microstructure array with patterned metallic coatings.* Sensors and Actuators a-Physical, 2009. **150**(2): p. 296-301.
172. Arora, A., M.R. Prausnitz, and S. Mitragotri, *Micro-scale devices for transdermal drug delivery.* International Journal of Pharmaceutics, 2008. **364**(2): p. 227-236.
173. Matteucci, M., et al., *A compact and disposable transdermal drug delivery system.* Microelectronic Engineering, 2008. **85**(5-6): p. 1066-1073.
174. Lee, J.W., J.H. Park, and M.R. Prausnitz, *Dissolving microneedles for transdermal drug delivery.* Biomaterials, 2008. **29**(13): p. 2113-2124.
175. Park, J.H., M.G. Allen, and M.R. Prausnitz, *Biodegradable polymer microneedles: Fabrication, mechanics and transdermal drug delivery.* Journal of Controlled Release, 2005. **104**(1): p. 51-66.
176. Rajaraman, S. and H.T. Henderson, *A unique fabrication approach for microneedles using coherent porous silicon technology.* Sensors and Actuators B-Chemical, 2005. **105**(2): p. 443-448.
177. Noh, Y.W., et al., *In vitro characterization of the invasiveness of polymer microneedle against skin.* International Journal of Pharmaceutics, 2010. **397**(1-2): p. 201-205.
178. S Brzezinski, G.M., T Nowak,H Schmidt, D Marcinkowska, A Kaleta, *Structure and Properties of Microporous Polyurethane Membranes Designed for Textile-Polymeric Composite Systems.* Fibres and Textiles in Eastern Europe, 2005. **13**(6): p. 54.
179. Wang, J., *In vivo glucose monitoring: towards 'Sense and Act' feedback-loop individualized medical systems.* Talanta, 2008. **75**(3): p. 636-41.
180. Jeong, R.A., et al., *In vivo calibration of the subcutaneous amperometric glucose sensors using a non-enzyme electrode.* Biosens Bioelectron, 2003. **19**(4): p. 313-9.
181. Kim, K., et al., *A tapered hollow metallic microneedle array using backside exposure of SU-8.* Journal of Micromechanics and Microengineering, 2004. **14**(4): p. 597-603.
182. Ho Shim, J., H. Do, and Y. Lee, *Simple Fabrication of Amperometric Nitric Oxide Microsensors Based on Electropolymerized Membrane Films.* Electroanalysis. **22**(3): p. 359-366.
183. Castner, J.F. and L.B. Wingard, Jr., *Mass transport and reaction kinetic parameters determined electrochemically for immobilized glucose oxidase.* Biochemistry, 1984. **23**(10): p. 2203-10.
184. Mikkelsen, S.R. and R.B. Lennox, *Rotating disc electrode characterization of immobilized glucose oxidase.* Anal Biochem, 1991. **195**(2): p. 358-63.
185. Doretti, L., et al., *Acetylcholine biosensor involving entrapment of acetylcholinesterase and poly(ethylene glycol)-modified choline oxidase in a poly(vinyl alcohol) cryogel membrane.* Enzyme and Microbial Technology, 2000. **27**(3-5): p. 279-285.

186. Thibault, J.-F., C. Garreau, and D. Durand, *Kinetics and mechanism of the reaction of ammonium persulfate with ferulic acid and sugar-beet pectins.* Carbohydrate Research, 1987. **163**(1): p. 15-27.
187. Ju, Y.M., et al., *A novel porous collagen scaffold around an implantable biosensor for improving biocompatibility. I. In vitro/in vivo stability of the scaffold and in vitro sensitivity of the glucose sensor with scaffold.* J Biomed Mater Res A, 2008. **87**(1): p. 136-46.
188. Fernandez, J.L., C. Hurth, and A.J. Bard, *Scanning electrochemical microscopy #54. Application to the study of heterogeneous catalytic reactions-hydrogen peroxide decomposition.* J Phys Chem B, 2005. **109**(19): p. 9532-9.
189. Wittstock, G., *Modification and characterization of artificially patterned enzymatically active surfaces by scanning electrochemical microscopy.* Fresenius J Anal Chem, 2001. **370**(4): p. 303-15.
190. T. Wilhelm, G.W.a.R.S., *Scanning electrochemical microscopy of enzymes immobilized on structured glass-gold substrates* Fresenius' Journal of Analytical Chemistry, 1999. **365**(1-3): p. 163-167.
191. Frankenthal, R.P. and D.J. Siconolfi, *The Anodic Corrosion of Gold in Concentrated Chloride Solutions.* Journal of The Electrochemical Society, 1982. **129**(6): p. 1192-1196.
192. Bantle, J.P. and W. Thomas, *Glucose measurement in patients with diabetes mellitus with dermal interstitial fluid.* Journal of Laboratory and Clinical Medicine, 1997. **130**(4): p. 436-441.
193. Srinivasan, V., V.K. Pamula, and R.B. Fair, *An integrated digital microfluidic lab-on-a-chip for clinical diagnostics on human physiological fluids.* Lab on a Chip, 2004. **4**(4): p. 310-315.
194. Brivio, M., W. Verboom, and D.N. Reinhoudt, *Miniaturized continuous flow reaction vessels: influence on chemical reactions.* Lab on a Chip, 2006. **6**(3): p. 329-344.
195. Wu, M.H., S.B. Huang, and G.B. Lee, *Microfluidic cell culture systems for drug research.* Lab on a Chip, 2010. **10**(8): p. 939-956.
196. Winkle, R.F., et al., *Towards microfluidic technology-based MALDI-MS platforms for drug discovery: a review.* Expert Opinion on Drug Discovery, 2008. **3**(11): p. 1281-1292.
197. Baxter, G.T., *Hurel (TM) - an In Vivo-surrogate Assay Platform for Cell-based Studies.* Atla-Alternatives to Laboratory Animals, 2009. **37**: p. 11-18.
198. Park, T.H. and M.L. Shuler, *Integration of cell culture and microfabrication technology.* Biotechnology Progress, 2003. **19**(2): p. 243-253.
199. Mustafic, A., et al., *Imaging of flow patterns with fluorescent molecular rotors.* J Fluoresc. **20**(5): p. 1087-98.
200. Ratner, B.D., et al., *Biomaterials Science - An Introduction to Materials in Medicine (2nd Edition)*, Elsevier.
201. Mohomed, K., F. Moussy, and J.P. Harmon, *Dielectric analyses of a series of poly(2-hydroxyethyl methacrylate-co-2,3-dihydroxypropyl methacylate) copolymers.* Polymer, 2006. **47**(11): p. 3856-3865.
202. Lord, M.S., et al., *Lysozyme interaction with poly(HEMA)-based hydrogel.* Biomaterials, 2006. **27**(8): p. 1341-1345.
203. Garrett, Q., B. Laycock, and R.W. Garrett, *Hydrogel lens monomer constituents modulate protein sorption.* Invest Ophthalmol Vis Sci, 2000. **41**(7): p. 1687-95.

204. Duran, J.A. and J.A. Meyer, *Exothermic Heat Released during Catalytic Polymerization of Basswood-Methyl Methacrylate Composites.* Wood Science and Technology, 1972. **6**(1): p. 59-&.
205. Doria-Serrano, M.C., et al., *Poly(N-vinyl pyrrolidone) Calcium Alginate (PVP Ca-alg) Composite Hydrogels: Physical Properties and Activated Sludge Immobilization for Wastewater Treatment.* Industrial & Engineering Chemistry Research, 2002. **41**(13): p. 3163-3168.
206. Ulbricht, M., *Advanced functional polymer membranes.* Polymer, 2006. **47**(7): p. 2217-2262.